Particle & Particle Systems Characterization
www.particle-journal.com

Noble Metal Clusters: Applications in Energy, Environment, and Biology

*Ammu Mathew and Thalappil Pradeep**

Sub-nanometer-sized metal clusters, having dimensions between metal atoms and nanoparticles, have attracted tremendous attention in the recent past due to their unique physical and chemical properties. As properties of such materials depend strongly on size, development of synthetic routes that allows precise tuning of the cluster cores with high monodispersity and purity is an area of intense research. Such materials are also interesting owing to their wide variety of applications. Novel sensing strategies based on these materials are emerging. Owing to their extremely small size, low toxicity, and biocompatibility, they are widely studied for biomedical applications. Primary focus of this review is to provide an account of the recent advances in their applications in areas such as environment, energy, and biology. With further experimental and theoretical advances aimed at understanding their novel properties and solving challenges in their synthesis, an almost unlimited field of applications can be foreseen.

1. Introduction

The unique physiochemical properties of soluble/dispersible noble metal and semiconducting nanomaterials have contributed to several areas of research pertaining to energy, environment, and medicine in the past few decades.[1–6] For noble metals, the excitement has been largely due to plasmonic (metallic) nanoparticles (NPs) of diverse shapes.[3,7,8] In the recent past, a new class of nanoscale materials made of a few to tens of atoms, having size <2 nm, often called nanoclusters or quantum clusters (QCs)[9] are receiving large attention due to their unique physical and chemical properties. They are believed to have greater implications to the aforementioned areas. Consequently, precise control of the clusters by developing easy synthetic strategies became an active area of research. These materials fall in the NP-to-atom/molecule transition region and exhibit molecule-like properties owing to the gradual emergence of discrete electronic states.[10] Analogous to the size-dependent bandgap and quantum confinement effects in semiconductor quantum dots, QCs with sizes comparable to the Fermi wavelength of electrons show interesting properties such as size-dependent fluorescence, making them distinctly different from their NP counterparts. Unlike semiconductor quantum dots, QCs are less toxic and are smaller in dimension, making them superior candidates than the former in terms of biological applications. This review is an attempt to look at the emerging applications of this fascinating branch of materials science.

Naming of these materials is still a point of debate and a fully acceptable terminology has not appeared so far. As a result, authors use a number of names, which include nanomolecules, nanoclusters, NPs, faradaurates, monolayer-protected clusters (MPCs), artificial atoms, super atoms, QCs, etc. MPC has been a more acceptable name in the literature, although this has been used before in the context of plasmonic NPs, since 1995.[11] As clusters being discussed these days are atomically precise, naming them as MPCs seems inappropriate and often makes one confuse them with particles of the past. The name "clusters" is suggestive of gas-phase analogues of these materials, which are unprotected and unstable in the condensed phase. The name "nanomolecule" appears to imply that other prefixes such as pico, femto, etc. are possible for molecules, which does not make chemical sense, although we note that macromolecules do exist. "Faradaurate" is not appropriate as the suffix "ate" appears to imply a complex ion. Superatom and artificial atom would have been acceptable if the system was only an aggregate of atoms, while the materials are indeed molecules and possess properties of ligands quite distinctly. It is in fact these properties that are being used extensively in many of the applications. Moreover, with the recent addition of the crystal structures of non-superatomic systems such as $[Au_{23}SR_{16}]^-$, where SR is SC_6H_{11}, the term "superatoms" fails to describe this class of materials appropriately. It is in this context that a more suitable name, QCs, is used, which suggests distinct optical and electronic properties of the system and also resembles the name, quantum dots which indeed they are, although the former are composed of metals. Molecules are indeed quantized and therefore, the prefix "quantum" is, at least, partly redundant. We do note that search for a more appropriate name is continuing.

A. Mathew, Prof. T. Pradeep
DST Unit of Nanoscience (DST UNS) and Thematic Unit of Excellence (TUE)
Department of Chemistry
Indian Institute of Technology Madras
Chennai 600036, India
E-mail: pradeep@iitm.ac.in

DOI: 10.1002/ppsc.201400033

Although noble metals generally refer to eight elements (ruthenium, rhodium, palladium, silver, osmium, iridium, platinum, and gold), QCs of gold,[10,12–15] silver,[16,17] as well as their alloys[18–20] are the most studied, although several clusters of copper,[21–23] platinum,[24–26] and palladium[27,28] are also reported. Over the past two decades, metallic QCs of various core sizes and ligands with unique properties have been utilized in diverse applications of energy, environment, and biomedicine, as depicted in **Figure 1**.

Syntheses and isolation of such clusters can be achieved by different means. The current synthetic capabilities allow the large-scale synthesis of several stable and isolable clusters.[9,29] Discrete molecule-like electronic transitions, size-dependent physicochemical properties, especially photoluminescence as well as other properties such as magnetism and electrochemical properties have generated wide interest. Catalytic activities of both supported and unsupported Au clusters[30–33] have been explored intensely. Additionally, the possibility of tuning optical and electrical properties of QCs by independently modifying their surface chemistry has given another handle to control their properties. A range of organic, biological, and polymeric molecules such as thiols, aminoacids, proteins, dendrimers, and DNA and their derivatives have been exploited for tuning the surface chemistry of QCs. Although several noble metal clusters have been studied for catalytic applications, they are largely unprotected and distinct molecular formulae cannot be assigned to many.[34–37]

Several excellent reviews exist on diverse synthetic strategies,[9,17,29,38,39] unique structure,[10,40,41] properties,[13,15,16,32,38,41–45] and bio-applications[17,46–49] of Au and AgQCs. Practical applications of these materials in environment, energy, and biology become possible due to their distinct chemistry (both of the ligand and the core). The diverse optical and catalytic properties of these systems, being used in the application areas mentioned, are mostly manifested in the solution state. Even in the case of supported clusters, the role of ligands is important. Solubility and compatibility with the solvent system are a crucial requirement, which is enabled by the ligand chemistry. Use of the core electronic structure in the biological context is enabled by surface conjugation. From the above, it is evident that practical utility of these materials is largely due to their unique chemistry. In this review, we highlight the molecular properties of QCs enabling applications. Structure of the review is as follows. Brief descriptions of the common synthetic techniques utilized are presented in Section 2, which is followed by a discussion of their unique properties in Section 3. Applications of QCs are discussed in Section 4. Finally, a summary and future prospects of this area are provided in Section 5. In the discussion, clusters are often described using their core size such as Au_{35}, Au_{38}, etc. without reference to their ligand structure such as $Au_{25}L_{18}$, $Au_{38}L_{24}$, etc. (where "L" denotes the ligand) as the cluster composition is well defined even with the metal core itself in such cases. In other words, most of the clusters except Ag_{32} (which is reported to have 19 and 21 ligands) have a fixed number of ligands. Clusters whose atomic compositions are ill defined are also discussed. They are labeled as M@L, where there is no atomic precision in the composition, while distinct cluster properties such as visible luminescence exist.

Ammu Mathew holds an M.Sc. in chemistry from Stella Maris College, Chennai, and is currently pursuing her Ph.D. under the guidance of Prof. T. Pradeep in the Department of Chemistry, Indian Institute of Technology Madras, Chennai. Her work is concerned with the chemistry of noble metal quantum clusters, applications of mesostructures in ultra-trace detection of analytes, and creation of hybrid structures of the two.

T. Pradeep, after his Ph.D. from the Indian Institute of Science and postdoctoral training at University of California, Berkeley, and Purdue University, West Lafayette, joined IIT Madras in 1993, where he is a full professor since 2004. Prof. Pradeep's research interests are in molecular and nanoscale materials, and he develops instrumentation for those studies. He is involved in the development of affordable technologies for drinking water purification, and some of his technologies have been commercialized.

2. Common Synthetic Approaches

Creation of clusters with varying core sizes and ligands is fascinating as it opens up immense opportunities to study the emergence of novel physical and chemical properties and provides an insight into their structure–property relationships. While for NPs, changes in the physiochemical properties are manifested by change in size (diameter) or shape of the particles, modification of a single metal atom in the core can alter properties in the cluster size regime. Several protocols have been developed and they have been documented in several excellent reviews.[9,17,29,38,39]

After the pioneering work of Brust and co-workers in 1994,[50] the two-phase system of synthesis of thiol stabilized ≈3 nm AuNPs, comprising an organic layer (toluene) and an aqueous layer gained much interest. A phase-transfer agent was used to transfer the metal ion precursor to the thiol containing organic phase. Efficient routes for the synthesis of monolayer protected sub-nanometer-sized clusters of various ligands using both biphasic and monophasic solvent mixtures were realized later using modified versions of the initial Brust–Schiffrin method.[51–54] Following this, several protocols were developed to make atomically precise, monodisperse clusters. Based on the precursors used, synthetic protocols

Part. Part. Syst. Charact. **2014**,
DOI: 10.1002/ppsc.201400033

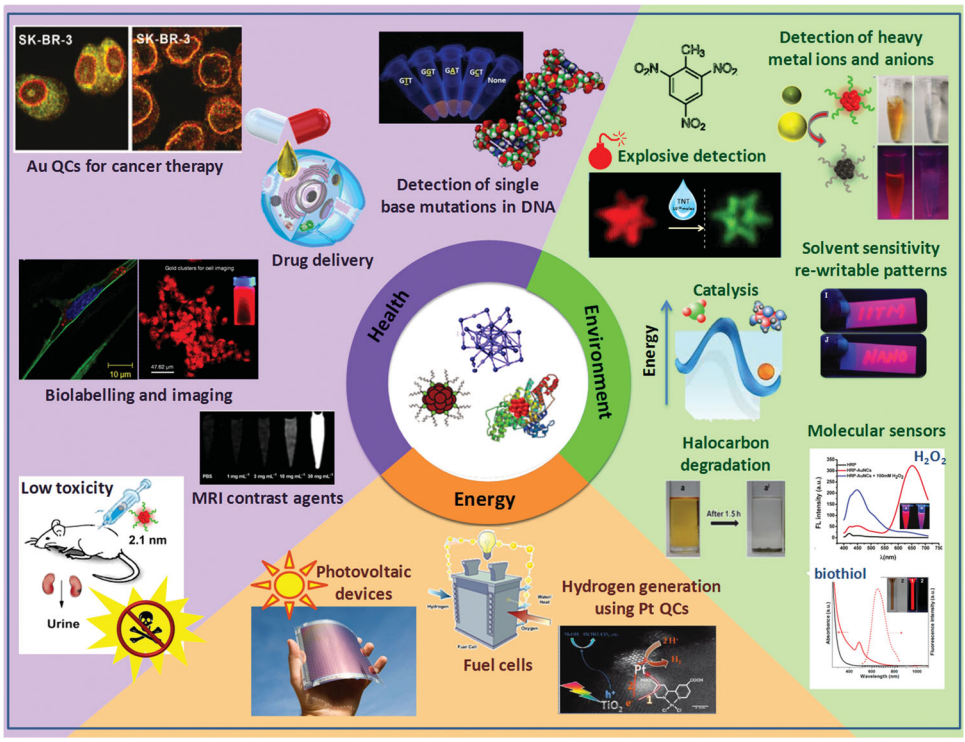

Figure 1. Applications of QCs are spanned over three major domains: energy, environment, and biology. Images in the figure reproduced with permission.[94,170,264,269,273,290] Copyright 2010, 2011, and 2012, American Chemical Society; Reproduced with permission.[135,173,206] Copyright 2010, 2011, and 2012, Wiley-VCH; Reproduced with permission.[210] Copyright 2013, Royal Society of Chemistry; Reproduced with permission.[291] Copyright 2010, Springer.

can be broadly classified into two major categories, bottom up and top down methods, as shown in **Figure 2**. In the bottom up synthesis of QCs, metal ions are used as precursors. Here, the choice of ligands, reducing agent, metal precursor, and experimental conditions plays significant roles in determining the core size, purity, and yield of the clusters. Apart from traditional wet chemical routes (solution-phase synthesis), new protocols such as solid-state synthesis, interfacial synthesis, gel-mediated synthesis, etc. offer alternate ways of making clusters with diverse properties. In a typical solid-state synthesis, the reactants, namely, the metal ion precursor, reducing agent and ligand are ground well in their native form in air and the cluster is extracted into a suitable solvent. Ag_9,[55] Ag_{32},[56] Ag_{44},[57] and Ag_{152}[58] were synthesized utilizing the above protocol. Cluster synthesis using various templates such as polymers,[59,60] proteins,[61–63] dendrimers,[64,65] gels,[66,67] DNA,[68,69] etc. are widely employed for the synthesis of fluorescent QCs of Au, Ag, Cu, etc. Such templates can serve as suitable environments for cluster synthesis owing to their size, distinct conformation, and multiple binding sites, leading to distinct core sizes. After the synthesis of Au clusters protected by bovine serum albumin (BSA) by Xie et al.,[70] protein-protected clusters have emerged as an area of research due to their immense potential in biological studies. They are summarized well in several reviews.[17,39,47,71] Photoreduction method,[60,67] sonochemical method,[72] microemulsion method,[73] radiolytic method,[74,75] electrochemical method,[76] microwave-assisted synthesis,[77] etc. are other routes for making clusters. Among the various top down routes used for the synthesis of clusters, ligand-mediated etching from larger NPs[78] or clusters[79] is a useful method. Ligand-exchange[80,81] or place-exchange[82] reactions from preformed clusters is another popular protocol. The above synthetic routes, upon careful control of precursor metal ion and ligand concentration yields fairly monodisperse clusters of definite nuclearity. However, it is important to note that an additional purification step is often employed, post-synthesis, in order to discard other impurities in solution such as excess ligands, metal complexes, other clusters, etc. Isolation and separation of clusters are carried out via various techniques such as polyacrylamide gel electrophoresis (PAGE),[55,83,84] solvent selective precipitation,[85,86] size-exclusion chromatography,[87] etc. Recently, high-resolution separation and isolation of mixed ligand clusters containing a distribution of chemical compositions to yield individual clusters have been realized using high-performance liquid chromatography (HPLC) for clusters of various metal cores such as $PdAu_{24}$, Au_{25}, and Au_{38} as well as various regioisomers of Au_{38}.[81,88] The difference in polarity between the clusters induced by various ligand functionalization was used for the separation of the products. Enantiomeric separation of Au_{38} cluster protected by achiral thiolates was achieved by chiral HPLC.[89]

Studies of gas-phase clusters of Au and Ag were initiated way back in 1980s.[90] Chemical sputtering of metal targets of gold and silver by pulsed laser or inert gas ions produced metal atoms, which later coalesced and nucleated to form "naked" (without ligand protection) clusters. While the reports of QCs stabilized by various ligands are numerous, synthesizing their corresponding gas-phase analogues poses a major challenge to

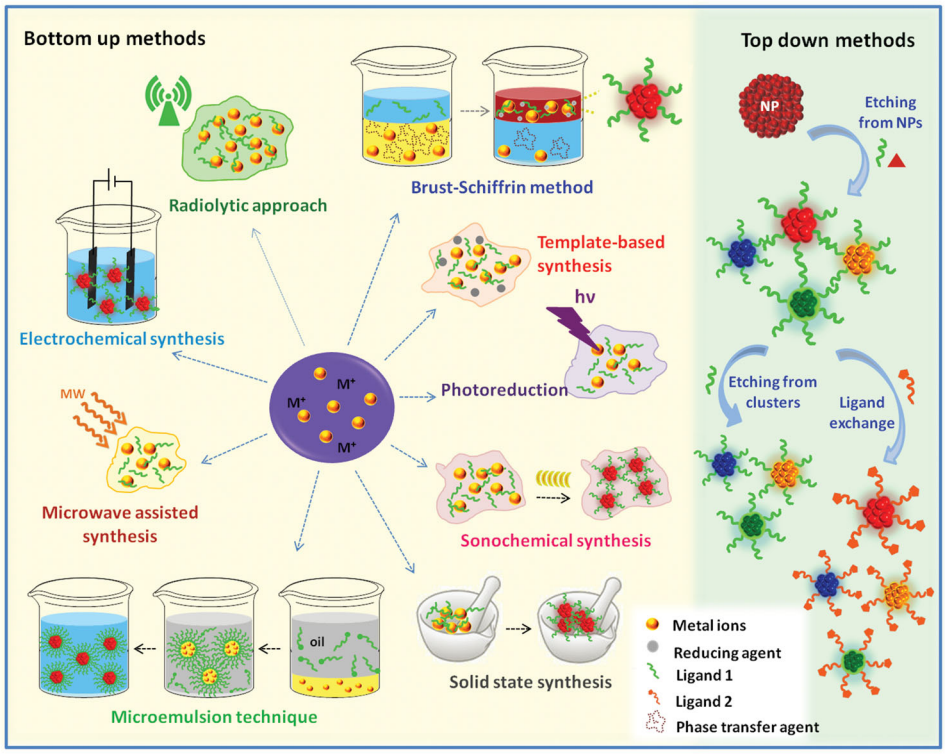

Figure 2. Various routes for the synthesis of atomically precise, sub-nanometer-sized, noble metal quantum clusters.

researchers. Dissipation of the excess internal energy of such clusters in the form kinetic energy leading to gas-phase collisions and subsequent nucleation is a major limiting factor for the stability and isolation of such clusters. Recently, creation of clusters of magic numbered unprotected metal cores such as Au_{18}^+, Au_{25}^+, Au_{38}^+, and Au_{102}^+ with unusual stability in the gas phase was demonstrated in laser desorption ionization experiments using protein templates.[91] It was proposed that the cluster nucleation occurred in the vicinity of the protein, in the gas phase, leading to the formation of magic numbered Au clusters. Later, naked alloy clusters of the type $Au_{24}Pd^+$ were also detected in the gas phase using a similar approach.[92] A recent perspective article by Rao and Pradeep[29] summarizes advances in the synthesis of atomically precise QCs of silver, gold, and their alloys with special emphasis on silver QCs. **Table 1** highlights several synthetic routes discovered so far along with a few examples.

3. Unique Characteristics

3.1. Structure

Understanding the crystal structure of QCs is important in exploiting their unique properties for various applications in diverse fields. Information on the nature of Au–S interaction, atomicity of the core, orientation of the ligands around the metal core in the form of staples, etc. is derived by solving the crystal structure of the material. Moreover, observation of crystals from such clusters serves as an irrefutable confirmation of their existence in solution. X-ray crystallography and computational studies have led to significant progress in deriving the total structure of atomically precise nanoclusters. Many crystal structures of gold clusters such as $Au_{102}SR_{44}$,[93] $Au_{25}SR_{18}$,[94,95] $Au_{38}SR_{24}$,[96] $Au_{36}SR_{24}$,[97] $[Au_{24}(PPh_3)_{10}(SR)_5Cl_2]^+$,[98] $Au_{28}SR_{20}$,[99] and $[Au_{23}SR_{16}]^-$[100] (where SR = thiolate) were reported in the past few years mainly due to their better stability, resistance to oxidation, and optimized synthetic protocols, facilitating the growth of large single crystals. However, crystal structures of silver clusters such as Ag_{14},[101] Ag_{16},[102] Ag_{32},[102] and $Ag_{44}SR_{30}$[103,104] as well as bimetallic alloy clusters such as $Au_{13}Cu_x$ (x = 2, 4, 8) clusters[105] and $Au_{12}Ag_{32}SR_{30}$[103] were reported recently.

Gold clusters such as Au_{102}(p-MBA)$_{44}$, $Au_{25}(SCH_2CH_2Ph)_{18}$, and $Au_{38}(SCH_2CH_2Ph)_{24}$ are composed of non-FCC (face-centered cubic) kernels such as decahedral Au_{79}, icosahedral Au_{13}, and face-sharing bi-icosahedral Au_{23}, respectively. Surface of each $Au_n(SR)_m$ clusters contain unique "staple"-like motifs such as dimeric staples (—SR—Au—SR—Au—SR—) and monomeric staples (—SR—Au—SR—). $Ag_{44}SR_{30}$ cluster has a double-shell core made of concentric shells of an inner Ag_{12} icosahedron cage within an Ag_{20} dodecahedron cage. These 32-atom cages were further protected by six $Ag_2(SR)_5$ units in which Ag(I) ion binds to three SR ligands in a $Ag(SR)_3$ planar configuration, which is unlike the case of Au clusters, in which Au(I) ions were coordinated linearly to two thiolate ligands.

The very first crystal structure, among thiolated noble metal QCs was of Au_{102}(p-MBA)$_{44}$ in 2007 by Kornberg and co-workers.[93] The structure is composed of a central Marks decahedron core made of 49 gold atoms, two 20-atom caps

Part. Part. Syst. Charact. **2014**,
DOI: 10.1002/ppsc.201400033

Table 1. List of various common synthetic approaches for making noble metal QCs along with some examples. Schematic of the synthetic procedures is shown in Figure 2.

Method				Some examples of QCs synthesized	Refs.
Bottom up approach	Brust–Schiffrin method and its modifications			$Au_{25}SR_{18}$,[94,152,307] $Au_{44}SR_{28}$,[51] Pt@DT,[308] Cu@MPP[23]	[23, 51,152,307–309]
	Template-based synthesis	Polymers		Ag@LA-PEG,[310] Ag@(PG-b-PAA),[59]	[59,60,310]
		Proteins		Au_{25}@BSA,[70] Ag_{15}@BSA,[62] Au@NLf,[63] Cu@BSA,[21] AuAg@BSA,[20]	[61–63]
		Dendrimers		Ag@PMAA,[72],311 Ag@PAMAM,[65]	[64,65,72,311]
		Gels		Ag_{25}@SG,[66] Au_{15}@CD,[170]	[66,67,170]
		DNA		Ag@DNA,[69],312-315	[68,69,312–315]
		Thiol- or amine-functionalized small molecules		Ag_7DMSA_4,[52] $Ag_8(H_2MSA)_8$ and $Ag_7(H_2MSA)_7$,[169] $Ag_{\sim 4,5}$@DHLA,[193] $Au_{25}SG_{18}$,[79],83	[52,169,193]
	Photoreduction			Ag@PAMAM,[65]	[60,65,67]
	Sonochemical synthesis			Ag@PMAA[69],72	[72]
	Solid-state synthesis			Ag_9,[55] Ag_{32},[56] Ag_{44},[57] and Ag_{152}[58]	[55–58]
	Microemulsion technique			Ag_n QCs ($n < 10$)[73]	[73]
	Microwave-assisted synthesis			Ag@L-GSH[77]	[77]
	Electrochemical synthesis			Cu@TBAN[76]	[76]
	Radiolytic approach			Ag_3^{2+},[43] Ag_4^{2+}[44]	[74,75]
Top down approach	From NPs	Etching	Using excess ligand	$Au_{25}SG_{18}$,[79]	[79]
			High temperature	Au@DT,[316] $Ag_{38}MSA_{24}$,[78] $Ag_{75}SG_{40}$[317]	[78,316]
			Other	$Ag_8(H_2MSA)_8$ and $Ag_7(H_2MSA)_7$	[169]
	From other QCs	Etching		$Au_{25}SR_{18}$,[79] $Au_{38}SR_{24}$,[318] Au_{75}[319]	[79,318,319]
		Ligand exchange		$Au_{25}(DDT_{18-n}SBB_n)$,[81] $Pd_1Au_{24}(DDT_{18-n}\ SBB_n)$[81]	[80–82]
		Alloying		$Ag_7Au_6(H_2MSA)_{10}$,[320] $(Cu_nAu_{25-n})SR_{18}$ (n = 1–5), [163],321 $(Pd_1Au_{24})SR_{18}$,[164] $(Au_{24}Pt)SR_{18}$[322]	[163,164,320–322]

*Abbreviations used: Dodecanethiol-stabilized platinum clusters (Pt@DT), 2-mercapto-5-n-propylpyrimidine (MPP), polyethylene glycol appended with lipoic acid groups (LA-PEG), polyglycerol-block-poly(acrylic acid) (PG-*b*-PAA), meso-2,3-dimercaptosuccinic acid (DMSA), mercaptosuccinic acid (H_2MSA), dihydrolipoic acid (DHLA), bovine serum albumin (BSA), glutathione (GSH), poly(amidoamine) (PAMAM), poly(methacrylic acid) (PMAA), single-stranded DNA (ssDNA), tetrabutylammonium nitrate (TBAN), L-glutathione (L-GSH), mercaptosuccinic acid (MSA/(H_2MSA), dodecanethiol (DDT).

with fivefold rotational (C5) symmetry on opposite poles, and a 13-atom equatorial band. The sulfur atom of the ligands (p-MBAs) binds to two gold atoms in a bridge conformation and thus forms a rigid surface layer on the metal core. The crystal structure also revealed the chiral nature of the cluster due to the number and specific geometry of the atoms in the equatorial band. Chirality in atomically precise clusters was later studied in greater detail using several clusters (described below). Later Murray and co-workers[94] and Jin and co-workers[95] reported the crystal structure of $Au_{25}(SCH_2CH_2Ph)_{18}$ clusters. It consists of three types of gold atoms:

1. a central gold atom with coordination number 12;
2. 12 gold atoms with coordination number 6 forming the vertices of an icosahedron around the central atom (where five bond to gold atoms and one to a sulfur atom) and
3. 12 gold atoms stellated on 12 of the 20 faces of the Au_{13} icosahedron (with six orthogonal semi-rings of $Au_2(SCH_2CH_2Ph)_3$ around the Au_{13} core, wherein each sulfur atom on the central Au_{13} core is connected to two gold atoms).

In 2010, the total structure of $Au_{38}(SC_2H_4Ph)_{24}$, derived by Jin and co-workers,[96] showed a face-fused Au_{23} bi-icosahedral core with three monomeric $Au(SR)_2$ staples capped at the waist of the Au_{23} rod and six dimeric $Au_2(SR)_3$ staples. Due to the staggered arrangement of the dimeric $Au_2(SR)_3$ staples, three on the top icosahedron and the other three on the bottom icosahedron, $Au_{38}SR_{24}$ cluster framework has a C_3 rotational axis. Following these, several reports on total structure of clusters of various atomicities emerged. Though a vast number of clusters of various metal cores, ligands, and functionalities are known to date, only a few of them have been successfully crystallized. **Table 2** lists the noble metal cluster crystals reported till date in the order of their publication. Details of conditions used for crystallization are also provided. **Figure 3** shows their crystal structures.

Table 2. List of crystal structures of noble metal quantum clusters reported till date in the order of their publication. The crystal structures are shown in Figure 3.

No.	Year	Cluster*	Core	Shell/staples	Solvents and crystallization conditions	Refs.
1.	2007	Au_{102}(p-MBA)$_{44}$	Au_{39}	2[RS—(AuSR)$_2$] and 19(RS—Au—SR)	Water (solvent) 300×10^{-3} M NaCl, 100×10^{-3} M sodium acetate, pH 2.5, 46% methanol	[93]
2.	2010	$[N(C_8H_{17})_4][Au_{25}(PET)_{18}]$	Au_{13}	6(RS—Au—SR—Au—SR)	DCM (solvent)1:1 mixture of PET and thiophenol, excess methanol	[94]
3.	2010	$Au_{25}(PET)_{18}$	Au_{13}	6(RS—Au—SR—Au—SR)	20 mg mL^{-1} cluster in ethanol:toluene (4:1)	[95]
4.	2010	$Au_{38}(PET)_{24}$	Au_{23}	3(RS—Au—SR) and 6(RS—Au—SR—Au—SR)	Toluene/ethanol (solvent), ambient conditions	[96]
5.	2011	$[Au_{25}(PPh_3)_{10}(PET)_5Cl_2]^{2+}$	2(Au_{13})	5 bridging (—SR—), 10 terminally coordinated (PPh_3) and 2Cl	DCM/ethanol (1:1)	[323]
6.	2012	Au_{36}(SPh-tBu)$_{24}$	Au_{28}	4(SR—Au—SR—Au—SR) and 12 bridging (—SR—)	Toluene (solvent) ≈5 mg cluster in 1.5 mL DCM and 1 mL ethanol	[97]
7.	2012	$Ag_{14}(SC_6H_3F_2)_{12}(PPh_3)_8$	$(Ag_6)^{4+}$	8[$Ag^+(SC_6H_3F_2^-)_2PPh_3$] tetrahedra sharing one ($SC_6H_3F_2^-$) between them	DCM/hexane solvent mixture at 4 °C	[101]
8.	2012	$[Au_{24}(PPh_3)_{10}(PET)_5X_2]^+$	2(Au_{12})	5 bridging (—SR—), 10 terminally coordinated (PPh_3) and 2X	Vapor diffusion of hexane into a toluene solution of clusters	[98]
9.	2013	$Ag_{16}(DPPE)_4(SPhF_2)_{14}$	$(Ag_8)^{6+}$	$[Ag_8(DPPE)_4(SPhF_2)_{14}]^{6-}$	Clusters in DCM/hexane solvent mixture at 4 °C in presence of 5.0 mg PPh_4Br	[102]
10.	2013	$[PPh_4]_2[Ag_{32}(DPPE)_5(SPhCF_3)_{24}]$	$[Ag_{22}]^{12+}$	1[$Ag_6(DPPE)_3(SPhCF_3)_{12}]^{6-}$, 2[$Ag_2(DPPE)(SPhCF_3)_4]^{2-}$ and 4($SPhCF_3$)$^-$		
11.	2013	$[Au_{13}Cu_2(PPh_3)_6(SPy)_6]^+$	Au_{13}	6(PPh_3) and 6(SPy) holds two face-capping Cu atoms	DCM/hexane solvent mixture at 4 °C	[105]
12.	2013	$[Au_{13}Cu_4(PPh_2Py)_4$(SPh-tBu)$_8]^+$ $[ClO_4]^-$	Au_{13}	4(PPh_2Py) and 8(SPh-tBu) holding four surface-capping Cu atoms		
13.	2013	$[Au_{13}Cu_8(PPh_2Py)_{12}]^+$	Au_{13}	2[$Cu(PPh_2Py)_3$] and 6[$Cu(PPh_2Py)$]		
14.	2013	Au_{28}(SPh-tBu)$_{20}$	Au_{20}	4(—SR—Au—SR—Au—SR—) and eight bridging (—SR—)	1.5 mL DCM and 1 mL ethanol solvent mixture	[99]
15.	2013	Na_4Ag_{44}(p-MBA)$_{30}$	Ag_{12}@Ag_{20} two shell core	6[$Ag_2(SR)_5$]	Water/methanol (solvent); cluster washed with 1% acetic acid in DMF; crystallized from DMF	[104]
16.	2013	$[PPh_4]_4[Ag_{44}(SPhF_2)_{30}]$	Ag_{12}@Ag_{20} two shell core	6[$Ag_2(SR)_5$]	Layering hexane into the DCM solutions of clusters at 4°C	[103]
17.	2013	$[PPh_4]_4[Ag_{44}(SPhCF_3)_{30}]$				
18.	2013	$[PPh_4]_4[Ag_{44}(SPhF)_{30}]$				
19.	2013	$[PPh_4]_4[Au_{12}Ag_{32}(SPhF)_{30}]$	Au_{12}@Ag_{20} two shell core			
20.	2013	$[PPh_4]_4[Au_{12}Ag_{32}(SPhF_2)_{30}]$				
21.	2013	$[PPh_4]_4[Au_{12}Ag_{32}(SPhCF_3)_{30}]$				
22.	2013	$[Au_{23}(c\text{-}C_6)_{16}]^-$	Au_{15}	2[$Au_3(SR)_4$], 2[$Au(SR)_2$] and 4 bridging (—SR—)	≈4 mg cluster in 1 mL DCM followed by vapor diffusion of pentane into the cluster solution for 1–2 d	[100]
23.	2014	$Au_{18.3}Ag_{6.7}(PET)_{18}$	$Au_{6.3}Ag_{6.7}$	6(RS—Au—SR—Au—SR)	Incoming Au/Ag molar ratio was 1:0.25. Toluene or DCM was used as solvent and EtOH or MeOH as the nonsolvent	[324]
24.	2014	$Au_{30}S$(S-t-Bu)$_{18}$	Au_{20}	2(—SR—Au—SR—Au—SR—Au—SR—) units and 4(—SR—Au—SR—) units and 2 bridging (—SR—)	Vapor–vapor diffusion of ethanol into a toluene solution of cluster	[325]

*Abbreviations used are p-mercaptobenzoic acid (p-MBA), phenylethane thiol (PET), dichloromethane (DCM), 4-tert-butylbenzenethiol (SPh-tBu), pyridine-2-thiol (SPy), triphenylphosphine (PPh_3), diphenylphosphinopyridine (PPh_2Py), 3,4-difluorothiophenol ($SPhF_2$), 4-fluorothiophenol (SPhF), 4-(trifluoromethyl)thiophenol ($SPhCF_3$), dimethylformamide (DMF), 1-cyclohexanethiol (c-C_6), 1,2-bis(diphenylphosphino)ethane (DPPE), 2-Methyl-2-propanethiol (S-t-Bu).

Part. Part. Syst. Charact. **2014**,
DOI: 10.1002/ppsc.201400033

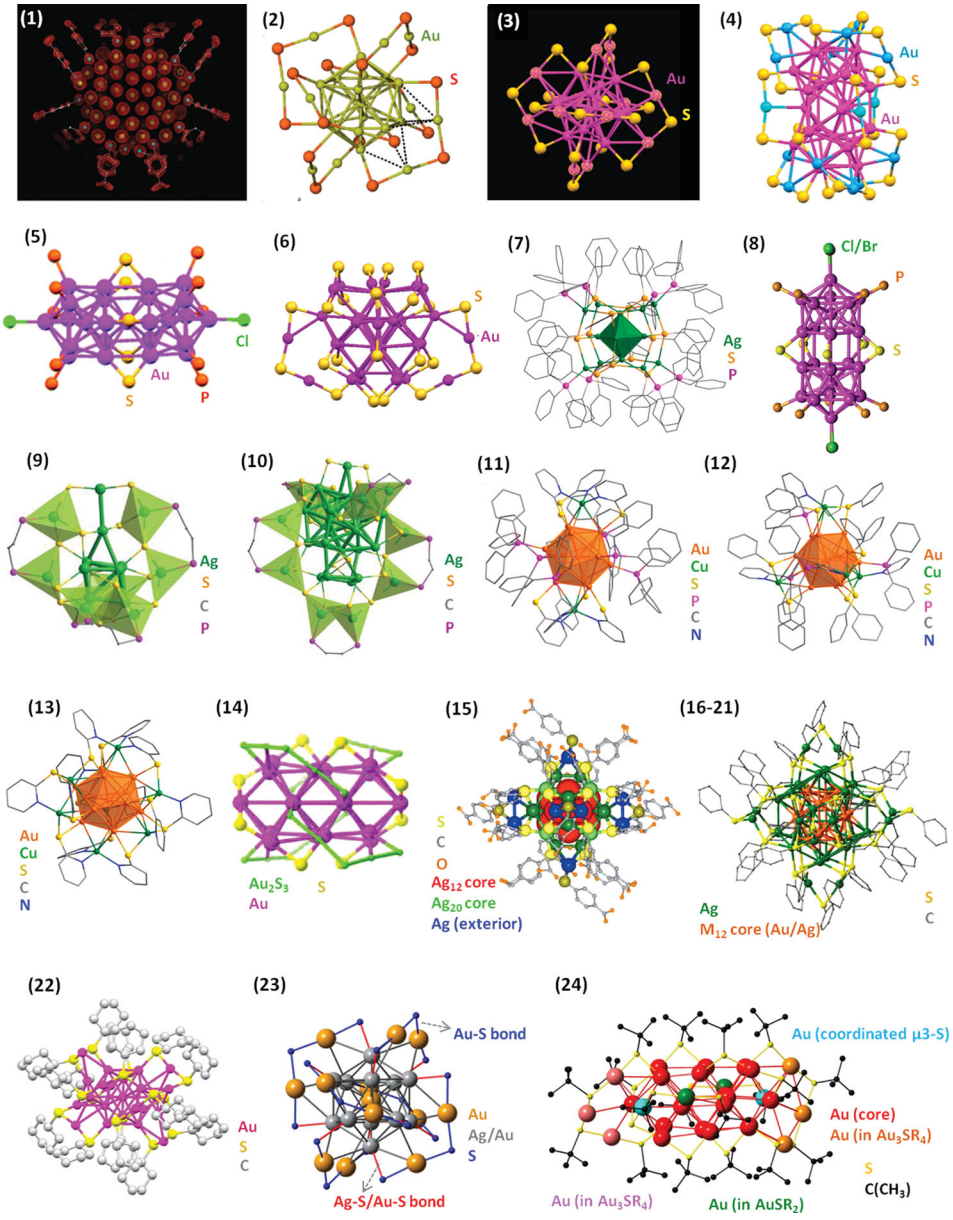

Figure 3. Crystal structures of the various noble metal clusters crystallized till date. Note that the clusters are numbered as shown in Table 2. Panel 1 reproduced with permission.[93] Copyright 2007, American Association for the Advancement of Science. Panels 2–5, 8, 11–14, 22–24 reproduced with permission.[94–96,98–100,323–326] Copyright 2010, 2011, 2012, 2013, and 2014, American Chemical Society. Panel 6 reproduced with permission.[97] Copyright 2012, Wiley-VCH. Panels 7, 9, 10 reproduced with permission.[101,102] Copyright 2012 and 2013, Royal Society of Chemistry. Panels 15–21 reproduced with permission.[103,104] Copyright 2013, Macmillan Publishers Ltd.

3.2. Absorption Spectroscopy

Appearance of distinct molecule-like absorption features is often treated as the fingerprint of QCs.[106–110] In this size regime, plasmon band, typically observed in metal NPs, is absent and unique step-like features in the absorption spectra due to molecular highest occupied orbitals and the lowest unoccupied orbitals (HOMO–LUMO) transitions emerge. This happens as a result of the conversion of the electronic band structure to discrete energy levels.[107,110,111] Density functional theory (DFT) calculations help in providing an in-depth understanding of the optoelectronic properties of the clusters.[95,112–114] Tsukuda and co-workers[83] observed distinct optical absorption and emission profiles for glutathione (GSH)-protected AuQCs [$Au_{10}SG_{10}$, $Au_{15}SG_{13}$, $Au_{18}SG_{14}$, $Au_{22}SG_{16}$, $Au_{22}SG_{17}$, $Au_{25}SG_{18}$, $Au_{29}SG_{20}$, $Au_{33}SG_{22}$, and $Au_{39}SG_{24}$], which confirm their quantized electronic states. For example, $Au_{25}SR_{18}$ (where SR = phenylethane thiol) show multiple absorption bands. Three distinct bands at 670 nm (intraband sp ← sp, LUMO ← HOMO transition), 450 nm (mixed intraband (sp ← sp), and interband (sp ← d) transitions), and 400 nm (interband (sp ← d) transition) are found and they assert the role of quantum size effects in the

QCs. The labels of the energy levels (sp, d, etc.) are due to the Au 6s and Au 6p or Au 5d levels, which make the bands. Interband and intraband transitions refer to those between states derived from the same (6s6p to 6s6p) or different (5d to 6s6p) principal quantum numbers. The observed spectrum is in good agreement with time-dependent DFT calculations of the observed crystal structure.[95] The band at ≈670 nm is associated with the electronic transitions within the Au_{13} core of the cluster, clearly demonstrating the significance of the optical absorption features in determining the cluster structure. A superatom picture has been proposed by Grönbeck and co-workers[115] to account for the stability of $[Au_{25}SR_{18}]^-$. According to them, each SR ligand localizes one 6s electron of gold. Though the nominal 8 electron shell closure in the case of $[Au_{25}SR_{18}]^-$ appears to conform to the superatom model, stability of $[Au_{25}SR_{18}]^0$ and $[Au_{25}SR_{18}]^+$ is not explained by this. In the case of $Au_{38}SR_{24}$ QCs, the prominent absorption band at 700 nm is due to the overlap of the absorption features at 675 and 770 nm.[86,116] The face-fused bi-icosahedral Au_{23} core of the Au_{38} cluster[96] is attributed to such an effect. The absorbance band edge at 1.33 eV matched with the calculated bandgap energy for the Au_{38} cluster. The optical absorption spectrum of $[Ag_{44}SR_{30}]^{4-}$ cluster[117] in solutions exhibited multiple bands and as a result they were initially described as IBANs (intensely and broadly absorbing NPs).[118] Eight distinct absorption bands were observed in their optical spectra ranging from 380 to 850 nm with extinction cross-sections as high as 2.59×10^5 L $mol^{-1}cm^{-1}$. Change of ligand from thiolate[117,118] to selenolate[57] seemed to have little or no effect in their absorption features. Recently, crystal structures of various $[(M_{12}Ag_{32})SR_{30}]^{4-}$ clusters where M stands for Au[103] and Ag[103,104] were reported using various ligands. While the absorption spectrum showed no apparent change in peak positions for clusters with different thiols for M = Ag, a distinct shift was observed in the case of alloy clusters were M = Au, clearly indicating the significance of the core metal atoms in the overall optical properties of the clusters.[103]

Recently, Häkkinen and co-workers[119] studied the changes in the localized surface plasmon resonance (LSPR) of Au clusters upon growth of their core size from 1.5 to 2 nm, using ab initio calculations and atomistic models. Using time-dependent density functional perturbation theory (TD-DFPT), the threshold size for the occurrence of LSPR in gold clusters was predicted to fall between metal cores of diameter between 1.5 and 2 nm. In 1.5 nm clusters, the protecting layer confined the plasmon-like resonance within the core and for clusters above 2 nm, the LSPR was enhanced. The origin of plasmonic features in QCs or the threshold at which plasmonic behavior emerges has been probed by various groups.[109,111,120] In 1997, Whetten and co-workers[109] studied the changes in optical absorption spectra for thiol-protected nanocrystal gold molecules with core diameters ranging from 1.4 to 3.2 nm. From their studies, a systematic broadening of the surface plasmon (SP) band was observed with decreasing core size of the crystallites, however, the SP band becomes unidentifiable and onset of step-like structure emerges in the absorption spectrum for crystallites of sizes less than 2.0 nm. Murray and co-workers[111] interpreted this loss of the SP band with decrease in core size as the onset of quantum size effects in AuQCs. Emergence of a distinct plasmonic feature at 495 nm in the optical absorption spectrum was observed from a 76.3 kDa AuQC.[120]

3.3. Photoluminescence

Photoluminescence, yet another interesting property exhibited by these clusters. It originates as a result of the breakdown of the continuous energy bands of NPs into discrete energy levels and subsequent electronic transitions between the HOMOs–LUMOs. The resulting strong emission from these materials can be used for a wide array of applications. It has been proposed that the high-energy visible fluorescence can be attributed to the radiative interband recombination between sp and d bands. Whereas the low-energy near-infrared (NIR) emission originates from the radiative intraband transitions within the sp-band across the HOMO–LUMO gap. The fluorescence property of QCs largely depends on their chemical environments such as the cluster core size, protecting ligands, solvents, etc.[9,43,121,122] Synthesis of different luminescent QCs with emission ranging from blue to red and NIR was realized by tuning the core size as well as the protecting ligand shell of the clusters.

While luminescence from metal films was noticed much earlier,[123,124] NIR photoluminescence from 1.1 and 1.7 nm Au nanocrystals at room temperature was reported by Whetten and co-workers[125] in 2000. The observed emission had a quantum yield of $(4.4 \pm 1.5) \times 10^{-5}$, five orders of magnitude greater than bulk gold, and was attributed to the intraband sp to sp-like transitions. Following the discovery of its crystal structure, $Au_{25}SR_{18}$ clusters had been studied intensely and visible and NIR emissions of these clusters (originally thought as Au_{28})[126] were correlated to their structure.[121,127,128] Though the luminescence observed was independent of the protecting ligands and was mainly ascribed as a core property,[128] use of ligands with electron-rich atoms and groups can indeed enhance the luminescence.[121] Link et al.[126] in 2002 reported the presence of two luminescence maxima (at 1.5 and 1.15 eV) for Au_{28} (later identified as Au_{25}) clusters with a total quantum yield of approximately $(3.5 \pm 1.0) \times 10^{-3}$. The steady-state luminescence studies of Au_{25} QCs show two distinct features, a strong feature in the NIR region and a weaker luminescence in the visible region. Luminescence in the NIR region has a higher quantum yield ($\approx 1 \times 10^{-3}$) compared to the latter ($\approx 10^{-6}$–10^{-7}). NIR luminescence of Au_{25} QCs was used as a probe to follow the excited state dynamics of the core Au states by Ramakrishna and co-workers.[128] Unlike larger clusters, ultrafast growth and decay kinetics were observed in the luminescence decay traces of $Au_{25}SR_{18}$ QCs. While the time constants of emergence of luminescence were independent of the passivating ligands, the luminescence decay was influenced by the same. This indicates that though luminescence arises from the Au_{25} core states and is independent of the protecting ligands, its decay happens via relaxation of the core Au states to S—Au—S—Au—S semi-ring states. A finite luminescence lifetime of 200 fs up to a few picoseconds (ps) was observed for Au_{25} QCs using femtosecond time-resolved measurements. An extremely fast (<200 fs) internal conversion process was observed within the Au_{13} core, while the core to semi-ring relaxation required

DOI: 10.1002/ppsc.201400033

1.2 ps.[129] Photoluminescence from various QCs passivated using diverse ligands has been studied in great detail.[17,39,43] Visible luminescence is mostly observed in case of water-soluble clusters with hydrophilic ligands. Among them clusters entrapped in dendrimers, proteins, DNA, polymers, biothiols, etc. are most studied as they are relatively more stable than their thiolate counterparts owing to better protection of the cluster core against destabilizing agents. Size-dependent emission, ranging from UV to IR, was observed from dendrimer-protected Au clusters of different sizes such as Au_5, Au_8, Au_{13}, Au_{23}, and Au_{31}.[130] However, change in visible emission might not always be an indication of change in core size of the cluster. In Ag_{15}@BSA clusters,[62] the emission observed from the cluster solution undergoes a sequential color change, from green to yellow to orange and finally to red, upon addition of $NaBH_4$. Further examination using matrix-assisted laser desorption ionization (MALDI) MS and photoluminescence (PL) studies revealed the existence of both green emitting Ag–BSA conjugate and red emitting Ag_{15}@BSA clusters in solution and the observed change in visible luminescence under UV lamp was attributed to increasing formation of red emitting Ag_{15}@BSA in solution compared to the former. It is important to mention that the luminescence from such clusters is now identified as fluorescence. Tang and co-workers[131] studied the fluorescence from red-emitting BSA-protected Au_{25} QCs in detail and observed the presence of dual fluorescence bands at 710 (band I) and 640 nm (band II) via temperature-dependent measurements. From their studies, band I originates exclusively from the icosahedral Au_{13} core while the [—S—Au—S—Au—S—] staples are responsible for band II. Time-resolved photoluminescence and transient absorption measurements[132] revealed that the fluorescence seen in these clusters consisted of both fast (nanoseconds) and slow (microseconds) components due to prompt fluorescence and thermally activated delayed fluorescence. The unusually efficient intersystem crossing found in these systems was attributed as a consequence of the small energy gap (30 meV) between the triplet and the singlet states.

Solvatochromism from clusters, demonstrated by Ras and co-workers[122] in silver clusters protected by poly(methacrylic acid) (PMAA), wherein emission from the clusters showed a shift upon change in polarity of the dispersing medium (water–methanol mixtures) is yet another interesting phenomenon. This was followed by several reports of Ag clusters protected by DNA,[30] polystyrene-block-PMAA block copolymer,[133] and polyethyleneimine[134] exhibiting such solvent polarity-dependent emission tunability.

The luminescence property of these clusters is widely utilized in most applications involving QCs (discussed later). Owing to their tunable emission, high quantum yields, large stokes shift, resistance to photodegradation, etc. such fluorescent Au and AgQCs are used in diverse applications.[17,39,48]

3.4. Metal-Enhanced Luminescence

Another interesting phenomenon exhibited by these clusters is metal-enhanced luminescence (MEL). MEL from Au@BSA QCs in presence of AgNPs was first demonstrated by Pradeep and co-workers[61] A fluoropohore in close proximity to a metal NP typically experiences quenching of its luminescence whereas when it is separated from the NP by a distance, it experiences an enhancement. This effect is called MEL. Approximately, ninefold enhancement in luminescence of Au@BSA QCs was observed in the presence of AgNPs. Though an exact mechanism is not known yet, here the protein shell on the QC was acting as the spacer between the luminescent cluster and the NPs. Absence of luminescence enhancement in the case of Au and Au/AgNPs could be attributed to the poor matching between the excitation wavelength of the cluster and the SP oscillations of the NPs. MEL was also observed in the case of Ag_{15}@BSA clusters when coated on bimetallic Au/Ag mesoflowers (MFs).[135] As mentioned previously, this phenomenon is still in its infancy with regard to QCs and needs to be understood in greater detail.

3.5. Chirality

Chirality is a common structural property exhibited by many natural molecules. Stable structures of bare gold QCs show interesting chiroptical properties as a function of cluster size and the way they respond to circularly polarized light. This was first reported by Whetten and co-workers,[136] when they found that 38-atom Au clusters are very sensitive for the polarization of light as evidenced by CD in the near-IR, visible, and near-UV regions.

Kornberg and co-workers[93] established the existence of chirality in Au_{102}(p-MBA)$_{44}$ cluster from their crystal structure studies. The electron density map of Au_{102}(p-MBA)$_{44}$ is shown in **Figure 4**A. The chirality in Au_{102}(p-MBA)$_{44}$ structure is apparent from a view of the cluster down the Marks decahedral (MD) axis (Figure 4B). Both the number and geometry of the equatorial atoms in the cluster core are imparting chirality to the cluster core. Sulfur atoms bonded to Au atoms in two different shells and to a phenyl ring are also found to be the chiral centers in the cluster. One enantiomer has R configuration with 22 sulfur centers while S configuration had 18. Apart from this, two sulfur centers with no readily assigned chirality were also found, as they are bonded to two gold atoms in the same shell.

In 2010, Aikens and co-workers[137] reported the structural, electronic, and optical properties of thiolate-protected $Au_{38}(SR)_{24}$ cluster by density-functional theory calculations (R=CH_3 and R=C_6H_{13}) and powder X-ray crystallography (R=$C_{12}H_{25}$). This study provided a new mechanism for the strong chiral activity of thiolate-protected gold clusters with achiral metal cores and ligands. They verified the existence of a stable cluster unit that consists of a bi-icosahedral core and a chiral arrangement of the protecting gold-thiolate $Au_x(SR)_y$ units. The low-energy structure of this cluster has been assigned to Au_{23}@$(Au(SR)_2)_3(Au_2(SR)_3)_6$, which is in excellent agreement with the theoretically predicted structure (for R=C_6H_{13}). This isomer was found to have an intrinsically chiral structure due to special arrangement of the protective $SR(AuSR)_x$ units on the surface of its Au_{23} core. The computed absorption and circular dichroism (CD) spectra of the lowest energy structure of $Au_{38}(SCH_3)_{24}$ was in agreement with the previously measured low-energy CD signal of GSH-protected $Au_{38}(SG)_{24}$. Recently, Bürgi and co-workers[89] successfully separated the enantiomers of Au_{38} cluster, covered

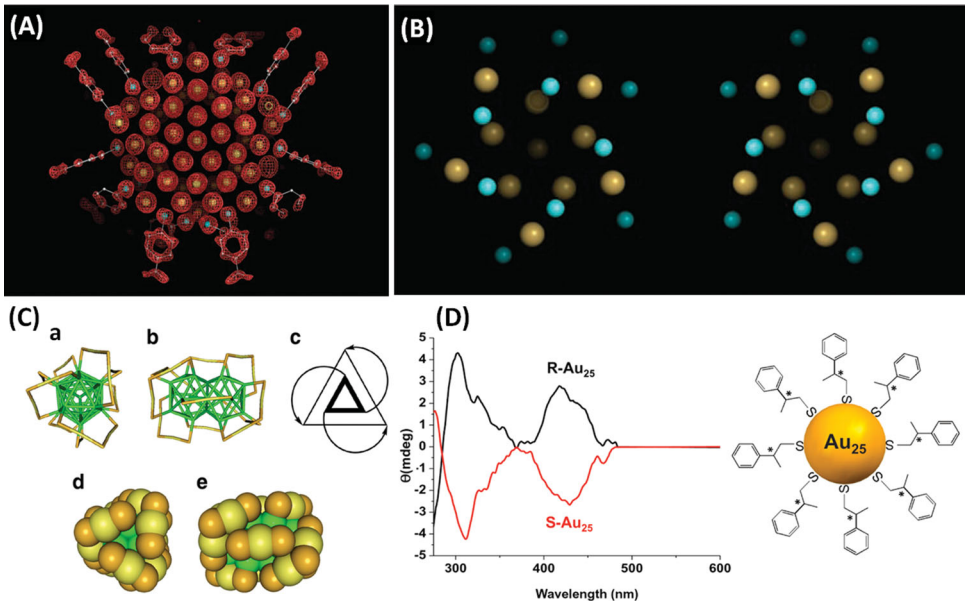

Figure 4. A) Electron density map depicting the X-ray crystal structure of the $Au_{102}(p\text{-}MBA)_{44}$ clusters. Gold, sulfur, carbon, and oxygen atoms are shown as yellow, cyan, gray, and red spheres, respectively). B) The two enantiomeric $Au_{102}(p\text{-}MBA)_{44}$ clusters, as viewed down from the cluster axis indicating chirality. Gold and sulfur atoms are depicted as yellow and cyan spheres in the image. Panels A, B reproduced with permission.[93] Copyright 2007, American Association for the Advancement of Science. C-a) Top and b) side-view of the crystal structure of the left-handed enantiomer of $Au_{38}SR_{24}$ (where SR = SCH_2CH_2Ph). Gold adatoms are shown in yellow, Au core atoms in green and sulfur atoms in orange; CH_2CH_2Ph units in the thiol were removed for clarity. c) Schematic representation of a top view of the $Au_{38}SR_{24}$ cluster along the C3 axis highlighting the handedness of the QC. The top three core atoms binding to the long staples are represented by the inner triangle while the outer triangle denotes the core Au atoms binding to the "end" of the staple. The long staples are represented by arrows and the two triangles are not in the same plane. d) Top and e) side view of the cluster in space-filling mode. Reproduced with permission.[89] Copyright 2012, Macmillan Publishers Ltd. D) CD spectra of Au_{25} nanoclusters capped by chiral thiol ligands ($SCH_2C^*H(CH_3)Ph$). Inset of figure shows a schematic of the cluster. Reproduced with permission.[140] Copyright 2011, American Chemical Society.

with achiral thiolates (2-phenylethylthiolate, denoted as PET) by HPLC. Crystal structure of the left-handed enantiomer of $Au_{38}(SCH_2CH_2Ph)_{24}$ is shown in Figure 4C. This cluster has a prolate shape with face-fused biicosahedral Au_{23} core, which is protected by three short $Au(SR)_2$ and six long $Au_2(SR)_3$ staples (Figure 4C). The staples are arranged in a chiral fashion, wherein the long staples have a staggered configuration of two triblade fans (composed of three staples), which can rotate either clockwise or anti-clockwise, depending on the enantiomer. The short staples at the equator of the cluster follow the handedness of the long staples, but are slightly tilted with respect to the threefold axis.

Among $Au_{25}(SR)_{18}$ QCs, GSH-protected Au_{25} clusters [$Au_{25}(SG)_{18}$] showed distinct CD signals whereas phenylethylthiolate-protected Au_{25} i.e. [$Au_{25}(SCH_2CH_2Ph)_{18}$] did not.[138,139] This was due to the intrinsic chiral nature of the former ligand. Whereas, $Au_{25}(PET^*)_{18}$ clusters synthesized using chirally modified phenylethylthiols [($HSCH_2C^*H(CH_3)Ph$, abbreviated as PET*] at the second position, showed mirror-imaged CD spectra.[140] The CD spectra of $Au_{25}(PET^*)_{18}$ showed intense bands at 310 and 425 nm with positive sign for the peaks of the *R*-Au_{25} isomer and negative for the *S*-Au_{25} isomer (Figure 4D). The observed CD signals are not from the R- or S-pet* ligands, as the ligand itself shows neither absorption nor CD signals in this wavelength region. On the basis of the atomic structure and electronic properties of well-defined Au_{25} nanoclusters, it was found that the chirality of $Au_{25}(SR^*)_{18}$ is not caused by the metal core but by the surface ligands and surface gold atoms of the cluster.[41,140]

3.6. Two-Photon Absorption

The noble metal QCs behave differently from NPs in terms of their emission lifetimes as well as two-photon cross-sections. In view of their biological applications, the nonlinear optical properties such as two/multi-photon-excited emissions are beneficial for low power medical imaging as two-photon excitation (TPE) in the NIR region increases the penetration depth, spatial resolution, and minimizes autofluorescence. Two photon absorption (TPA) properties of AuQCs have been extensively investigated by Goodson and co-workers[141] two-photon excited emission was first observed for Au_{25} QCs under 1290 nm excitation, showing an emission peak at 830 nm (**Figure 5**A). The pump-power dependence of fluorescence with a slope of ≈2 indicates that it is a two-photon excited emission (Figure 5B). The TPA cross-section of Au_{25} in hexane was measured to be 42 700 GM (Göppert-Mayer unit, 10–50 cm^4s), which is superior to the TPA cross-sections of many organic chromophores. Apart from the NIR luminescence for Au_{25} clusters, the additional luminescence observed in the visible region with maximum around 510 nm was later found to be two-photon allowed.[141]

In 2008, Dickson and co-workers developed three water-soluble Ag clusters, emitting at 660, 680, and 710 nm, using

Part. Part. Syst. Charact. **2014**,
DOI: 10.1002/ppsc.201400033

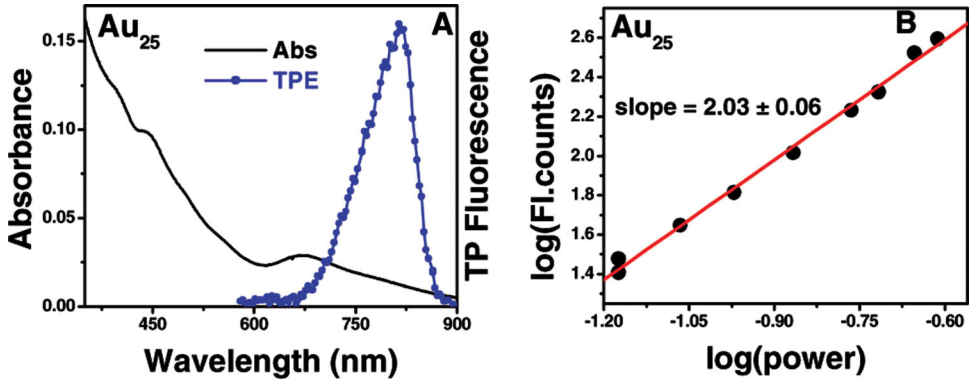

Figure 5. A) Two-photon excited fluorescence from Au_{25}. B) Pump power dependence of Au_{25} for the two-photon excited emission. Reproduced with permission.[141] Copyright 2008, American Chemical Society.

single-stranded (ss) DNA, which exhibited large two-photon cross-sections of ≈50 000 GM providing bright, photostable emission with versatile tunability of excitation and emission wavelengths.[142] Recently, two-photon excited fluorescence from a DNA-templated Ag QC, showing an emission at 630 nm when excited at 800 nm, with a two-photon absorption cross-section of ≈3000 GM was reported.[143]

3.7. Magnetism

In 2004, ferromagnetic behavior was observed in 1.4 nm[144] and 1.9 nm[145] thiol-capped gold NPs. This generated much interest as bulk Au is diamagnetic. The hysteresis loops were measured at 5 and 300 K for thiol-capped AuNPs of ≈1.4 nm diameter.[144] From the curve, the ferromagnetic behavior exhibited by the NPs is evident and high coercive field values, ranging between 250 and 860 Oe at 300 and 5 K, respectively, were observed. Magnetic moment of the gold atoms was estimated to be 0.036 μB. However, diamagnetic behavior was observed in the case of similar sized Au particles protected by a surfactant. Thus the localized magnetic moment arises due to the 5 d localized holes generated through Au—S bonds, which in turn is a result of the high spin-orbit coupling (1.5 eV) of Au and the reduction in symmetry associated with Au—Au and Au—S bonds. Miyake and co-workers[146] discussed the observance of Au ferromagnetism and studied the diameter-dependent magnetization behavior of Au particles and predicted a maximum magnetic moment per Au atom in the particles of 3 nm diameter. The ferromagnetic polarization mechanism of metallic Au is different from that of transition metals and existence of a spin-correlation effect at the nanoscale was proposed by the authors.

Paramagnetism has been reported in several noble metal QCs.[41,147,148] Jin and co-workers[148] reported the paramagnetic behavior exhibited by charge neutral Au_{25} nanoclusters, $[Au_{25}SR_{18}]^0$. The magnetic properties of these monodisperse Au_{25} QCs were evaluated with electron paramagnetic resonance (EPR) spectroscopy using microcrystal powders of these QCs, which showed an $S = 1/2$ signal with $g = 2.56$, 2.36, and 1.82. EPR quantification indicates that $[Au_{25}(SR)_{18}]^0$ has one unpaired spin per particle. Magnetism is strongly dependent on the charge state of the cluster. $(Au_{25}SR_{18})^0$ is magnetic and $(Au_{25}SR_{18})^{-1}$ is nonmagnetic and this enabled the reversible switching of magnetism in such clusters (**Figure 6**B). The reason for the observed magnetic property has been attributed to the presence of one unpaired spin per particle, delocalized in the Au_{13} core. This is contrary to the previous belief that the magnetism in gold arose from the particle surface via charge transfer in the Au—S bonds. Magnetization measurements of the clusters using superconducting quantum interference device (SQUID) magnetometer also revealed their paramagnetic nature between 5 and 300 K with no hysteresis at 5 K.

Magnetic moment measurements using X-ray magnetic circular dichroism (XMCD) of various GSH-protected AuQCs (Au_nSR_m) by Tsukuda and co-workers[147] showed an increase in magnetic moment with increase in cluster size. However, the magnetic moment observed per Au—S bond remained constant. Thus, the inherent spin polarization observed in the gold QCs was identified as a consequence of the localized hole created by Au—S bonding at the Au—S interface rather than due to a quantum size effect. XMCD data on $Au_{18}SG_{14}$ cluster revealed its paramagnetic nature with a magnetic moment of 0.0093 μB per Au—S obtained from SQUID measurements. The absence of hysteretic behavior in the magnetization curves of $Au_{18}SG_{14}$ at 2, 5, 200, and 290 K, as shown in Figure 6C, suggests the paramagnetic nature of the cluster. Induced magnetism in clusters via chemical oxidation was demonstrated recently in the case of $Au_{102}MBA_{44}$ QCs.[149]

3.8. Stability

Stability of QCs is important for their application in diverse fields. Thiolate-protected gold clusters (Au_nSR_m) of certain compositions show higher stability compared to others. Stability of QCs is governed by various electronic and geometric factors and is often explained in terms of magic numbers,[84] superatom model,[150] closing of electronic shells,[151–153] etc. Tsukuda and co-workers[84] isolated various GSH-protected magic numbered AuQCs such as $Au_{18}SG_{11}$, $Au_{21}SG_{12}$, $Au_{25\pm1}SG_{14\pm1}$, $Au_{28}SG_{16}$, $Au_{32}SG_{18}$, and $Au_{39}SG_{23}$ using PAGE and distinct optical properties were observed for each composition. Role of electronic factors in deciding the stability of clusters is also evident from

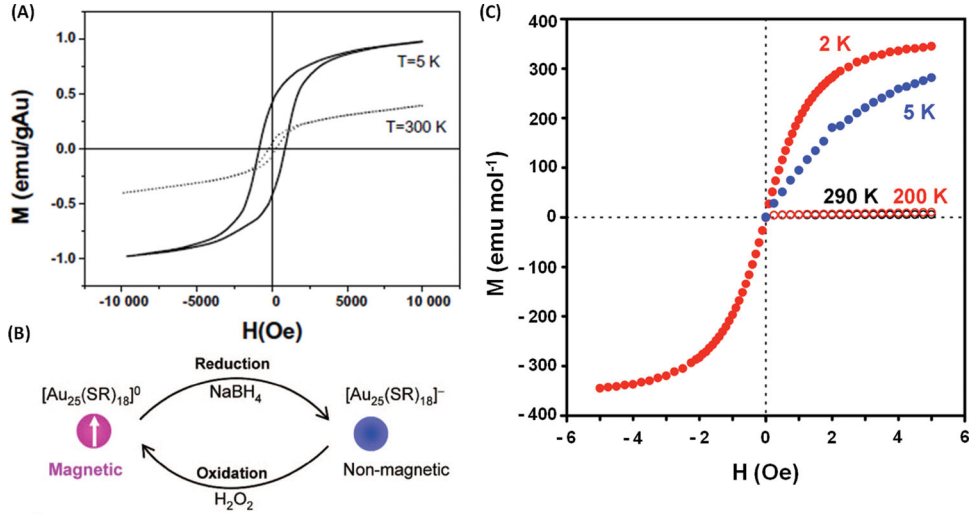

Figure 6. A) Hysteresis loops for thiolate-protected Au particles at 5 K and 300 K. Reproduced with permission.[144] Copyright 2004, American Physical Society. B) Schematic showing the magnetic reversibility of neutral and anionic Au_{25}QCs. Reproduced with permission.[148] Copyright 2009, American Chemical Society. C) Magnetization curves of $Au_{18}SG_{14}$ clusters at 2, 5, 200, and 290 K. Reproduced with permission.[147] Copyright 2006, American Chemical Society.

the isolation of charged Au clusters such as Au_{147},[151] Au_{44},[51] and Au_{25}.[152,153] The unusual stability of $Au_{25}SR_{18}$ QCs has been a subject of intense research, both experimentally and theoretically.[79,115,154,155] Passivating ligands play an important role on the electronic and thermodynamic stability of the QCs.[153,156–159] Among the water-soluble AuQCs, captopril-protected Au_{25} exhibited improved thermal stability compared to their GSH-protected analogues.[160] Another interesting report by Negishi and co-workers[161] describes the increased stability of Au_{25} QCs made with selenolate ligands compared to thiolate ligands against degradation in solution. In general, the thermal stability of AuQCs is higher than that of AgQCs.[155,162] Decomposition of GSH-protected Ag_{25} clusters above 50 °C to yield Ag_2S NPs (3 ± 1 nm),[150] crystallizing in monoclinic acanthite polymorph, via S—C bond cleavage of the cluster monolayer, illustrates this phenomenon.[162]

Core alloying of Au_{25} QCs with foreign atoms, such as Pd and Cu, affects their stability differently. While copper doping distorted the geometric structure and stability of Au_{25} QCs,[163] mono-Pd-doped Au_{25} ($Pd_1Au_{24}SR_{18}$) enhanced their stability against degradation.[164] Recently, enhanced stability of Au_{25} QCs in solution was demonstrated by supramolecular functionalization of β-cyclodextrin (CD) on 4-(*t*-butyl)benzyl mercaptan (BBSH) protected Au_{25} QC, via host–guest interactions.[157] CD molecules act as an umbrella protecting the fragile cluster core from the direct interaction with destabilizing agents such as metal ions, ligands, etc.

4. Applications

Unique properties of clusters combined with their robust nature enable them to be developed into useful materials. Energy, environment, and biology are the three main domains in which clusters have shown significant promise. Applications in each of these domains are discussed in the following sections.

Owing to their extremely small size and high reactivity, sensors made of such materials can markedly improve the sensitivity and specificity of analyte detection. For an efficient sensing strategy, the sensor material should be structurally robust and stable under ambient conditions. Combining the unique properties of QCs with other nanoscale materials can lead to creation of hybrid materials with enhanced properties of both. In spite of their highly sensitive nature, clusters are highly amenable for loading on various substrates without loss of properties enabling their use in diverse avenues. Several reports of clusters loaded on various substrates such as chitosan films,[165] silica particles,[166–168] alumina,[169] cyclodextrin gels,[170] graphene sheets,[171,172] bimetallic Au/Ag MFs,[135] crystals of polypeptide hormone (insulin),[173] boron nitride sheets,[174] SnO_2 nanowire networks,[175] etc. exist. **Figure 7** shows a few examples of clusters embedded/coated on various substrates. Such hybrid materials can serve as functional multimodal materials for diverse applications. For example, a strategy for sub-zeptomole level visual detection of TNT, an explosive molecule, was developed using a hybrid material combining materials of two different size regimes, namely, Au MFs and fluorescent AgQCs.[135] Apart from advantages of the unique morphological features of Au MFs and the optical properties of the QCs, anchoring QCs on Au MFs can lead to surface-enhancement of their luminescence and thus ultrasensitive detection (discussed later).

4.1. Applications in Environment

Recent research shows great promise of QCs in providing solutions to a number of environmentally relevant issues, which include pollution control and access to clean water. In view of

Part. Part. Syst. Charact. **2014**,
DOI: 10.1002/ppsc.201400033

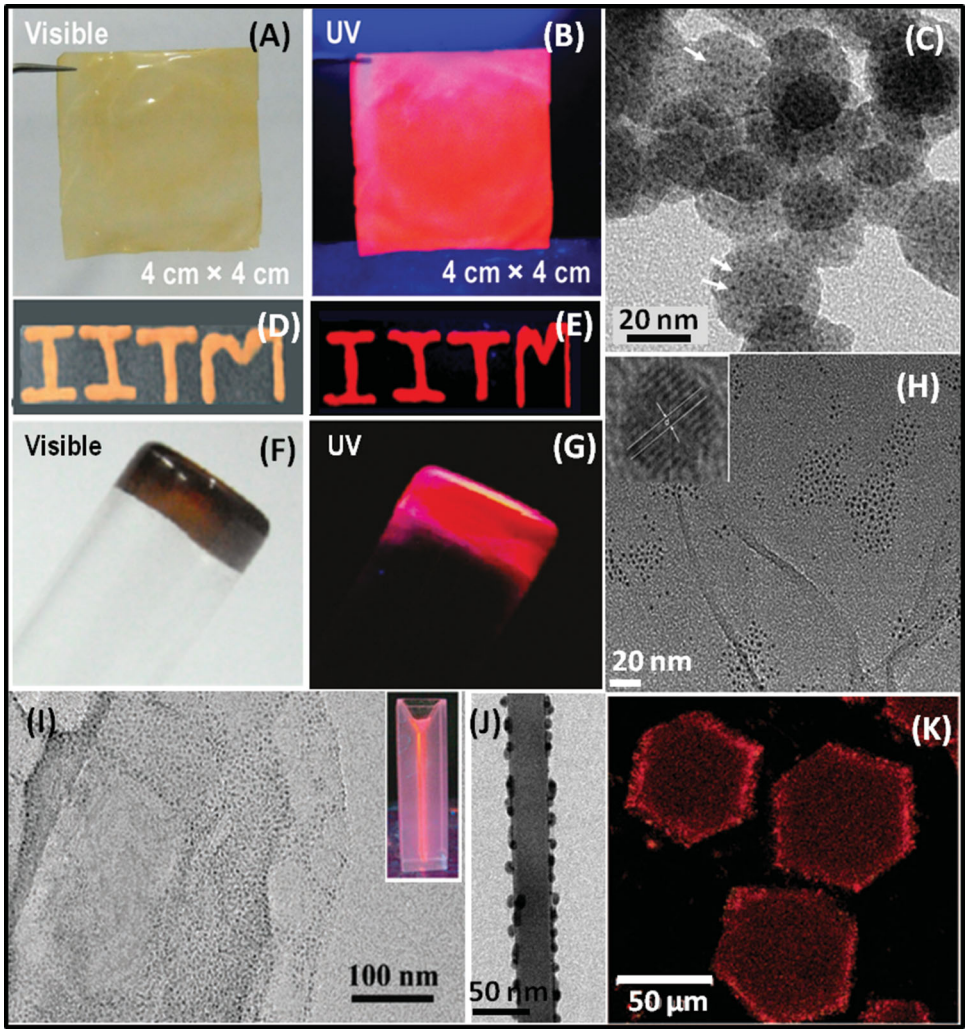

Figure 7. QCs embedded/supported on various substrates. Photographs under A,D, and F) visible light and under B,E, and G) UV light of clusters loaded on A,B) chitosan film, D,E) alumina, and F,G) cyclodextrin gels. TEM images of C) Au clusters on SiO_2 nanoparticles, H) AuQCs on graphene sheets, I) AuQCs on boron nitride sheets, and J) AgQCs on SnO_2 nanowires. K) Fluorescence microscopic image of AuQCs in insulin crystals. Panels A–C, F-G, and J reproduced with permission.[165,166,170,175] Copyright 2012 and 2011, American Chemical Society. Panels D-E, H, and K reproduced with permission.[169,171,173] Copyright 2011, Wiley-VCH. Panel I reproduced with permission.[174] Copyright 2013, Royal Society of Chemistry.

this, some noteworthy applications of QCs are described in the subsequent sections.

4.1.1. Chemical Sensing

For chemical sensing applications, optical absorption and luminescence are two most employed optical properties utilized in sensor development. Advantages such as selectivity, sensitivity, and miniaturizability in addition to properties such as strong luminescence, good colloidal stability, and ease of functionalization make QCs better optical sensors than NPs and other molecules. In the case of QCs, both the ligand and the metal core are important in sensing molecules and their well-defined structures and compositions allow detailed exploration of the underlying mechanisms. Furthermore, owing to their small size, QCs can be anchored on NPs and thus used to create hybrid materials, having properties of both constituents, which can serve as novel platforms for ultrasensitive detection of various analytes of societal interest.[135]

Heavy Metal Ion Sensing: Heavy metal contamination in drinking water is a major problem faced by the global community.[176,177] Though heavy metals such as Mn, Cu, Fe, Zn, etc. are nutritionally essential in trace quantities to the body, they have significant toxicological and carcinogenic effects beyond a certain safe limit. Apart from their non-biodegradable nature, their inherent tendency to form complexes with biomolecules leading to rupture of hydrogen bonds, changes in the conformation and structure of proteins, inhibition of enzymes, etc. pose a threat to the society. Heavy metal ions are known to have adverse effects to humans, especially to the central nervous system, kidneys, liver, skin, bones, teeth, etc.[50,178,179] Limits of permissible contamination of such species in drinking water have been recommended by WHO (World Health Organization) and EPA (Environmental Protection Agency).[180]

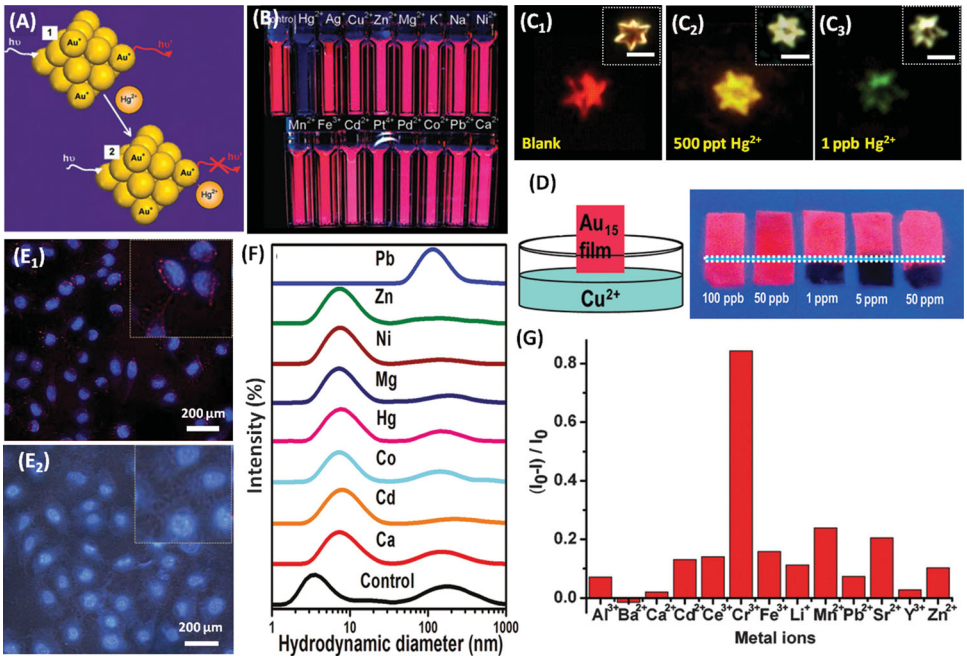

Figure 8. A) Schematic illustration of fluorescence quenching of Au clusters in presence of Hg^{2+} ions due to formation of metallophilic Hg^{2+}–Au^{+} bonds. B) Photographs showing the selective quenching of Au cluster solution with Hg^{2+} ions in presence various metal ions (at 50×10^{-6} M), under UV light. Reproduced with permission.[188] Copyright 2010, Royal Society of Chemistry. Fluorescence images (C_1–C_3) showing the gradation of color with addition of Hg^{2+} ions of different concentrations into Au@SiO_2-FITC@Ag_{15} MFs. Scale bars in the optical images of the MFs shown as inset correspond to 3 μm. Reproduced with permission.[135] Copyright 2012, Wiley-VCH. D) Illustration of Cu^{2+} ion sensing approach using an Au_{15} cluster embedded chitosan film and corresponding photographs showing the luminescence quenching of the film before and after exposing to varying concentrations of Cu^{2+} solutions. Reproduced with permission.[165] Copyright 2012, American Chemical Society. Fluorescence images of cells incubated with red emitting Au@BSA clusters before (E_1) and after (E_2) treatment with Cu^{2+} ions. Inset shows corresponding higher magnification images. Reproduced with permission.[204] Copyright 2011, Royal Society of Chemistry. F) Dynamic light scattering spectra of Cu@BSA clusters in presence of different metal ions validating the induction of protein–protein interaction and spherical aggregation of the cluster in presence of Pb^{2+} ions. Reproduced with permission.[21] Copyright 2011, American Chemical Society. G) Plot showing the effect of fluorescence quenching $[(I_0–I)/I_0]$ of the Ag clusters at 575 nm with different metal ions (20×10^{-3} M) and its high selectivity towards Cr^{3+} ions. Reproduced with permission.[200] Copyright 2011, Royal Society of Chemistry.

Tolerance limits for Pb^{2+}, Cd^{2+} and Hg^{2+} in drinking water are 0.015, 0.002, and 0.005 mg L^{-1}, respectively. Although various conventional techniques such as atomic absorption spectroscopy, inductively coupled plasma optical emission/mass spectrometry, UV–vis absorption spectroscopy, etc[181–185] provides sensitive and selective analysis of metal ions in solution; tedious sample preparation, pre-concentration steps, sophisticated instrumentation and need of skilled professionals are disadvantages aspects of such methods.

QCs of gold and silver with bright luminescence in the visible window are utilized for sensing toxic metal ions.[135,186–188] Among the heavy metal ion contaminants, mercuric ions are the most studied ones using QCs of Au, due to the strong metallophilic interaction between the d^{10} centers of Au^{+} ($5d^{10}$) and Hg^{2+} ($5d^{10}$) ions. Relativistic effects and huge dispersion forces between these closed shell atoms are responsible for this effect. Selective detection of Hg^{2+} ions has been demonstrated by many groups using luminescent clusters of gold[188–191] and silver.[66,192,193] Compared to the absorption bands, fluorescence originating from QCs are much more sensitive to changes in their immediate environment. Thus most studies on metal ion sensitivity are carried out based on changes in fluorescence as it is more sensitive to the changes in particle size. Protein-protected clusters of Au and Ag are promising candidates for metal ion sensing experiments due to their high quantum yields (6%–10%). In most cases, intrinsic luminescence from the clusters is quenched upon interaction with the Hg^{2+} ions as a result of formation of Hg^{2+}—Au^{+} or Hg^{2+}—Ag^{+} bonds with the cluster core as shown in the schematic in **Figure 8**A. Selective interaction of mercury ions with BSA-protected Au clusters was reported by Ying et al.[188] Red luminescence from the clusters was quenched instantaneously upon addition of Hg^{2+} ions in comparison to other ions (Figure 8B) and the intensity of quenching was found to be linearly dependent on the concentration of mercury ions with a detection limit of 0.5×10^{-9} M. This method was also extended to a paper test strip system using nitrocellulose membrane as a support for the clusters facilitating rapid visual detection. Several other reports on selective interaction of mercury ions with BSA-protected clusters of Au and Ag exist.[188,190,194] Mercury ions were detected visually at sub-zeptomole level from solution among other metal ions using 15 atom silver clusters[62] anchored on silica-coated gold mesoflowers (denoted as Au@SiO_2@Ag_{15} MFs).[135] Incorporation of an additional dye, fluorescein isothiocyanate (FITC) on the hybrid sensor enabled visual color change of the MFs from red to green in presence of the analyte. Figures 8(C_1-C_3) show the distinct change in fluorescence of the MFs from red to green upon exposure to increasing Hg^{2+} concentration. The

Part. Part. Syst. Charact. **2014**,
DOI: 10.1002/ppsc.201400033

intermediate yellow (Figure 8C_2) color could be due to the additive effect of the unquenched red luminescence of the cluster on the MF surface and the underlying green luminescence of FITC-incorporated silica shell.

Interaction of mercury ions with the passivating ligands on the cluster surface and subsequently quenching the cluster luminescence is yet another strategy for sensing. However, multivalent ions such as Pb^{2+} and Cd^{2+} possess similar binding affinity with carboxylic anions of the ligand. Quenching of the green luminescence of 11-mercaptoundecanoic acid (MUA)-protected Au clusters upon addition of Hg^{2+} ions reported by Chang and co-workers[195] was attributed to a similar ion-templated chelation process but the clusters were unable to differentiate Hg^{2+} ions from Pb^{2+} and Cd^{2+} ions. Thus an additional chelating ligand 2,6-pyridinedicarboxylic acid (PDCA), known to form highly stable complexes with Hg^{2+} compared to other ions, was introduced into the solution. The adsorbed PDCA ligands on the cluster surface effectively masked other ions and improved the selectivity of the cluster towards Hg^{2+} ions via a cooperative effect. A luminescent, freestanding film for the detection of Cu^{2+} ions, in aqueous solution was developed utilizing the sensitivity of Au_{15} cluster towards Cu^{2+} ions.[165] The cluster-embedded chitosan film, similar to the pH paper, showed a visual sensitivity to Cu^{2+} ions up to 1 ppm (Figure 8D). Several other reports also exist on the detection of Cu ions using Ag[196] NPs, core–shell polymer NPs[197,198] and Au[199] clusters. Zhu and co-workers[200] demonstrated a fluorescent silver cluster probe for the detection of Cr^{3+} ion with high sensitivity and selectivity, based on the fluorescence quenching of the cluster. The detection limit was found to be 28×10^{-9} M.

As yet another strategy, aggregation-induced fluorescence quenching mechanism of clusters was utilized to detect ions such as Hg^{2+}, Fe^{3+},[201] Pb^{2+},[202] Cu^{2+}[61,63,203] etc. Mercury ions can form chelation complexes with free carboxylic acid groups of the ligands such as dihydrolipoic acid (DHLA),[193] GSH, etc. resulting in interparticle aggregation and loss of cluster luminescence. Compared to the chelation tendencies of other ions, the relatively high binding affinity of mercury ions with simple carboxylic acids in water may be the reason for the greater quenching observed in presence of Hg^{2+}. Similar strategy was utilized for the detection of copper ions in live cells (Figure 8E) using BSA-protected Au clusters under various pH conditions.[204] The red emission observed from the cells incubated with Au–BSA (Figure 8E_1) was completely quenched upon exposure of Cu^{2+} ions (Figure 8E_2). Copper ions are known to chelate with GSH in 1:2 (Cu^{2+}:GSH) ratio. This principle was utilized to demonstrate a "turn-on" luminescence sensor for GSH using Au@BSA clusters.[61] Addition of GSH to a mixture containing QCs and Cu^{2+} ions led to the formation of a complex between Cu^{2+} ions and GSH resulting in the deaggregation of clusters and thereby luminescence recovery. Bovine serum albumin-protected copper clusters (Cu@BSA) were demonstrated as a potential sensor for Pb^{2+} ions in water up to ppm concentrations.[21] The quenching was associated to the complexation between BSA and Pb^{2+} ions via the carboxylate groups leading to cluster aggregation. DLS measurements of the system showed an increase in the hydrodynamic diameter (Figure 8F) of the cluster solution post-treatment with Pb^{2+} ions due to the protein–protein interaction and subsequent spherical aggregation of the cluster.

Another plausible mechanism for the luminescence quenching of clusters in presence of metal ions was the transfer of electron density from the clusters to the adsorbed cations leading to partial oxidation and subsequent amalgam formation[205] of the cluster. A simple static quenching mechanism was proposed by Wang and co-workers[192] using Ag@oligonucleotide clusters based on the resulting unchanged fluorescence lifetime and the linear Stern–Volmer plot observed upon interaction with mercury ions with the cluster. Here, formation of a nonfluorescent complex as a result of the interaction was associated with the quenching of cluster luminescence. Use of Ag_{25} clusters for the detection of Hg^{2+} ions at low concentrations (LOD – 1 ppb) has been demonstrated.[66] Both colorimetric and fluorescence detection were demonstrated and the changes in cluster features were utilized for the quantitative analysis of the ions. Detection of Cr^{3+} ions from solutions with high sensitivity was demonstrated by fluorescent Ag nanoclusters[200] in presence of other metal ions such as Al^{3+}, Ba^{2+}, Ca^{2+}, Cd^{2+}, Ce^{3+}, Fe^{3+}, Li^{+}, Mn^{2+}, Pb^{2+}, Sr^{2+}, Y^{3+}, and Zn^{2+} (Figure 8G). **Table 3** lists some of the cluster-based heavy metal ion sensors and their properties.

Anion Sensing: QC-based sensors for the detection of anions such as halides, sulfides, cyanides, nitrites, etc are also known. These anions have significant role in environmental pollution. A gold-cluster-based fluorescent sensor for the detection of cyanide ions from aqueous solutions was demonstrated by Lu et al.[206] The authors proposed a cyanide etching-induced fluorescence quenching of the gold clusters (**Figure 9**A) based on the unique Elsner reaction (given below) between cyanide and gold atoms.

$$4Au + 8CN^- + 2H_2O + O_2 \rightarrow 4Au(CN)_2^- + 4OH^-$$

The quenching effect was strongly dependent on the pH of the solution and maximized at pH 12, because under low pH conditions CN^- ions can capture available protons in solution to form hydrocyanic acid (HCN). The detection limit of 200×10^{-9}M achieved was much lower than the allowed limit of CN^- in drinking water (2.7×10^{-6} M) stipulated by WHO. Moreover, the technique was demonstrated to be effective in detecting CN^- from real water samples such as local groundwater, tap water, pond water, and lake water spiked with cyanide. A fluorescent and colorimetric platform (Figure 9B) for the sensitive and selective detection of halide ions (e.g., Cl^-, Br^-, and I^-) was developed by Luo and co-workers[207] using hyperbranched polyethyleneimine-functionalized Ag clusters based on halide-induced oxidative etching and aggregation of Ag nanoclusters. Reaction between halide ions and silver atoms and the difference in solubility constants (Ksp) of the silver compounds serve as the indicators for detection. Though oxidative etching is proposed as the dominant mechanism at lower halide concentrations, an increase in halide ions chemisorbed on the surface of the clusters could neutralize the surface charge of Ag@PEI clusters thereby giving rise to an increase in van der Waals forces among the particles leading to their aggregation at higher halide concentrations. LODs for Cl^-, Br^-, and I^- ions are 200×10^{-9}, 65×10^{-9}, and 40×10^{-9}M, respectively. Besides,

Table 3. List of various clusters exhibiting metal ion sensitivity and associated properties.

Detection technique	Analyte	Cluster/hybrid system used	Selectivity among other ions	LOD	Sample matrix	Ref.
Fluorescence quenching	Hg^{2+}	Ag@oligonucleotide	Co^{2+}, Ni^{2+}, Pb^{2+}, Zn^{2+}, Cu^{2+}, Fe^{2+}, Fe^{3+}, Mn^{2+}, and Cd^{2+}	5×10^{-9} M (1 ppb)	Aqueous media	[192]
		Au_{25}@BSA	Ag^{+}, Cu^{2+}, Zn^{2+}, Mg^{2+}, K^{+}, Na^{+}, Ni^{2+}, Mn^{2+}, Fe^{3+}, Cd^{2+}, Pt^{4+}, Pd^{2+}, Co^{2+}, Pb^{2+}, Ca^{2+}, Cl^{-}, NO_3^{-}, SO_4^{2-}, and PO_4^{3-}	0.5×10^{-9} M (0.1 ppb)	Aqueous media	[188]
		Ag@DHLA	K^{1+}, Cs^{1+}, Sr^{2+}, Ba^{2+}, Mg^{2+},Mn^{2+}, Fe^{2+},Co^{2+}, Pb^{2+},Cu^{2+}, Zn^{2+}, Sn^{2+}, and Pd^{2+}	1×10^{-9} M	Aqueous media	[193]
		Au@MUA	Li^{1+}, Na^{1+}, K^{1+}, Mg^{2+}, Ca^{2+}, Sr^{2+}, Ba^{2+} Cu^{2+}, Co^{2+}, Ni^{2+}, Zn^{2+}, Pb^{2+}, Hg^{2+}, Cd^{2+}, Fe^{2+}, Al^{3+}, Cr^{3+}, and Au^{3+}	5×10^{-9} M (1 ppb)	Aqueous media	[189]
		Au@BSA	Na^{1+}, K^{1+}, Mg^{2+}, Ca^{2+}, Ba^{2+}, Pb^{2+}, Mn^{2+}, Fe^{3+}, Ni^{3+}, Zn^{2+}, Cd^{2+}, Al^{3+}, Cr^{3+}, Cu^{2+}, Br^{-}, I^{-}, NO_3^{-}, SO_3^{-}, Ac^{-}	80 nm	Aqueous media	[327]
		Au@SiO_2@Ag_{15} MFs	Pb^{2+}, Ni^{2+}, Cd^{2+}, and Cu^{2+}	0.1 zeptomoles	Aqueous media	[135]
		Ag_{25}@GSH	Cr^{3+}, Mn^{2+}, Fe^{3+}, Co^{2+}, Ni^{2+}, Cu^{2+}, Zn^{2+}, Pd^{2+}, Cd^{2+}, Pt^{2+}, Au^{3+}	1 ppb	Aqueous media	[66]
	Hg^{2+} and CH_3Hg^{+}	Au@Lys VI	Li^{+}, Na^{+}, K^{+}, Mg^{2+}, Ca^{2+}, Sr^{2+}, Ba^{2+}, Fe^{2+}, Fe^{3+}, Co^{2+}, Ni^{2+},Cu^{2+}, Zn^{2+}, Mn^{2+}, Ag^{+}, Cd^{2+}, Pb^{2+}, Cr^{3+}, F^{-}, Cl^{-}, Br^{-}, I^{-}, ClO_4^{-}, BrO_3^{-}, IO_3^{-}, NO_3^{-}, CO_3^{2-}, HCO_3^{-}, SO_3^{-}, SO_4^{2-}, $S_2O_3^{2-}$, PO_4^{3-}, HPO_4^{2-}, $H_2PO_4^{-}$, AcO^{-}, citrate^{3-}, BO_3^{3-}	3×10^{-12} M (Hg^{2+}) and 4×10^{-9} M (CH_3Hg^{+})	Aqueous media and sea water	[191]
	Cr^{3+}	Ag@PMAA-Na	Al^{3+}, Ba^{2+}, Ca^{2+}, Cd^{2+}, Ce^{3+}, Fe^{3+}, Li^{+}, Mn^{2+}, Pb^{2+}, Sr^{2+}, Y^{3+}, and Zn^{2+}	28×10^{-9} M	Aqueous media	[200]
	As^{3+}	Au@Cys	Ba^{2+}, Co^{2+}, Mn^{2+}, Mg^{2+}, Fe^{2+}, Pb^{2+}, Zn^{2+}, Ni^{2+},Ca^{2+}, Sr^{2+}, Sb^{3+}, Bi^{3+}, Al^{3+}, Cr^{3+}, and Au^{3+}	53.7×10^{-9} M	Aqueous media	[328]
	Pb^{2+}	Cu@BSA (Cu_5 and Cu_{13} core)	Hg^{2+}, Ca^{2+}, Co^{2+}, Zn^{2+}, Ni^{2+}, Cd^{2+}, Mg^{2+}, Na^{+}, and K^{+}	>20 ppm	Aqueous media	[21]
	Cu^{2+}	Ag@PMAA	K^{+}, Na^{+}, Ag^{+}, Ca^{2+}, Ba^{2+}, Zn^{2+}, Mg^{2+}, Pb^{2+}, Co^{2+}, Ni^{2+}, Al^{3+} and Fe^{3+}, F^{-}, Cl^{-}, Br^{-}, ClO_4^{-}, BrO_3^{-}, IO_3^{-}, Ac^{-}, $C_2O_4^{-}$, NO_2^{-}, $B_4O_7^{2-}$, SO_3^{2-}, SO_4^{2-}, PO_4^{3-} and citrate^{-}	8×10^{-9} M	Reversible aqueous media	[329]
		Au@GSH	Hg^{2+}, Pb^{2+}, Cd^{2+}, Fe^{2+}, Co^{2+}, Ni^{2+}, Zn^{2+}, Mn^{2+}, Ca^{2+}, Mg^{2+}, Ba^{2+}, Al^{3+}, Fe^{3+}	3.6×10^{-9} M	Aqueous media	[203]
		Au_{15}@αCD	Fe^{3+}, Zn^{2+}, Ag^{1+}, Cd^{2+}, Hg^{2+}	$<1 \times 10^{-6}$ M Not tested	Aqueous media	[170]
		Au@NLf	Ag^{1+}, Ca^{2+}, Ni^{2+}, Co^{3+}, Fe^{3+}, and Zn^{2+}	10 ppm	Aqueous media	[63]
		Au@BSA	Ni^{2+}, Co^{2+}, Fe^{2+}, Fe^{3+}, Cd^{2+}, Pb^{2+}	50×10–6 M	Live cells	[204]
Fluorescence enhancement		Cu/Ag@DNA	Na^{+}, K^{+}, Mg^{2+}, Ca^{2+}, Zn^{2+}, Pb^{2+}, Cd^{2+}, Ni^{2+}, Cr^{2+}, and Fe^{3+}	2.7×10^{-9} M	Aqueous media	[198]
	Ag^{+}	Au_{16}@BSA	Al^{3+}, Ca^{2+}, Cd^{2+}, K^{+}, Mg^{2+}, Mn^{2+}	1×10^{-6} M	Aqueous media	[18]
	Al^{3+}	AgAu@MSA	Fe^{3+}, Fe^{2+}, Hg^{2+}, Cu^{2+}, Pb^{2+}, Mg^{2+}, Zn^{2+}, Ni^{2+}, Mn^{2+},Cr^{3+}, Cd^{2+}, Co^{2+} and Ba^{2+}	0.8×10^{-6} M	Aqueous media	[330]

*Abbreviations used are, limit of detection (LOD), bovine serum albumin (BSA), dihydrolipoic acid (DHLA), mercaptoundecanoic acid (MUA), Ag_{15} cluster- functionalized silica-coated Au mesoflower (Au@SiO_2@Ag_{15} MFs), glutathione (GSH), lysozyme type VI (Lys VI), sodium salt of polymethacrylic acid (PMAA-Na), α-cyclodextrin (α-CD), native lactoferrin (NLf), polyethyleneimine (PEI), DNA-templated bimetallic Au/Ag nanoclusters [(Au/Ag)@DNA)] and mercaptosuccinic acid (MSA).

selective detection of Br^{-} and I^{-} ions coexisting with Cl^{-} ions was demonstrated under conditions of higher ionic strength. This sensor has been successfully applied for the detection of Cl^{-} in real water samples. Sulfide ions have been detected with a LOD of 0.83×10^{-9} M from solutions utilizing the fluorescence quenching of DNA-templated gold/silver nanoclusters (Au/Ag@DNA QCs) in presence of sulfide ions.[208] Changes to the conformation of the DNA template from packed hairpin to random coil structures as a result of interaction between sulfide ions and gold/silver atoms were responsible for this effect. Addition of sodium peroxydisulfate to the mixture reduced the interference from I^{-} ions in the detection protocol. Yang and coworkers[209] constructed a molecular Boolean NAND logic gate for the detection of nitrite ion using Au@BSA clusters. Cluster luminescence, acting as the optical transducer signal, was quenched only in presence of both nitrous acid and hydrogen

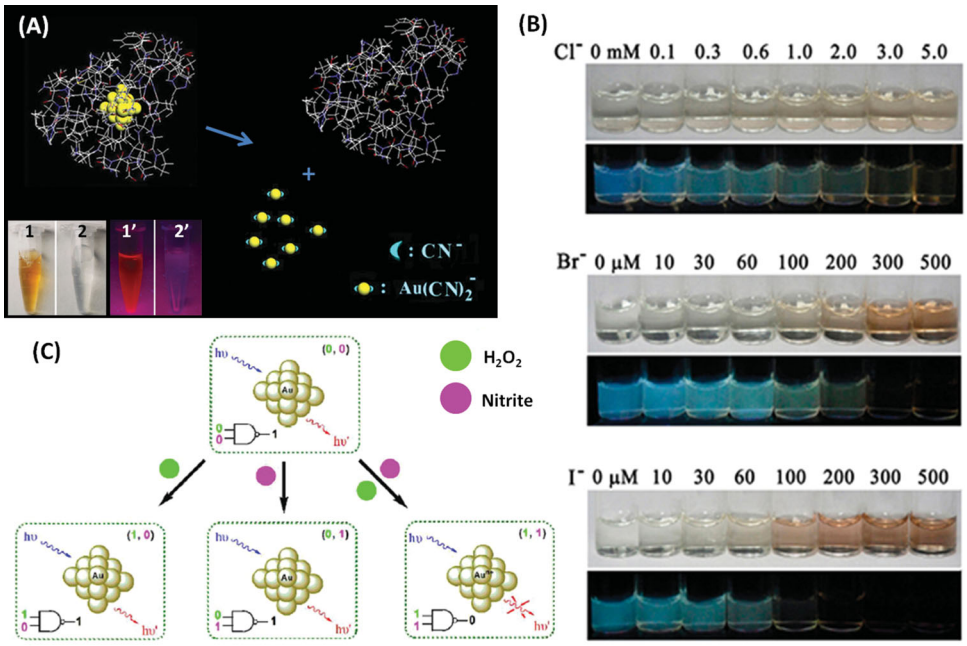

Figure 9. A) Schematic illustration of the detection of cyanide ions from aqueous solution using Au clusters. Inset shows photographs of the cluster solution 1 and 1′) before and 2 and 2′) after addition of 5×10^{-3} M cyanide ions under 1 and 2) visible and 1′ and 2′) UV light, respectively. Reproduced with permission.[206] Copyright 2010, Wiley-VCH. B) Photographs showing the colorimetric and fluorescence detection of halide ions using hyperbranched polyethyleneimine-capped Ag clusters upon addition of different concentrations of halide ions. Reproduced with permission.[208] Copyright 2012, American Chemical Society. C) Schematic representation of the binary Boolean NAND logic gate based on Au@BSA clusters with H_2O_2 and nitrite ions as inputs. Symbolic expressions for the logic gate are also shown in each case. Reproduced with permission.[209] Copyright 2013, Royal Society of Chemistry.

peroxide. This property was used as the readout to build the NAND logic gate and was used to monitor presence of nitrite ions in real samples.

TNT Sensing: Ultra trace sensors for analytes of societal interest such as 2,4,6-trinitrotoluene (TNT) is an ongoing quest due to their importance in national security and welfare of humanity. TNT is a man-made compound, which is used as an explosive material for military applications. TNT from the explosion and production sites is generally released into the environment through wastewater effluents where it can persist for many years. This nitroaromatic compound is toxic to many organisms including animals, plants, and microorganisms. A novel strategy for visual detection of TNT at sub-zeptomole level[135] was achieved using a hybrid material made by combining two systems and their variants with specific properties; one in the mesoscale regime (Au MFs)[7] having unique structural features observable under an optical microscope and another in the sub-nanometer regime (Ag_{15}@BSA)[62] having sensitivity to the analyte. **Figure 10**A shows a schematic of the sensing strategy. Change in the luminescence color in presence of an analyte being a more desirable indicator, a TNT-insensitive fluorophore, FITC was precoated on the MFs resulting in a bright green emission from the Au@SiO_2-FITC MFs (Figure 10B(1 and 1′)). After further functionalization with AgQCs, the Au@(SiO_2-FITC)@Ag_{15} MFs showed a red emission (Figure 10B(2 and 2′)) wherein the FITC emission was suppressed. Upon exposure to 10 ppb TNT, a green emission from the underlying FITC was observed (Figure 10B(4 and 4′)), as the red luminescence from the cluster had been completely quenched. Even at 100 ppt, an observable color change was evident (Figure 10B(3 and 3′)). The observation of green luminescence is in agreement with the solution-phase data, wherein the disappearance of cluster emission and the emergence of FITC emission are observed upon TNT exposure (Figure 10C). Owing to their highly anisotropic nature, MFs can act as highly sensitive probes for surface-enhanced Raman spectroscopy (SERS). Upon exposure to TNT, luminescence from the QCs on the bimetallic Ag-coated Au MFs (Au/Ag MFs) is lost and the Raman features from TNT (at 1209, 1361, 1535, 1619, and 2960 cm^{-1}) are detectable on the particle, as shown in Figure 10D. This method stands unique compared to other nanomaterials-based detection approaches as it involves the combination of multiple detection techniques such as SERS and luminescence to detect TNT at ultratrace levels and avoid false alarms. This approach can be used in terms of a single-particle, single-molecule detection technique, which is probably the ultimate in ultra-trace sensitivity with selectivity.

Halocarbon Sensing: Among the various contaminants present in the environment, halocarbons such as chlorofluorocarbons (CFC), C_2Cl_4, C_2ClF_3, CCl_4, etc. in water and air pose a threat to humanity owing to their potential for ozone depletion and global warming. In spite of regulations on their use, many of them find applications as industrial solvents, lubricants, plasticizers, and refrigerants due to lack of suitable replacements or financial constraints. Complete degradation of chlorocarbons such as CCl_4, $CHCl_3$, and $C_6H_5CH_2Cl$ at room temperature using mercaptosuccinic acid (MSA) protected Ag clusters, Ag_9MSA_7, was demonstrated by Pradeep and co-workers[210]

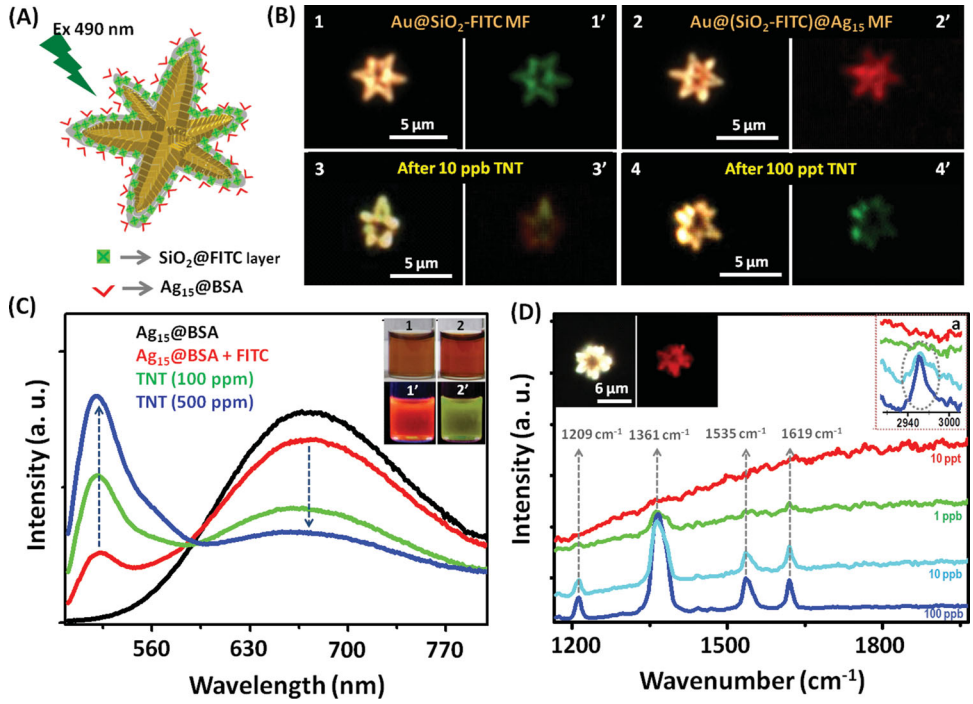

Figure 10. A) Schematic of the TNT sensor. B) Optical (1, 2) and fluorescence (1′, 2′) images of green emitting Au@SiO_2-FITC MFs before (1, 1′) and the red emitting Au@(SiO_2-FITC)@Ag_{15} MFs (2, 2′) after cluster functionalization. Optical (3, 4) and fluorescence (3′, 4′) images of the later upon exposure to 100 ppt (3, 3′) and 10 ppb (4, 4′) TNT, respectively. C) Effect of emission spectra of the bare cluster upon mixing with FITC dye and subsequent exposure to TNT of varying concentrations. The photographs of solution containing a mixture of FITC dye and Ag_{15} cluster before and after TNT addition, taken under visible (1 and 2) and UV light (1′ and 2′), respectively, are shown in the inset. D) Raman spectra showing the gradual evolution of TNT features from the Au/Ag@Ag_{15} MFs with addition of increasing concentration of TNT. Optical and fluorescence images of Au/Ag@Ag_{15} MFs are given in the inset. Gradual appearance of Raman feature at 2960 cm^{-1} is shown in the inset. Reproduced with permission.[135] Copyright 2012, Wiley-VCH.

From their studies, Ag clusters showed increased efficiency towards such halocarbon degradation compared to their NP analogues. Importance of isopropyl alcohol (IPA) for the reaction was highlighted as it can improve the solubility of halocarbons in water. The authors propose that Cl^- ions formed due to the cleavage of Cl_3C—Cl can replace the thiolates on the surface of the cluster leading to loss of its stability and formation of AgCl.

4.1.2. Catalysis

The field of gold catalysis has seen many advances over the past years. Extensive studies are carried out to fabricate novel catalysts with enhanced selectivity, activity, and stability. The excellent catalytic activity exhibited by gold in the NP regime is distinctly different from bulk. Gold was considered to be one of the least catalytically active metals until 1987 when gold NPs deposited on semiconducting transition-metal oxides showed surprising activity in carbon monoxide oxidation even at a temperature of –77 °C.[211] The remarkable catalytic ability demonstrated by the metal was ascribed to its size. The greater number of low coordination surface atoms present on particles of smaller size is considered to facilitate the chemisorption of reactant molecules on the surface of the metal leading to their high catalytic activity. Aptly pointed out by Bond and Thompson in their review, "The long neglect of gold as a catalyst is chiefly due to the failure to appreciate the necessity of creating particles that are sufficiently small and, for oxidations, of selecting a helpful support."[212] Subsequently, catalysts made of nanogold received enormous attention.[211,213–219] Studies of the onset of catalytic activity in gold clusters of various sizes, prepared on single crystalline titania surfaces showed that the activity of such QCs originates only when their diameters are less than 3.5 nm.[35] This threshold was associated to the metal-to-nonmetal transition observed upon the decrease of cluster size below ≈300 atoms per cluster.

Atomically precise clusters of gold, such as Au_{25}, Au_{38}, Au_{102}, Au_{144}, etc. have stimulated much interest in this area due to their unique structure–property relationships and known crystal structures. Recently, gold clusters stabilized by thiolate, phosphine, halides, and polymers as ligands have also been employed as catalysts for various reactions.[32,44,45] Apart from advantages due to monodisperse nature and large number of highly active surface sites for catalysis, correlation of their complete structure and catalytic properties stimulated much interest as it provided insights into their size-dependent catalytic properties. Catalytic activities of NPs are strongly dependent on their particle size. The broad size distribution of the NPs employed in such reactions hinders precise measurements of size-dependent catalytic performance, which is crucial for improving catalytic performance. Atomically precise QCs on the other hand, having solved X-ray crystal structures are advantageous in this context. For example, among

the three AuQCs (Au_{25} (diameter 1.0 nm), Au_{38} (diameter 1.3 nm), and Au_{144} (diameter 1.6 nm)) utilized for the selective oxidation of styrene, catalytic performance was found in the order, $Au_{25} > Au_{38} > Au_{144}$ indicating a strong size-dependence in catalytic performance.[220] Several reports exist on the catalytic activities of clusters for reactions such as oxidation of styrene,[219–222] carbon monoxide,[223–226] alcohol,[34,227–229] and cyclohexane,[230] hydrogenation of aldehydes and ketones,[33,231] reduction of nitrophenol,[232] and electrochemical reduction of O_2.[23,233–236]

Both supported and unsupported clusters have shown enormous potential for catalytic activities. Clusters immobilized on various supports such as, graphene, SiO_2,[222,225,237] titania,[238,239] iron oxide,[31] ceria,[240] etc. are important in the fabrication of heterogeneous catalysts. Gas-phase clusters deposited on various substrates are also excellent catalysts for various reactions. Carbon monoxide oxidation by Au_8 clusters deposited on MgO surfaces showed catalytic activity even at a temperature of 150 K.[241] Hutchings and co-workers[31] demonstrated similar CO oxidation activity using $Au_{\sim 10}$ clusters immobilized on iron-oxide supports. Similarly, sub-1 nm gold particles on ceria substrates were found to be highly active in methanol-steam-reforming and water-gas-shift reactions, compared to particles larger than 3 nm in size.[242,243] Ambient pressure X-ray photoelectron spectroscopy was used to study such reactions using various clusters of Au, Pt, Pd, and Cu clusters embedded in mesoporous ceria.[240] The oxidation of CO using mass-selected Pd_{13} clusters on thin MgO films was modeled using microkinetic simulation of the reaction by Heiz and co-workers.[244] The model allowed predictions of mole fractions, turn-over frequency, reaction probability, and sticking coefficients of the clusters in addition to providing an understanding of the substrate effects during catalysis. Effect of substrate on the cluster-ripening mechanisms was also studied by depositing monodisperse Pd clusters on three different model catalysts namely, (1) bare Rh(1 1 1), (2) superstructures of Moiré-patterned graphene grown on Rh(1 1 1) and Ru(0 0 0 1), and (3) hexagonal boron-nitride film that was grown on Rh(1 1 1).[245] Mechanism of CO oxidation catalyzed by AuQCs on a thin defect-free MgO film supported on a Mo(100) surface was predicted by Landman and co-workers[246] to occur via a Langmuir–Hinshelwood or an Eley–Rideal mechanism on 2D gold cluster islands. The excess electronic charge at the gold cluster/magnesia interface as a result of the penetration of metal states through the MgO thin film was considered to be the impetus for the observed catalytic activity. The dependence of the thickness of the substrate on the catalytic reaction was also studied using mass-selected Au_{20} clusters via first-principles DFT calculations.[247]

Zeng et al.[248] conducted ab initio studies of the catalytic properties of 12 different clusters in the size range of Au_{16}–Au_{35} towards CO oxidation reaction and proposed a quantitative assessment of the site-size–activity relationship. From their studies, anionic clusters showed stronger adsorbtion of CO and O_2 in comparison to their neutral counterparts. **Figure 11**A shows the computed reaction pathways of various anionic Au clusters towards CO oxidation. While both activation energy and size of the clusters were important parameters in deciding the strength of CO adsorption, the effective indicator to access

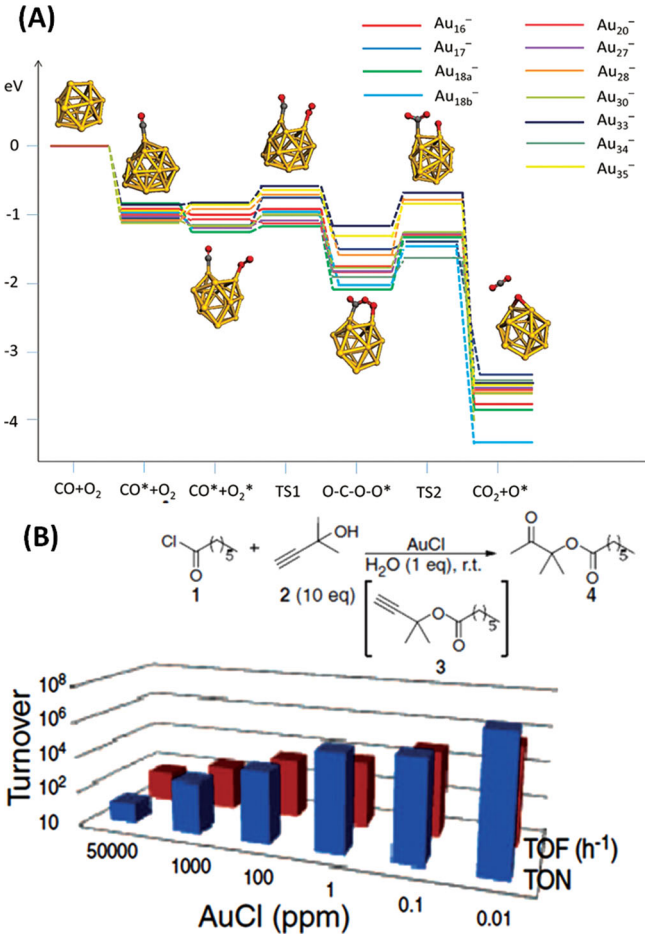

Figure 11. A) Computed pathways for the reaction, $CO + O_2 \rightarrow CO_2 + O$, catalyzed by various anionic gold clusters from Au_{16} to Au_{35}. The species adsorbed on the cluster is denoted by a star (*). Reproduced with permission.[248] Copyright 2011, American Chemical Society. B) Plot showing the extremely high turnover number (TON) and turnover frequency (TOF) for different amounts of AuCl in the ester-assisted hydration reaction (shown in the inset) of in situ-formed alkynes using small gold clusters (Au_3 to Au_{10}) as catalysts at room temperature. Reproduced with permission.[37] Copyright 2012, American Association for the Advancement of Science.

catalytic activities of the clusters was dependent on the CO and O_2 adsorption energies on them. Role of anionic clusters of gold Au_n^- (n = 1–7) on O_2 activation was probed by Wang et al.[249] using photoelectron spectroscopy.

Supported Au_{55} clusters were used as efficient catalysts for the selective oxidation of styrene by dioxygen.[219] The catalytic activity was associated with the altered electronic structure of the Au_{55} clusters. Further, the authors demonstrated that a sharp size threshold existed for the catalytic activity and particles with size (diameter) above 2 nm were completely inactive. Yet another promising report in this context was the huge turnover number of 10^7 atoms reported for the ester-assisted hydration reaction of alkynes using small gold clusters (Au_3 to Au_{10}) as catalysts at room temperature at parts per billion concentrations.[37] Turnover number (TON) of a catalyst denotes its catalytic activity, it is the number of substrate molecules that can be converted to products by one catalyst site/species before its

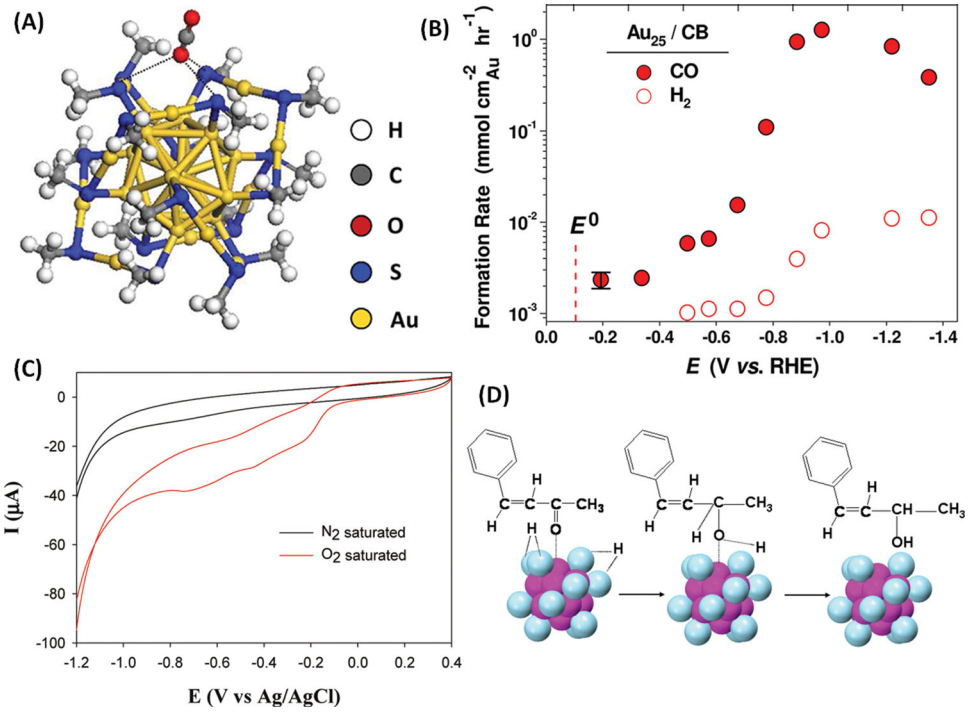

Figure 12. A) Density functional theory model of the stable Au_{25}–CO_2 couple denoting the interaction of oxygen atom (shown in red) with three sulfur atoms (blue) of the Au_{25} shell during the reduction of CO_2. B) Potential-dependent rate of formation of H_2 and CO for carbon black (CB) supported Au_{25} (denoted as Au_{25}/CB in figure) during electrolysis. Panels A,B reproduced with permission.[250] Copyright 2012, American Chemical Society. C) Cyclic voltammograms of Cu clusters deposited on glassy carbon electrode (0.1 M KOH) saturated with N_2 (black curve) or O_2 (red curve) under a potential scan rate of 0.1 V s^{-1}. Reproduced with permission.[23] Copyright 2011, American Chemical Society. D) Schematic illustration of the proposed mechanism of $Au_{25}SR_{18}$ catalyzed, chemoselective hydrogenation of α,β-unsaturated ketone to unsaturated alcohol. Au atoms of the core are shown in magenta and that of the shell are shown in cyan. Thiolate ligands are not shown for clarity. Reproduced with permission.[33] Copyright 2010, Wiley-VCH.

deactivation. The time component depicting the speed at which the catalyst operates is given by the turnover frequency (TOF), which is the number of substrate molecules converted per unit time. Plot showing the extremely high TON and TOF for different amounts of AuCl in the ester-assisted hydration reaction using small gold clusters (Au_3 to Au_{10}) as catalysts are shown in Figure 11B.

Reduction of CO_2, an important greenhouse gas, was studied both experimentally and theoretically using negatively charged atomically precise Au_{25} clusters by Jin and co-workers.[250] They investigated the effect of catalytic properties upon interaction between $Au_{25}(C_2H_4Ph)_{18}$ and CO_2.[250] A spontaneous and reversible electronic interaction similar to that seen during Au_{25} oxidation was observed spectroscopically and electrochemically. Atomic-scale determination of the favorable binding sites and adsorption structures were realized with the help of DFT calculations. DFT model of the Au_{25}–CO_2 couple (as shown in **Figure 12**A) shows the interaction of oxygen atom (shown in red) with three sulfur atoms (blue) of the Au_{25} shell during the reaction. Reversible perturbation of the electronic structure and CO_2 induced charge redistribution within Au_{25} cluster as a result of molecular physisorption on the cluster was associated to the change in its properties. The potential-dependent formation rate of the reaction products of CO and H_2, shown in Figure 12B, provided an insight into the mechanism of reduction and a two electron, two proton pathway through adsorbed CO_2•- intermediate was proposed.

In another report, sub-nanometer-sized Cu_n clusters (where $n \leq 8$ showed high electrocatalytic activity towards oxygen reduction).[23] Cyclic voltammograms of the Cu clusters deposited on glassy carbon electrode in 0.1 M KOH saturated independently with N_2 (black trace) and O_2 (red trace) are shown in Figure 12C. The onset potential of O_2 reduction of –0.07 V was comparable to commercial Pt catalysts. The catalytic capability of $Au_{25}SR_{18}$ clusters towards selective hydrogenation capability of the C=O bond in α,β-unsaturated ketones and aldehydes at low temperature (0 °C) with 100% chemoselectivity showed the efficiency of the clusters in catalytic reactions.[33] The unique structure of Au_{25} cluster with an electron-rich Au_{13} core and low-coordinated ($N = 3$) surface gold atoms are responsible for the observed high catalytic activity. Figure 12D shows the proposed mechanism.

In short, QCs have immense potential for developing novel catalysts for highly specific and selective reactions. A summary of the catalytic properties of thiolate-protected Au clusters can be found in elsewhere.[32,44,45,251] Experimental results and theoretical calculations can offer excellent inputs into understanding the high catalytic activities evidenced in this class of materials. Moreover, correlation of the crystal structures of the QCs with their catalytic properties will lead to an in-depth understanding of catalytic mechanisms, active centers involved, etc. and thus allow the design and development of new "nano" catalysts for specific reactions with improved selectivity. **Table 4** illustrates more examples of clusters acting as catalysts in various reactions.

Part. Part. Syst. Charact. **2014**,
DOI: 10.1002/ppsc.201400033

Table 4. Various clusters exhibiting catalytic activity.

Cluster	Size (diameter)	Support	Type of reaction	Conditions	Ref.
Au	1–6 nm	TiO_2	Carbon monoxide oxidation	Ultrahigh vacuum	[35]
Au_8	–	MgO		Soft landing conditions, 150 K	[241]
Pd_{13}		MgO		Soft landing conditions, 478 K	[244]
$Au_{\sim 10}$	0.5 nm	FeOOH		25 °C, air, pretreatment of catalyst at 120 °C	[31]
$Au_{25}(SCH_2CH_2Ph)_{18}$	–	TiO_2, CeO_2, and Fe_2O_3		60–80 °C, water vapor, O_2 pretreatment at 150 °C	[223]
$Au_{38}(SCH_2CH_2Ph)_{24}$	–	CeO_2		60–80 °C, water vapor, O_2 pretreatment at 175 °C	[224]
$Au_{144}(SC_2H_4Ph)_{60}$	–	$CuO–mSiO_2$		calcination at 300 °C in air prior to reaction	[225]
$Au_{25}SR_{18}$	–	HAP	Styrene oxidation	Toluene, TBHP	[221]
$Au_{25}SR_{18}$, $Au_{38}SR_{24}$, and $Au_{144}SR_{60}$	–	–		Toluene, O_2 atmosphere, 100 °C	[220]
$Pt_1Au_{24}SC_2H_4Ph_{18}$	–	TiO_2		Acetonitrile, N_2, 70 °C $PhI(OAc)_2$	[331]
$Au_{55}(PPh_3)_{12}Cl_6$	≈1.4 nm	SiO_2		Toluene, 100 °C, O_2 atmosphere	[222]
Au_{11}@TPP	0.8 ± 0.3 nm	$mSiO_2$	Alcohol oxidation	Water, 80 °C, H_2O_2	[237]
Au@PVP	≈1 nm	–		Water, air, 27 °C	[34,227,228]
Au@ poly(EOEOVE)	<4 nm	–			[332]
$Pd_1Au_{24}(SC_{12}H_{25})_{18}$	–	CNT		Water, 30 °C, 1 atm	[229]
AuAg@PVP	1.3–2.2 nm	–		Water, air, 25 °C	[333]
$Au_{25}(SCH_2CH_2Ph)_{18}$	–	CeO_2	Homocoupling of aryl iodides	DMF, 130 °C, K_3PO_4	[334]
$Au_{25}SR_{18}$	–	TiO_2	Photocatalytic degradation of methyl orange	water, hν, air	[335]
Au_nSG_m, (n, m) = (10, 10), (18, 14), (25, 18), and (39, 24)	<2 nm	HAP	Cyclohexane oxidation	150 °C, TBHP	[230]
Cu@(PAMAM-OH)	–	–	Hydrogenation of carbonyl and olefin groups	Water, 25–10 °C	[336]
$Au_{25}(SCH_2CH_2Ph)_{18}$	–	TiO_2, Fe_2O_3, and CeO_2	Oxidation of sulfide to sulfoxide	DCM, 40 °C, N_2 atmosphere	[337]
$Au_{25}SR_{18}$, $Au_{38}SR_{24}$, and $Au_{144}SR_{60}$	–	–	Hydrogenation of aldehydes and ketones	Toluene:acetonitrile (1:1), H_2 atmosphere, 60 °C	[220]
$Au_{25}SR_{18}$	–	–		Toluene:ethanol, 0 °C, H_2 atmosphere	[33]
$Au_{25}(SCH_2CH_2Ph)_{18}$	–	–		Ethanol:toluene (10:2), RT, H_2 atmosphere	[231]
$Ag_{7,8}(H_2MSA)_{7,8}$	–	SiO_2, TiO_2, Fe_2O_3, and Al_2O_3	Reduction of nitrophenol	Water, 35 °C, air	[338]

*Abbreviations: tert-butyl hydroperoxide (TBHP), polyvinylpyrrolidone (PVP), 2-(2-ethoxy)ethoxyethyl vinyl ether (EOEOVE), poly(amidoamine) dendrimer with hydroxyl surface groups (PAMAM–OH), carbon nanotubes (CNT), hydroxyapatite (HAP), triphenylphosphine (TPP), iodobenzene diacetate ($PhI(OAc)_2$), room temperature (RT), mesoporous silica ($mSiO_2$), mercaptosuccinic acid (H_2MSA).

4.1.3. Surface-Enhanced Raman Scattering Substrates

Noble metal NPs of diverse shapes and sizes have been employed as SERS-active substrates[7,252,253] for enhancing the Raman signals of many different molecules.[254–256] The most commonly used substrates include colloidal silver and gold particles between 10 and 50 nm in size and their films. Recently, Pradeep and co-workers[257] described the use of thiolate-protected Ag_{152} cluster as an efficient SERS substrate using several dyes and biomolecules. An enhancement factor of 1.58×10^9 was obtained in the case of crystal violet molecules using the QC substrate. The unusually high SERS enhancement observed was attributed to the formation of Ag_{152} crystallites in solution, which could act as hot spots for Raman enhancement. Absence of visible luminescence from the cluster and its plasmonic nature may also be the reasons for its better SERS

activity compared to other smaller QCs and larger NPs. Use of atomically precise QCs as efficient SERS-active substrates thus opens up hitherto unprecedented possibilities of such QCs to a number of analytes in various areas.

4.2. Applications in Energy

Recent research focuses on developing new materials for clean and affordable energy along with means to reduce energy consumption and lessen toxicity on the environment. Noble metal nanoclusters have shown their capability for H_2 production and solar cells applications. Research in organic and inorganic photovoltaic materials has seen considerable growth worldwide due to the increasing need to make materials with lower cost and higher power conversion efficiencies. Though hybrid systems consisting of multiple components can be an efficient solution, increased complexity of the device structure can hinder commercial applications. Studies on the efficiency of QCs in solar cell applications were pursued owing to the improved efficiency achieved using metallic NPs-incorporated polymer solar cells.[258–261] Zhu and co-workers[262] demonstrated the use of Au nanocluster decorated multi-layer graphene as transparent anode in polymeric solar cells. Apart from the better power conversion efficiencies and enhanced fill factor of these electrodes compared to other modified multi-layer graphene devices, they showed improved interfacial contact, which substantially decreased the series resistance of the nanocluster-embedded polymer solar cells.

Recently, thiolate-protected AuQCs were used to develop high-efficiency solar cells by incorporating them in mesoscopic TiO_2 films.[263] A stable photocurrent of 3.96 mA cm^{-2} with a relatively high power conversion efficiency of 2.3% was demonstrated under AM 1.5 illumination. The higher photovoltage observed was attributed to the effective electron injection as a result of the greater HOMO–LUMO gap of QCs and their stronger interaction with TiO_2. The overall absorption features and cell performance of the QC-sensitized solar cells, with an open-circuit voltage of 832 mV and fill factor of 0.7, were comparable to that of their quantum dot analogues emphasizing their potential as viable candidates for the next generation of solar cells.

Hydrogen's potential role as a way to store renewable energy has been hampered due to challenges in production and storage. Despite the potential to reduce environmental pollution, use of this fuel is severely hampered due to challenges in its production and storage. Generation of hydrogen through methanolysis of ammonia-borane (AB) using poly(*N*-vinyl-2-pyrrolidone) (PVP)-stabilized palladium(0) nanoclusters at room temperature was demonstrated by Özkar and co-workers[27] The clusters showed high stability and turnover number of 23 000 in 27 h at room temperature. Kinetic studies on the catalytic methanolysis of AB triggered by PVP-stabilized Pd clusters showed a first-order reaction with activation energy of 35 ± 2 kJ mol^{-1}. Castellano and co-workers[264] demonstrated the use of Pt clusters in hydrogen production. The clusters supported on a titania surface was used to photocatalyze the reduction of protons to hydrogen. The net catalytic ability for the heterogeneous hydrogen production, was however, dependent on various factors including the surface coverage of the metal precursor, $Pt(dcbpy)Cl_2$ (dcbpy = 4,40-dicarboxylic acid-2,20-bipyridine).

Another interesting report was the impressive electrocatalytic performance of a hybrid system comprising Au clusters on reduced graphene oxide (rGO) towards oxygen reduction reaction (ORR).[240] The Au/rRO hybrid system showed superior methanol tolerance, enhanced electrocatalytic stability, and comparable onset potential to commercially available Pt/C catalyst. This work is promising in view of developing low cost and high- performance alternatives for Pt catalysts in fuel cells.

High oxygen reduction activity of Pt clusters embedded on genomic DNA/graphene oxide nanocomposites was demonstrated by Kim and co-workers[26] The strong interaction between the Pt clusters and the DNA/graphene oxide nanocomposite can cause modulation in the electronic structure of the cluster leading to its high performance in electrocatalysis of ORR. Such hybrid materials can be utilized for applications in high-performance fuel cells and batteries.

Use of hydrogen as a means of storing energy produced from other sources can help in solving our ever-increasing energy demand owing to its abundance and non-contaminating nature. Use of noble metal clusters in this area is still in its infancy. Combining such catalytically active materials with atomic tunability in various aspects of this science can possibly yield new and better candidates for clean energy applications.

4.3. Applications in Biology

Medicinal benefits of noble metals, especially gold, date back to several thousands of years.[265,266] Optical properties of metal NPs (Au/Ag) such as absorption, scattering, and their surface-enhancing characteristics offered promising results in medical diagnosis and treatment. But their huge size limits their applications in biological matter to a large extent. The lower QYs of plasmonic NPs indeed hinder their applications in terms of bioimaging and labeling applications. The ultrasmall size (<2 nm), enhanced photoluminescence and better QYs exhibited by QCs in comparison to metal NPs prove them to be better candidates in biological applications. Moreover, the smaller sizes of the QCs lead to lower cytotoxicity and thus efficient renal clearance unlike NPs. In vivo applications of noble metal NPs are still severely hampered mainly by their slow renal clearance and high nonspecific accumulation in the organs of the reticuloendothelial system (RES), such as liver and spleen. Owing to their small size, these materials can be used to target-specific areas inside cells hitherto inaccessible to larger sized NPs. While good photostability, lower toxicity, and smaller size make QCs advantageous in bioapplications over semiconductor quantum dots; large Stokes shift, ease of functionalization, and better stability against photobleaching are the added advantages of QCs in comparison with traditional fluorescent dyes. In addition, tendency of aggregation and multivalency is concerns for quantum dots that hinder their use in both in vitro and in vivo applications. The QYs of protein-protected QCs are much higher than that of thiolate-capped clusters. For example, red emitting Au@BSA clusters have a QY of 6%,[70,267] Au@Lyz clusters[268] exhibit a QY of 5.6% and Ag_{15}@BSA clusters[62] show a QY as high as 10.7%. Though QYs of QCs are much

Part. Part. Syst. Charact. 2014,
DOI: 10.1002/ppsc.201400033

lower than fluorescent dyes, capabilities of QCs such as luminescence tunability (based on core size), surface modification without compromising luminescence, better sensitivity (luminescence quenching/enhancement, etc.) to external events in the cells, etc. make them ideal candidates for bioimaging, therapy, and drug delivery applications. QCs functionalized with drug molecules can serve multiple purposes; 1) they can be used as efficient drug carriers due to their small size, which allows easy cell penetration, 2) luminescence from the QC can be used to simultaneously track the payload and thus ensure their delivery in targeted areas, and 3) release of drugs in cell organelles and subsequent changes can be monitored using changes in luminescence of the QC. Thus, fluorescent metal QCs having better biocompatibility, high quantum yields, excellent photostability, and NIR luminescence are better candidates for multiple applications in molecular biotechnology and biomedical engineering. Towards this aim, synthesis of various clusters of Au and Ag protected by biocompatible ligands such as proteins, DNA, biothiols, etc. has been well explored.[47]

4.3.1. Biomolecular Sensing

Sensing biomolecules and reactive oxygen species (ROS) is important in biomedical diagnosis as it can provide vital information on the stages of many diseases including cancer. Florescent noble metal clusters have also been utilized for detection of biomolecules such as biothiols (cysteine, GSH etc.), small molecules, aminoacids, proteins, DNA, nucleic acids, etc. In addition, they have also used for sensing ROS such as H_2O_2.

Fluorescent gold clusters protected by the enzyme horseradish peroxidase (HRP) were used to detect the presence of hydrogen peroxide in solutions.[269] Addition of H_2O_2 quenched the cluster luminescence quantitatively, as shown in **Figure 13**A, indicating that HRP enzyme remains active even after cluster formation and possesses its intrinsic catalytic capability. A change in the structure/conformation of HRP in presence of H_2O_2 that can further change the microenvironment of the clusters was attributed as the reason for the loss of fluorescence. A linear quenching was observed over the range of 100×10^{-9} M to 100×10^{-6} M with a detection limit of 30×10^{-9} M. ROS plays a very important role in cellular metabolism. Reactivity of Au@HRP clusters towards other ROS such as O_2^-, *t*-butyl hydroperoxide (TBPH), OCl^-, and $^{\bullet}OH$ also showed a quenching of cluster luminescence. The quenching mechanism was attributed to the oxidation of the Au-S bond between Au core and the HRP scaffolds by the catalytic effect of HRP enzyme resulting in fewer HRP molecules protecting the cluster and therefore leading to aggregation of clusters. Fluorescent probes for other important molecules such as glutaraldehyde,[270] methotrexate (antimetabolite drug),[271] etc have also been reported.

Biothiols such as cysteine (Cys) and GSH commonly seen in biological systems have numerous functions in cellular metabolism and redox reactions.[272] Deficiency of Cys can lead to various medical ailments such as edema, depigmentation of hair, liver damage, etc. Thus, a facile analysis of Cys level in our body is important for early diagnosis and treatment. Xie and co-workers[273] demonstrated a simple method of detection of Cys using GSH-protected Ag clusters combining the thiol-silver chemistry and steric hinderence of the ligand shell protecting the cluster surface. Ag@GSH clusters showed a superior selectivity for Cys compared to the other 19 non-thiol containing-natural aminoacids (Figure 13B) due to the specific thiol–Ag interaction. Further differentiation based on size of thiol molecules compared to the GSH ligand on the cluster provided additional sensitivity for Cys and a detection limit of $<3 \times 10^{-9}$ M was achieved. A dual optical signal change for detection of Cys, both fluorometrically and colorimetrically, avoids false positives. The change is attributed to the decomposition of the cluster to smaller species. Ag cluster-based sensors for biothiols[274–276] involving luminescence quenching of the cluster as a result of thiol-adsorption-accelerated oxidation are also

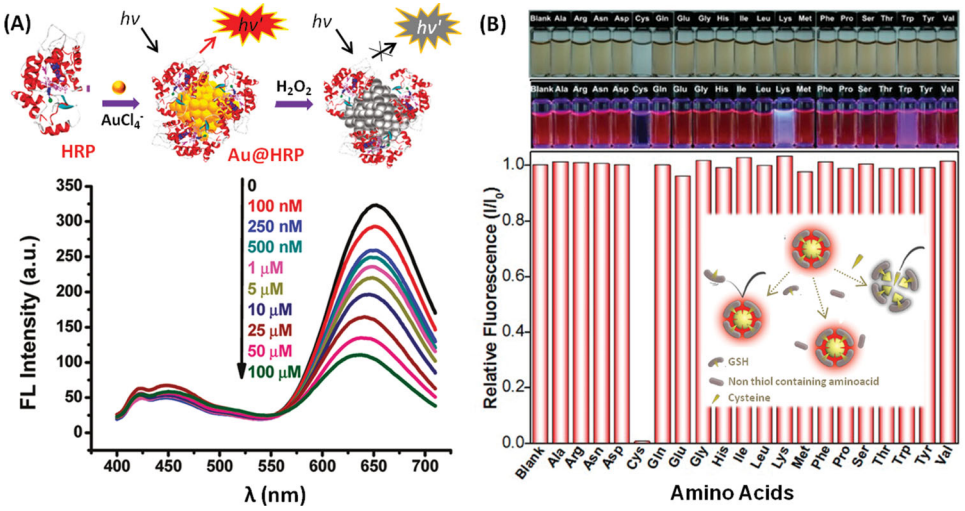

Figure 13. A) Change in emission spectra of Au@HRP clusters with increasing addition of H_2O_2. Inset of (A) shows the schematic of the formation of Au@HRP clusters and its quenching with H_2O_2. Reproduced with permission.[269] Copyright 2011, American Chemical Society. B) Photographs of the Ag@GSH cluster solution in presence of different aminoacids, under visible (top panel) and UV (bottom panel) light. Relative fluorescence intensities of the corresponding solutions are shown. Schematic of the sensing mechanism is also shown. Reproduced with permission.[273] Copyright 2012, American Chemical Society.

Table 5. Various sensors used for biopolymer detection along with their properties.

Analyte	Detection technique (Fluorescence)	Cluster/material used	Analyte/Antigen	Antibody/additional conditions used	LOD	Sample matrix	Ref.
Proteins	Turn off	Au@PAMAM	hIgG	Goat-derived polyclonal anti-human IgG	mM to nM levels	Aqueous solution	[277]
	Turn on	Au@MUA and Au NPs	PDGF AA	Thiol-derivatized aptamer (Apt) molecules	0.5×10^{-9} M	Cell media, urine etc	[278]
	Turn on		α-Thrombin	$Apt_{thrombin}$	0.15×10^{-9} M		
	Turn off	Au@S-Man	Con A	α-mannopyranosyl residues	75×10^{-12} M	Aqueous solution	[279]
		Ag@DNA	DNA, ATP	Formation of G-Quadruplex/ Hemin complex			
	Turn on	Au@Man	Tg	Con A	48×10^{-12} M	Serum	[282]
	Turn on	Au@S-Man	Tg	Con A, BSA (50×10^{-6} M)	90×10^{-12} M	Solution	[283]
	Turn on	Au@Man + Au NPs@anti-*Tg*	Tg	Con A	$65 (\pm 16) \times 10^{-9}$ M	Complex serum samples	[282]
	Naked eye	Au@SG	GST-tagged proteins	–	750×10^{-9} M	Complex cell lysate samples	[281]
	Turn on	Au@PA	hIgG	–	10×10^{-9} M	Solution	[280]
	Turn on		Protein G	–	85×10^{-9} M	Plasma samples	
	Turn off	Ag@DNA-Apt	Thrombin	Aptamers APT15 and APT29	1×10^{-9} M	Solution	[285]
Oligonucleotides	Turn off	Ag@DNA	miRNA	–	0.5×10^{-6} M	Whole plant endogenous RNA	[339]
	Turn on	Ag@DNA	HBB-SCA	–	–	–	[314]
	Turn on	Ag@DNA	Human *Braf* oncogene	guanine-rich DNA sequences	10×10^{-9} M	Various DNA targets	[340]
	Turn on	$Ag_{\sim 10}$@DNA	DNA	–	$<1 \times 10^{-6}$ M	Blood and serum samples	[341]

*Abbreviations used are, poly(amido) amine (PAMAM), platelet-derived growth factor AA (PDGF AA), 11-mercaptoundecanoic acid (MUA), 27-nt DNA aptamer (Apt-thrombin), concanavalin A (Con A), mannose-conjugated Au NCs (Au@Man), adenosine triphosphate (ATP), glutathione S-transferase (GST), human immunoglobulin G (hIgG), protein A (PA), thyroglobulin (Tg), anti-Tg antibody conjugated Au NPs (Au NPs@anti-Tg), single-stranded DNA binding protein (SSB), DNA aptamer-templated AgNC (Ag@DNA-Apt), microRNA (miRNA), Homo sapiens hemoglobin beta chain (HBB) gene responsible for sickle-cell anemia mutation (HBB-SCA).

known. A "turn-on" assay for biothiols utilizing specific nature of the DNA template protecting the Ag clusters was reported by Qu and co-workers recently.[276] Apart from achieving a detection limit of 6.2×10^{-9} M, this study opens up the possibility of fabricating specific DNA templates for the selective detection of specific analytes by virtue of the template-dependent fluorescence properties of the cluster.

Detection of biopolymers such as proteins and DNA is yet another interesting application of these nanoclusters. Sensors employed for such applications typically use antibody or aptamer-functionalized clusters to selectively conjugate with the analyte. Leblanc and co-workers[277] developed an immunoassay for the detection of nanomolar concentrations of human IgG in aqueous solutions using PAMAM dendrimer encapsulated luminescent gold clusters. The immunofluorescent assay was based on the electrostatic conjugation of an antibody (polyclonal, goat-derived anti-human IgG antibody) to the human IgG antigen. Thus appropriate selection of the analyte specific antibody is pivotal in designing the sensor. Competitive fluorescence quenching demonstrated by Chang and co-workers[278] for analyzing proteins is yet another sensing strategy. A fluorescence "turn-on" strategy was proposed for platelet-derived growth factors (PDGFs) and their receptors using bioconjugated 13 nm Au NPs and luminescent Au clusters. Clusters have also been used for the sensitive detection of many other proteins such as concanavalin A,[279] immunoglobulin G,[280] GSH S-transferase-fusion proteins,[281] thyroglobulin,[282,283] single-stranded DNA binding protein,[284] thrombin,[285] etc. **Table 5** summarizes the literature on detection of various proteins and oligonucleotides using QCs.

Dual-detection strategies such as colorimetry and fluorescence were used to quantitatively determine the presence of Human IgG using an optical immunosensor employing fluorescent Au cluster as the signal transducing agent.[286] A schematic of the portable biosensor consisting of biomolecules immobilized on an ITO chip using poly(dopamine) film is shown in **Figure 14**A. A sensitivity of 5 pg mL^{-1} was achieved via this technique suggesting the potential of the sensor for clinical analysis. Fluorescent protein sensors based on the silver cluster aptamers, having strong binding affinities to specific proteins, were used for the detection of thrombin.[285] Figure 14B shows the effect of fluorescence emission spectra of the Ag cluster in presence of specific (thrombin) and nonspecific proteins (streptavidin, PDGF, and BSA).

Adenosine triphosphate (ATP), often described as the "molecular unit of currency" for intracellular energy transfer

Part. Part. Syst. Charact. **2014**,
DOI: 10.1002/ppsc.201400033

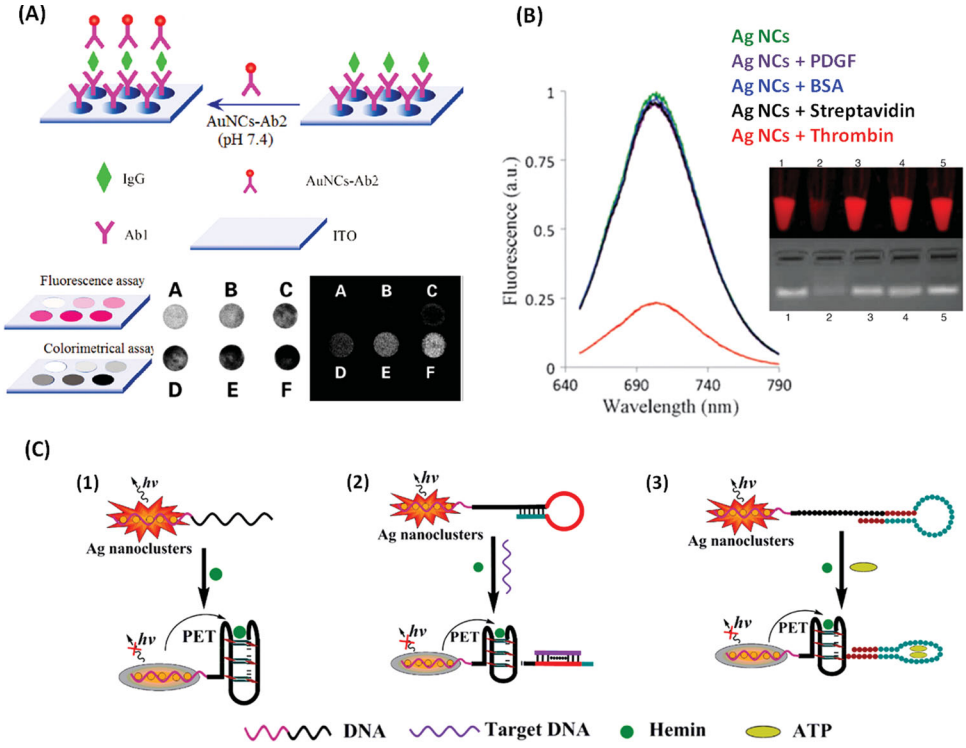

Figure 14. A) Schematic design of the optical immunosensor used for detection of biomolecules employing Au cluster as labels. Reproduced with permission.[286] Copyright 2011, American Chemical Society. B) Change in the fluorescence emission spectra of Ag clusters in presence of specific (thrombin) and nonspecific proteins (BSA, PDGF, and streptavidin). Inset shows the fluorescence (top panel) and gel shift analysis (bottom panel) of 1) aptamer–Ag clustersand its interaction with 2) thrombin protein, 3) streptavidin, 4) PDGF, and 5) BSA. Reproduced with permission.[285] Copyright 2011, Royal Society of Chemistry. C) Schematic illustration of the photoinduced electron transfer between Ag@DNA clusters and the 1) G-Quadruplex/Hemin Complex and that of analysis of 2) target DNA, and 3) ATP using the conjugates. Reproduced with permission.[258] Copyright 2013, American Chemical Society.

is an important constituent of the various metabolic processes taking place inside cells. A simple route using DNA-protected Ag clusters as fluorescent molecular beacons for selective detection of ATP was reported by Ye and co-workers[287] Guanine-rich DNA sequence on Ag nanoclusters was also used as the signal transducer to monitor the activity of the enzyme, adenosine deaminase in solutions.

Recently, selective detection of DNA and ATP molecules was demonstrated by Zhang et al.[258] based on the photoinduced electron transfer processes between luminescent DNA-protected Ag clusters and G-quadruplex/hemin complexes. Figure 14C shows the schematic of the sensing strategy employed. A parallel G-quadruplex blocked by a duplex is released upon specific combination of the target (DNA/ATP) allowing it to form a stable G-quadruplex/hemin complex. This triggers the electron transfer from the Ag@DNA clusters to the hemin Fe(III) center resulting in a decrease in the fluorescence intensity of the Ag@DNA QCs, thereby facilitating detection. Electrocatalytic activity of oligonucleotide-encapsulated Ag clusters utilized for the detection of microRNA (miRNA) was described by Zhang and co-workers[288] The efficient catalytic property of the cluster towards H_2O_2 reduction was used to design the electrochemical miRNA biosensor probe.

Recently, luminescent DNA-stabilized Ag nanoclusters were described to act as fluorescent labels for various biocatalytic transformations[289] such as oxidation of glucose, tyrosine, dopamine, or tyramine. Fluorescence quenching of Ag clusters by H_2O_2 and quinones enabled the detection of H_2O_2-generating oxidases and tyrosinase during biocatalytic processes. Moreover, use of Ag clusters as optical labels for bienzyme biocatalytic cascades was demonstrated using two such systems namely, 1) alkaline phosphatase/tyrosinase coupled hydrolysis and oxidation of o-phospho-l-tyrosine and 2) acetylcholine esterase/choline oxidase hydrolysis of acetylcholine and subsequent oxidation of choline. Ultrasensitve detection of alkaline phosphatase and o-phospho-l-tyrosine was also reported using this protocol.

4.3.2. Detection of Single-Nucleotide Polymorphism

Precise identification of genetic variations, such as single-nucleotide polymorphisms (SNPs), is critical as a slight alteration of a single base can cause diseases. In view of this, a new inexpensive method based on fluorescent silver QCs is reported for quick identification of base switches in a gene. It has been reported that certain nonemissive DNA-templated silver QCs can light up into distinct colors through interactions with different enhancer DNA sequences.[69] On the basis of this finding, Werner and co-workers[290] have designed a QC-based molecular probe, which fluoresce upon binding-specific DNA targets.

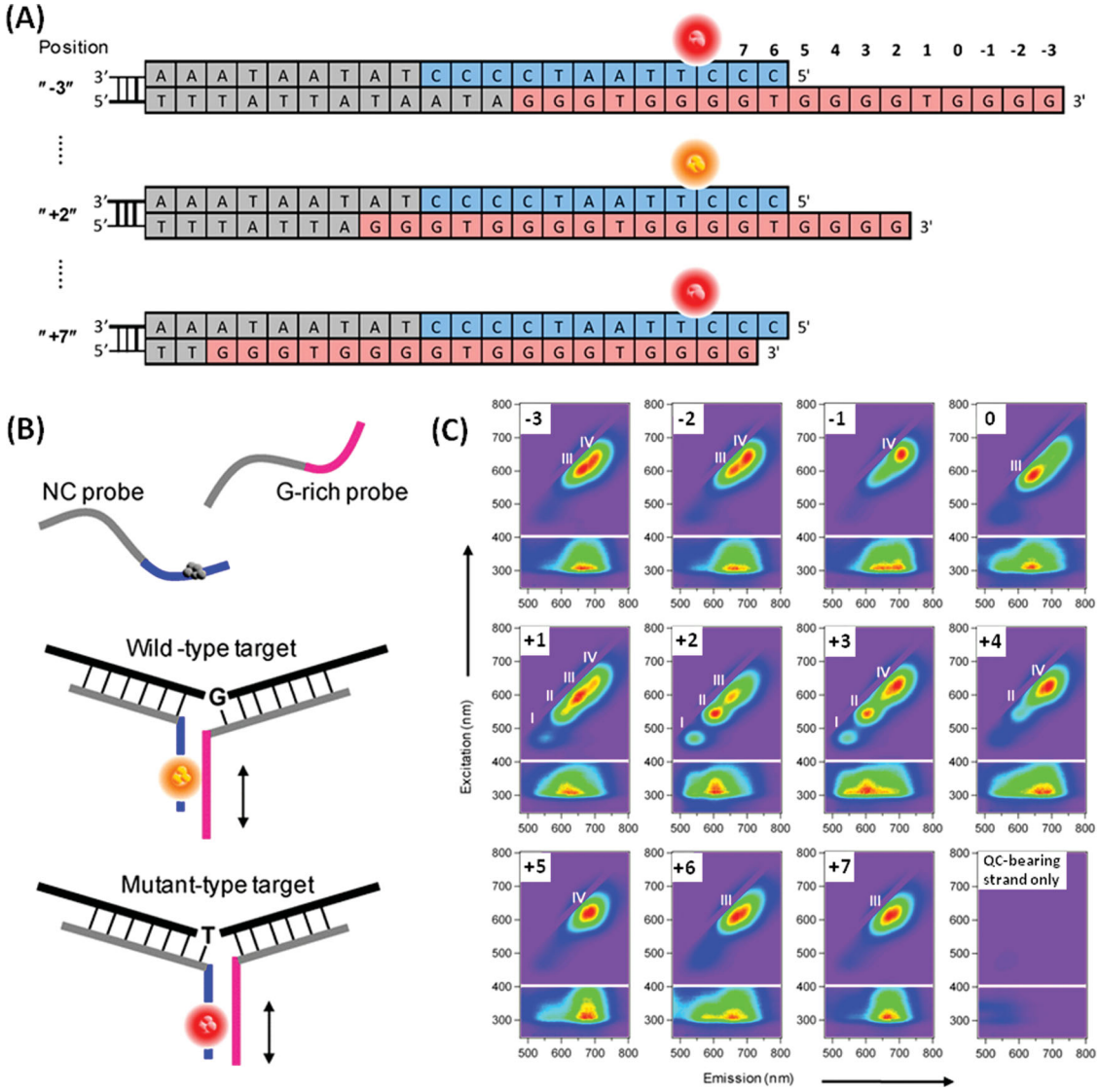

Figure 15. A) Schematic shows three relative positions (–3, +2, and +7) between the enhancer sequence (red fill) and the NC-nucleation sequence (blue fill). A cartoon of a Ag NC is shown for positions –3, +2, and +7, which results in a red light-up color for positions –3 and +7 and a yellow/orange color for position +2. B) DNA-templated Ag NC consist of a NC probe and a guanine (G)-rich probe lights up into different colors upon binding SNP targets. Probes remain dark in the absence of targets. Upon binding the wild-type target, the Ag NCs probe lights up into one color (orange) and upon binding the mutant type of target, the Ag NCs lights up into another color (red). The difference between wild-type and mutant-type targets is a single-nucleotide substitution. C) 2D Fluorescence contour plots of the 11 hybridized samples and a control sample having only the NC-bearing strand, with the corresponding position number shown on the upper left corner of each plot. Reproduced with permission.[290] Copyright 2012, American Chemical Society.

Different relative positions between the enhancer and the NC nucleation sequences were produced by hybridizing a common NC-bearing strand with 11 different guanine-rich (G-rich) strands (**Figure 15**A). The fluorescence emission of the AgQCs substantially changed (a shift of 60–70 nm in the emission maximum) depending upon the alignment between the AgQCs and the DNA enhancer sequence. A schematic representation of this phenomenon is given in Figure 15B. This new property has been exploited for the sensitive detection and identification of a number of disease-related SNPs. The hybridized samples generated multiple spectral peaks when excited in the visible to NIR region (450–800 nm), which was probed by the 2D fluorescence contour plots (Figure 15C). This method has been validated in three synthetic DNA targets with SNP and in two clinical samples taken from patients with ovarian cancer. In these samples, SNP can be easily identified by the naked eye under UV excitation, making this method reliable and cost effective.

In another study, Wang and co-workers[22] have successfully demonstrated the capability of an intelligent CuQC probe in distinguishing match and mismatch sequences with 15-mer probe DNA in solution. The high sensitivity of Cu nanoclusters to base types located in the major groove of DNA leading to associated modifications in their fluorescent property made these QCs fluorimetric indicators of the DNA hybridization event. This method allows the detection of not only a single mismatch but also its mismatch type in a specific DNA sequence.

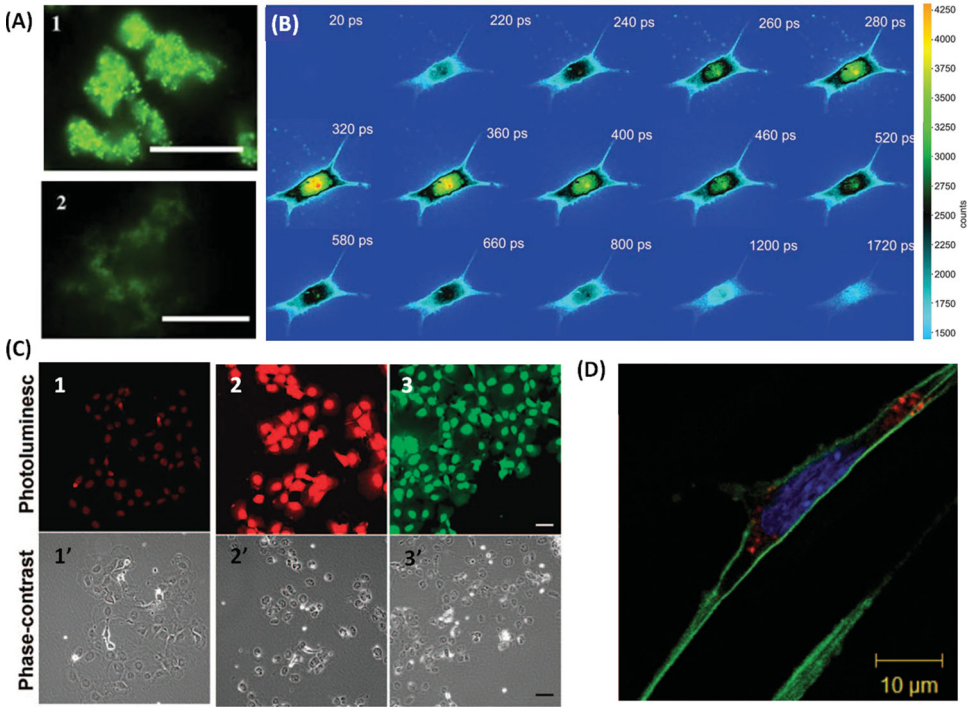

Figure 16. A) Epifluorescence microscopic images of amyloid fibrils stained with Ag clusters in combination with thioflavin T after an exposure time of 1) 0.02 s and 2) 1.6 s, respectively. The scale bars correspond to 10 μm. Reproduced with permission.[292] Copyright 2005, Elsevier. B) Time-gated luminescence microscopic images of NIH3T3 cells stained with silver nitrate showing the fast cluster emission at short times. Intensity scales for the images are also shown. Reproduced with permission.[293] Copyright 2007, Wiley-VCH. C) Endogeneous labeling of biotin within human hepatoma cells (HepG2) using Au clusters is demonstrated by the 1–3) fluorescence and 1′–3′) phase-contrast images from cells exposed to 1 and 1′) unconjugated Au clusters, 2 and 2′) streptavidin-conjugated Au clusters, and 3 and 3′) streptavidin-conjugated FITC. Scale bars in the images correspond to indicate 50 μm. Reproduced with permission.[295] Copyright 2009, American Chemical Society. D) Fluorescence image showing the internalization of Au@insulin clusters (red) inside C2C12 myoblast cells after exposure to the clusters for 2 h. Green and blue colors are from the dyes used to stain the cell boundary and cell nucleus, respectively, for ease of visual identification. Reproduced with permission.[173] Copyright 2011, Wiley-VCH.

4.3.3. Bioimaging and Biolabeling

The unique photophysical properties of noble metal QCs give rise to a myriad of applications in imaging techniques ranging from cellular staining to imaging specific proteins inside live cells. Size, biocompatibility, fluorescence quantum yield, and stability against photobleaching are essential components for any fluorescence based optical probe.

While limited photostability and small Stokes shift are problems crippling the use of conventional organic dyes as fluorescent reporters; bigger size and toxicity of semiconductor quantum dots hinder their use as biomarkers. Luminescent properties of fluorescent metal clusters make them excellent biological labels especially in the NIR region. Interference from the short-wavelength (400–600 nm) emission in biological media and scattering light can be avoided by use of such NIR probes wherein biological tissues are optically transparent. Smaller size, low cytotoxicity, high biocompatibility, high quantum yields, better emission rates, large Stokes shift, excellent photostability, and NIR luminescence make them better candidates than organic dyes and quantum dots for biomedical applications.[291]

Baskakov and co-workers[292] in 2005 demonstrated the use of Ag clusters in bioimaging for the first time in combination with a fluorophore, thioflavin T. The modified clusters were used to stain amyloid fibrils. The clusters showed bright green fluorescence in aqueous solution without any detectable photobleaching and could easily be detected using a fluorescence microscope (**Figure 16**A). Later Dickson and co-workers used intracellularly synthesized Ag clusters using argyrophilic proteins and imaged living cells using cluster emission.[293] The short fluorescence lifetimes [220 ps (33%) and 1760 ps (67%)] of the clusters allowed them to be monitored efficiently using time-gated luminescence microscopy (Figure 16B). Conjugation with biologically active molecules that can retain activity post-treatment is yet another way to target specific locations. Owing to their ease of functionalization, luminescence tunability and specific binding capabilities, QCs functionalized with aptamers are commonly employed for cellular labeling, nuclei staining and tumor detection. Dickson and co-workers[294] utilized DNA-encapsulated Ag clusters conjugated with proteins such as avidin for surface labeling in live cells by exploiting the specific avidin–biotin interactions. Ag clusters functionalized with avidin stained the cell surface and was internalized subsequently. Later Chang and co-workers[295] demonstrated that dihydrolipoic acid (DHLA)-protected water-soluble Au clusters can be conjugated effectively to biomolecules such as polyethylene glycol (PEG), BSA, avidin, and streptavidin via EDC coupling and used them for biological imaging applications. Endogeneous labeling of biotin inside human hepatoma cells

(HepG2) was demonstrated effectively by streptavidin-conjugated Au@DHLA clusters.[295] While unconjugated Au@DHLA clusters showed weak emission [Figure 16C (1 and 1′)] from the cells, streptavidin-conjugated clusters stained the biotin containing cells with high intensity [Figure 16C (2 and 2′)]. Streptavidin conjugated with FITC [Figure 16C (3 and 3′)] was used as the positive control as it is known to specifically bind biotin. Similar approach was used by Pradeep and co-workers to image human hepatoma cells (HepG2) using streptavidin-functionalized red emitting Au_{23} clusters[296] and oral carcinoma KB cells using folic-acid-conjugated Au@BSA clusters.[61] In both cases, the inherent luminescence of the internalized QCs was used in imaging the cells.

While use of various biopolymers for synthesis and subsequent imaging of clusters has been demonstrated by exploiting its luminescence, use of a biologically active protein such as insulin, for synthesis of clusters and retaining its biological activity was advantageous as it adds another modality towards diagnosis and imaging of such clusters. Chou and coworkers[173] synthesized fluorescent Au clusters using insulin and demonstrated its activity in blood glucose regulation. Figure 16D shows the internalization of the Au@insulin clusters in C2C12 mouse myoblasts cells. The red fluorescence in the image is from the clusters while the green and the blue are from the cell nucleus and cell boundary stained using dyes, 4′,6-diamidino-2-phenylindole and Alexa Fluor 488 phalloidin, respectively, for easy visual identification.

4.3.4. Cancer Therapy

In two early reports, the over expression of folic acid receptors in certain cancerous cells such as oral carcinoma KB cells was used to internalize and image folic-acid-functionalized Au clusters via receptor-mediated endocytosis.[61,267] Here, the higher internalization of folic acid (FA)-conjugated red luminescent BSA-protected Au_{25} QCs in FR +ve oral squamous cell carcinoma (KB) and breast adenocarcinoma (MCF-7) cell lines (compared to negative control cell lines) confirmed the receptor-targeted imaging and cancer detection capability of the clusters. A similar study conducted on mouse fibroblast L929 cells without folate receptors served as the negative control, wherein significant luminescence was not observed.[61] These studies demonstrated detection of cancerous cells for the first time using Au clusters. Later, potential of various Au and Ag clusters for simultaneous cancer cell targeting and imaging was demonstrated.[297,298] Efficacy of such materials for therapy was limited due to the lack of effective nuclear drug delivery vehicles to assist the transport of the drug from cytoplasm to the nucleus. Passage of the drug into the nucleus can significantly enhance its therapeutic capability. Irudayaraj et al.[299] reported nuclear localization and targeting capability of fluorescent BSA-protected Au clusters conjugated with Herceptin. Herceptin is a humanized monoclonal antibody capable of targeting ErbB2 receptors, which are overexpressed in breast cancer cells and tumour tissues. Combined use of fluorescent correlation spectroscopy (FCS) and fluorescence lifetime imaging microscopy (FLIM) was used to track the dynamics of the fluorescent cluster probes inside the nucleus of live cells with single particle sensitivity. **Figure 17**A shows the FLIM of SK-BR3 cells stained by Lamin A antibody labeled with Alexa350 and incubated with AuQCs. The presence of Au cluster inside the nucleus of the cell was clearly identified based on the difference in fluorescence lifetime of the Au clusters (1.5 ns) and Lamin A antibody labeled with Alexa350 (1.9 ns) as shown in the left panel of Figure 17A. Comparison of the FLIM from the cells for Herceptin conjugated and unconjugated clusters emphasized the advantage of the former for nuclear delivery. Moreover, the capability of escaping the endolysosomal pathway enhanced their potential to be efficient nuclear drug delivery vehicles. Figure 17B shows the confocal fluorescence images of endolysosomes of SK-BR3 cells incubated with Herceptin-conjugated Au clusters stained by lysosensor marker blue. Lysosensor, used to stain the endosomes and lysosomes of live SK-BR3 cells, was used to monitor the uptake of clusters after incubation. Majority of the clusters did not accumulate within the endosome (right panel of Figure 17B), signifying their endosomal escaping ability. Nuclear localization enhanced the anticancer therapeutic efficacy of Herceptin by the induction of DNA damage as shown in Figure 17C,D. Another report by Wang et al.[171] shows the transport of anticancer molecular drugs such as doxorubicin across HepG2 hepatocarcinoma cell membranes using Au cluster/reduced graphene oxide (GNC-RGO) nanocomposites. Furthermore, they used Raman spectroscopy to study the interaction of GNC–RGO nanocomposites and the proteins and DNA in cancer cells to gain mechanistic insights into their inhibitory action on cancer cells.

In a recent report, biosynthesis of fluorescent QCs by cancerous cells has been monitored by florescence imaging.[298] Clusters were formed inside human hepatocarcinoma (HepG2) and leukemia cell lines (K562) upon incubation with micromolar concentrations of chloroauric acid solutions, while noncancerous human embryo liver cells (L02) showed no such effect. Fluorescent biolabels formed as a result of subcutaneous injections of gold precursors near xenograft tumors in mouse models having hepatocellular carcinoma or chronic myeloid leukemia labels showed noninvasive tumor diagnostic capability (Figure 17E,F).

4.3.5. Other Diagnostic Tools (MRI and CT Imaging)

Magnetic resonance imaging (MRI) is a powerful and widely used imaging technique owing to its fast scan rate, excellent spatial resolution, and deep tissue penetration. However, requirement of large doses of gadolinium-based agents for adequate image contrast is a cause of concern. Use of Au@BSA clusters as bimodal MRI/optical nanoprobes was demonstrated by covalently grafting gadolinium complex of diethylenetriaminepentacetic acid (DTPA), denoted as Gd-DTPA, onto the Au clusters (**Figure 18**A).[300] T1-weighted MR images of the Gd-DTPA-conjugated cluster for various Gd^{3+} concentrations are shown in Figure 18B. These nanoprobes show a higher relaxivity of 23.7 mM^{-1} s^{-1} per Gd^{3+} relative to clinical Gd-DTPA (4.3 mM^{-1} s^{-1}), while their fluorescence emission intensity is preserved (Figure 18C) .

In another report, a similar strategy was used by Kong and coworkers.[301] for multimodal imaging using Gd^{3+}-functionalized

DOI: 10.1002/ppsc.201400033

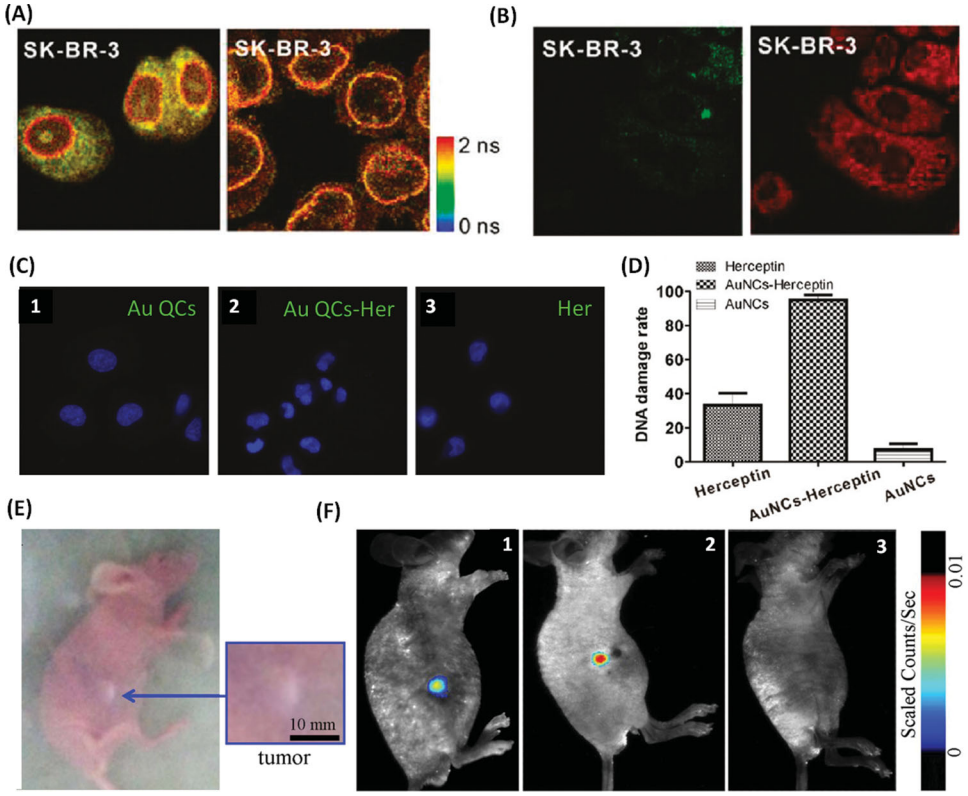

Figure 17. A) FLIM of SK-BR3 cells stained by Lamin A antibody labeled with Alexa350 showing the nuclear uptake of Herceptin-conjugated Au cluster (left) and unconjugated Au clusters (right) incubated for 4 h. Scale bar for FLIM is 0 to 2 ns. B) Confocal fluorescence images of endolysosomes of SK-BR3 cells incubated with Herceptin-conjugated Au clusters stained by lysosensor marker blue showing the emission from the lysosensor (Left panel) and from that of the Au cluster (right panel). C) Fluorescence images showing the induction of DNA damage and apoptosis by 1) unconjugated Au clusters, 2) Herceptin-conjugated Au clusters, and 3) Herceptin by staining the nucleus with Hoechst 33258. D) Bar diagram showing the quantitative evaluation of DNA damage of the cells as a percentage of the total number of cells for different treatments. Panels A-D reproduced with permission.[299] Copyright 2011, American Chemical Society. Representative xenograft tumor mouse models of hepatocellular carcinoma observed in visible light (E) and by in vivo fluorescence imaging (F1) 24 h after a subcutaneous injection of $HAuCl_4$ solution near the tumor. Inset shows an enlarged view of the xenograft tumor. Xenograft tumor mouse models of chronic myeloid leukemia observed by in vivo fluorescence imaging (F2) 24 h after a subcutaneous injection of 10 mmol L^{-1} $HAuCl_4$ solution near the tumor. (F3) Control mouse observed by in vivo fluorescence imaging 48 h after a subcutaneous injection of 10 mmol L^{-1} $HAuCl_4$ solution in the right side of their abdomen. Panels E,F reproduced with permission.[298] Copyright 2013, Nature Publishing Group.

gold clusters (Gd-AuQCs) protected by cyclodecapeptide (CP) for dual model (fluorescence/magnetic resonance) imaging. The Gd-Au QC probes emit bright red fluorescence under UV light, while exhibiting a high longitudinal relaxivity of 41.5 ± 2.5 mM^{-1} s^{-1} and low relaxivity ratio ($r2/r1$, where $r2$ and $r1$ are the relaxivities determined from the influence on the relaxation times $T2$ and $T1$) of 1.2 at 0.55 T. Figure 18D shows the unmodified intense red luminescence from the Gd-AuQCs under UV light along with remarkable $T1$ signal enhancement. The MR image of Gd-AuQCs was much brighter than Gd-CP and Gd-AuNPs under similar Gd^{3+} concentrations. Comparison of the $T1$-weighted MRI of Gd-AuQCs and Gd-DTPA showed better results for the former (Figure 18E) as also observed from their $r1$ relaxivity curves (Figure 18F).

Strong X-ray computed tomography(CT) signal elevation from Au clusters stabilized by insulin (Au@insulin)[173] brought to light yet another imaging modality using these clusters. Clusters showed a dose-dependent enhancement in contrast (Figure $18G_1$) when tested for CT imaging with C2C12 myoblast cells and the uptake was clearly distinguishable in the presence and absence of Au@insulin clusters (Figure $18G_2$).

4.3.6. The Issue of Toxicity

In spite of their applications in diverse avenues of biology, a primary concern for use of such materials in clinical trials is involving their toxicity to living organisms especially, humans. Efficient renal clearance is an important parameter as ideally any nanomaterial-based contrast agent or fluorescent label should be effectively cleared out of the body and show very little accumulation in organs. In vivo applications of noble metal NPs is still severely hampered mainly by their slow renal clearance and high nonspecific accumulation in the organs of the RES, such as liver and spleen, after systematic administration. NPs with smaller diameters (<10 nm) generally considered to be stealthy to the RES organs, are still often found in the liver (**Figure 19**A). In this context, sub-nanometer-sized clusters are advantageous compared to NPs for biomedical applications due

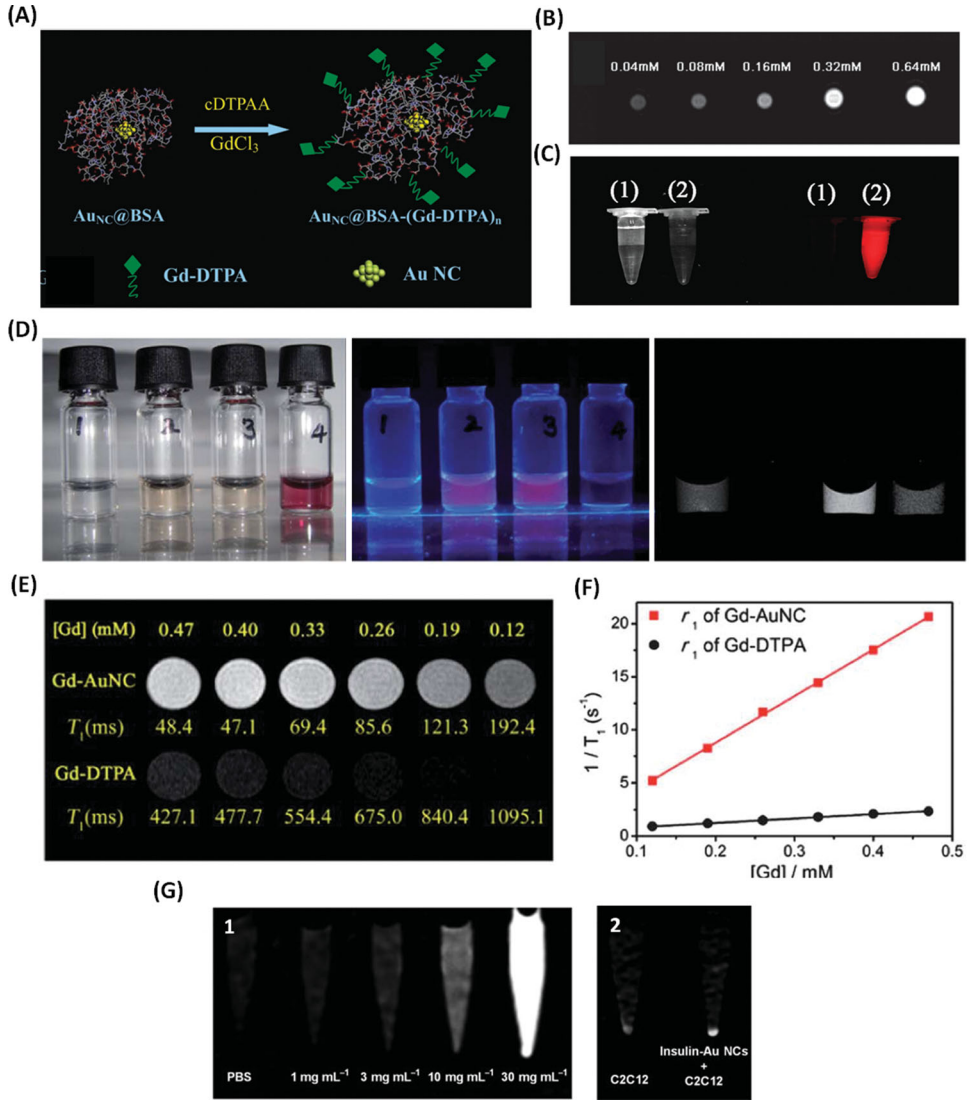

Figure 18. A) Schematic representation of functionalization of Au@BSA clusters with Gd-DTPA. B) T1-weighted MR image of Gd-DTPA-conjugated Au@BSA cluster for various Gd^{3+} concentrations in water from a 1.5 T clinical MRI system. C) Photographs of water (tube 1) and Gd-DTPA-conjugated Au@BSA cluster (tube 2) under white light (left) and under an excitation wavelength of 475 nm (right). Panels A-C reproduced with permission.[300] Copyright 2013, Royal Society of Chemistry. D) Photographs of the AuQCs under visible (left panel), UV light (middle panel), and their T1-weighted MR images (right panel) of the 1) Gd-CP, 2) AuQCs, 3) Gd-AuQCs, and Gd-AuNP samples. E) Comparison of the T1-weighted MRI of Gd-AuQCs (top) and Gd-DTPA for various Gd concentrations and r1 F) their relaxivity curves at 0.55 T. Panels D-F reproduced with permission.[301] Copyright 2013, Royal Society of Chemistry. G) CT imaging of Au@insulin QCs in sequential dosage (1) and differentiated C2C12 myoblasts with (right) and without (left) the clusters. Reproduced with permission.[173] Copyright 2011, Wiley-VCH.

to their extremely small size. Both the nature of the ligand and the particle size are crucial for efficient renal clearance.

Glutathione-protected luminescent Au clusters (Au@SG) showed efficient renal clearance through urine within 24 h after intravenous (IV) injection.[302] Real-time accumulation of the luminescent Au@SG clusters in the bladder of a live mouse was visualized by X-ray computed tomographic (CT) images as shown in Figure 19B. More than 50% of the cluster was excreted out of the body through urine within 24 h (Figure 19C) and up to 65% was observed in the urine, 72 h post-injection.

The importance of choice of the surface capping ligands during in vivo applications of clusters was revealed in experiments conducted with various ligand-protected clusters. Cliffel and co-workers[303] demonstrated that the histological damage to the renal tubules caused by the use of tiopronin-passivated Au clusters during in vivo applications can be eliminated by the incorporation of PEG on the clusters. The amount of PEGylation, chain length of the PEG chains, etc. had an effect on the clearance rate and thus the circulation lifetime of the particles in the body.[304] An optimum of 1% PEGylation using short-chain ligands and alcohol-terminated PEG was identified to achieve short circulation lifetimes in addition to zero toxicity, no immune response, and high water solubility.

However, it is important to mention that conflicting data exist in the literature about the cytotoxicity of small gold particles. A size-dependent toxicity study using gold NPs of sizes

DOI: 10.1002/ppsc.201400033

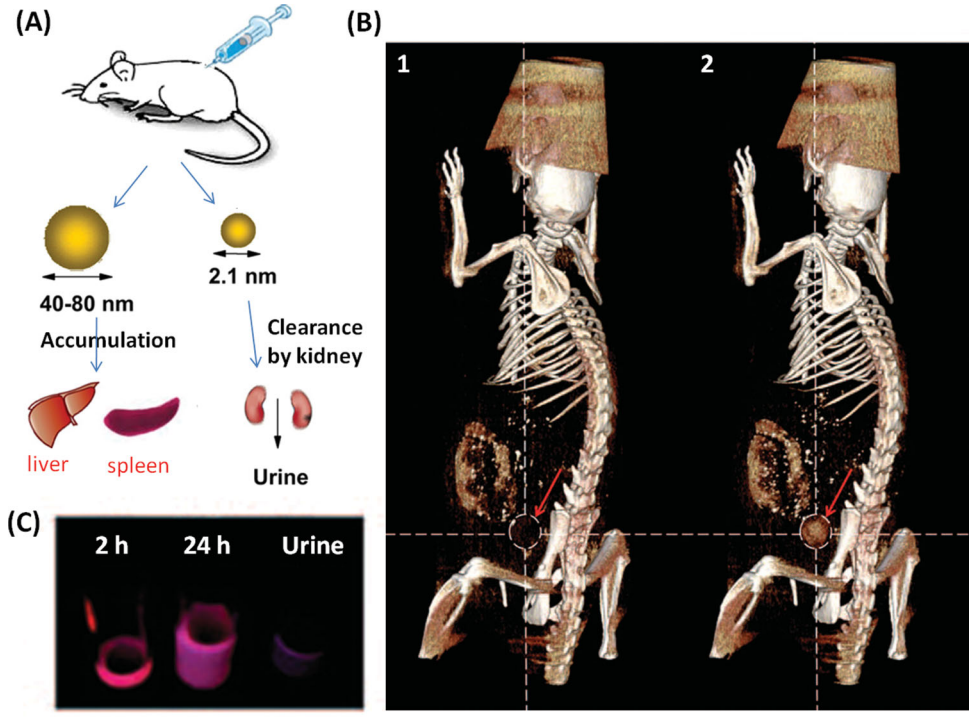

Figure 19. A) Schematic showing the efficiency of renal clearance of clusters in comparison with nanoparticles due to difference in particle size. B) X-ray computed tomography (CT) images of a live mouse 1) before and 2) after 30 min post-injection of Au@SG clusters. C) Fluorescence images of the urine after 1) 2 h and 2) 24 h post-injection of Au@SG clusters along with control urine (3) sample under UV light with a 630/75 bandpass filter. Panels B,C reproduced with permission.[302] Copyright 2011, Wiley-VCH.

ranging from 0.8 to 15 nm using various cell lines indicated that AuNPs of 15 nm size are nontoxic while the 1.4 and 1.2 nm AuNPs resulted in rapid cell death by necrosis and apoptosis, respectively, within 12 h of incubation.[305] Au_{55} clusters have also been shown to interact with DNA and cause significant toxicity towards various human cell lines compared to NPs,[306] but this enhanced reactivity shown by such clusters was envisioned as a possible mode for cancer treatment.

Thus, while water-soluble QCs have undoubtedly proven to have immense potential in biological applications, caution should be exercised in the choice of suitable ligand and their functionalization and core size in order to avoid additional effects.

5. Conclusions and Future Prospects

Novel properties arising as a result of size quantization in clusters, such as luminescence, a phenomenon not prominent in NPs, make such materials promising candidates for applications in diverse fields. Such sub-nanometer-sized materials can be easily conjugated with molecules, thus making them ideal candidates in biological applications such as multimodal imaging, sensors for biomolecules, nuclear targeting, drug delivery, oncotherapy, etc. Issues such as selectivity and stability of these clusters in complex media can be addressed by combining them with other molecular species or NPs, to obtain hybrid materials with multimodal properties. Novel sensing strategies based on these materials can be envisaged. Extremely small size and tunable luminescence properties of QCs may be useful for the development of hybrid, multimodal gold QCs-based nano-formulations for future therapeutics against various diseases, including cancer. Apart from this, the possibilities of conjugating QCs with various aptamers could possibly bring new capabilities in gene therapy. The recent progress in the computational capabilities and the current knowledge in the crystal structures of QCs provide sufficient background for designing new catalysts with predictable reactivity and selectivity. New capabilities in assembling nanoclusters precisely on various substrates may lead to the development of QC-based optical devices. Synthetic strategies in making hybrid QCs can open up new possibilities in more efficient and bio-friendly solar cells. The unique capabilities and biocompatibility make these materials promising candidates for the development of "next"-generation "quantum medicine" for disease diagnosis and treatment. As the properties of many of the QCs are studied only to a limited extent, many promising avenues in terms of their medical and materials science applications are yet to be explored. With further experimental and theoretical advances towards understanding these materials and by solving challenges in their synthesis, an almost unlimited field of applications can be foreseen. At present, it is necessary to a) have an appropriate terminology for describing such materials, b) crystallize as many of them as possible, c) correlate structures with associated properties, d) come up with a general rule or rules for the formation of these materials, and e) expand their science (chemistry, physics, biology, and applications). In this, inputs of computational studies will be highly beneficial. With

the expansion of computational power and developments in methodologies, accurate predictions of spectra become possible and this is demonstrated in a number of recent publications.[103,104] It is clear that expansion of science at the interface of molecules and NPs will be a result of strong overlap of experiments with theory.

Acknowledgements

Authors acknowledge the Department of Science and Technology for constant support. A.M. thanks CSIR for a research fellowship. The authors acknowledge the contributions of our co-workers, which made it possible to write this review.

Received: February 12, 2014
Revised: April 21, 2014
Published online:

[1] E. Boisselier, D. Astruc, *Chem. Soc. Rev.* **2009**, *38*, 1759.
[2] M.-C. Daniel, D. Astruc, *Chem. Rev.* **2004**, *104*, 293.
[3] P. R. Sajanlal, T. Pradeep, in *Kirk-Othmer Encyclopedia of Chemical Technology*, John Wiley & Sons, Inc., New York **2011**.
[4] K. E. Sapsford, W. R. Algar, L. Berti, K. B. Gemmill, B. J. Casey, E. Oh, M. H. Stewart, I. L. Medintz, *Chem. Rev.* **2013**, *113*, 1904.
[5] M. Amelia, C. Lincheneau, S. Silvi, A. Credi, *Chem. Soc. Rev.* **2012**, *41*, 5728.
[6] C. Wu, D. T. Chiu, *Angew. Chem. Int. Ed.* **2013**, *52*, 3086.
[7] P. R. Sajanlal, T. Pradeep, *Nano Res.* **2009**, *2*, 306.
[8] P. R. Sajanlal, T. Pradeep, *Langmuir* **2009**, *26*, 456.
[9] Y. Lu, W. Chen, *Chem. Soc. Rev.* **2012**, *41*, 3594.
[10] A. C. Templeton, W. P. Wuelfing, R. W. Murray, *Acc. Chem. Res.* **2000**, *33*, 27.
[11] M. Brust, M. Walker, D. Bethell, D. J. Schiffrin, R. Whyman, *J. Chem. Soc., Chem. Commun.* **1994**, 801.
[12] J. F. Parker, C. A. Fields-Zinna, R. W. Murray, *Acc. Chem. Res.* **2010**, *43*, 1289.
[13] S. H. Yau, O. Varnavski, T. Goodson, *Acc. Chem. Res.* **2013**, *46*, 1506.
[14] G. Schmid, *Chem. Soc. Rev.* **2008**, *37*, 1909.
[15] R. Jin, *Nanoscale* **2010**, *2*, 343.
[16] I. Diez, R. H. A. Ras, *Nanoscale* **2011**, *3*, 1963.
[17] S. Choi, R. M. Dickson, J. Yu, *Chem. Soc. Rev.* **2012**, *41*, 1867.
[18] H.-W. Li, Y. Yue, T.-Y. Liu, D. Li, Y. Wu, *J. Phys. Chem. C* **2013**, *117*, 16159.
[19] D. R. Kauffman, D. Alfonso, C. Matranga, H. Qian, R. Jin, *J. Phys. Chem. C* **2013**, *117*, 7914.
[20] J. S. Mohanty, P. L. Xavier, K. Chaudhari, M. S. Bootharaju, N. Goswami, S. K. Pal, T. Pradeep, *Nanoscale* **2012**, *4*, 4255.
[21] N. Goswami, A. Giri, M. S. Bootharaju, P. L. Xavier, T. Pradeep, S. K. Pal, *Anal. Chem.* **2011**, *83*, 9676.
[22] X. Jia, J. Li, L. Han, J. Ren, X. Yang, E. Wang, *ACS Nano* **2012**, *6*, 3311.
[23] W. Wei, Y. Lu, W. Chen, S. Chen, *J. Am. Chem. Soc.* **2011**, *133*, 2060.
[24] S.-I. Tanaka, J. Miyazaki, D. K. Tiwari, T. Jin, Y. Inouye, *Angew. Chem. Int. Ed.* **2011**, *50*, 431.
[25] S. Vajda, M. J. Pellin, J. P. Greeley, C. L. Marshall, L. A. Curtiss, G. A. Ballentine, J. W. Elam, C.-M. Stephanie, P. C. Redfern, F. Mehmood, P. Zapol, *Nat. Mater.* **2009**, *8*, 213.
[26] J. N. Tiwari, K. Nath, S. Kumar, R. N. Tiwari, K. C. Kemp, N. H. Le, D. H. Youn, J. S. Lee, K. S. Kim, *Nat. Commun.* **2013**, *4*, 2221.
[27] H. Erdogan, O. Metin, S. Ozkar, *Phys. Chem. Chem. Phys.* **2009**, *11*, 10519.
[28] M. Hyotanishi, Y. Isomura, H. Yamamoto, H. Kawasaki, Y. Obora, *Chem. Commun.* **2011**, *47*, 5750.
[29] T. Udayabhaskararao, T. Pradeep, *J. Phys. Chem. Lett.* **2013**, *4*, 1553.
[30] S. A. Patel, M. Cozzuol, J. M. Hales, C. I. Richards, M. Sartin, J.-C. Hsiang, T. Vosch, J. W. Perry, R. M. Dickson, *J. Phys. Chem. C* **2009**, *113*, 20264.
[31] A. A. Herzing, C. J. Kiely, A. F. Carley, P. Landon, G. J. Hutchings, *Science* **2008**, *321*, 1331.
[32] G. Li, R. Jin, *Acc. Chem. Res.* **2013**, *46*, 1749.
[33] Y. Zhu, H. Qian, B. A. Drake, R. Jin, *Angew. Chem. Int. Ed.* **2010**, *49*, 1295.
[34] H. Tsunoyama, N. Ichikuni, H. Sakurai, T. Tsukuda, *J. Am. Chem. Soc.* **2009**, *131*, 7086.
[35] M. Valden, X. Lai, D. W. Goodman, *Science* **1998**, *281*, 1647.
[36] J. Zhang, K. Sasaki, E. Sutter, R. R. Adzic, *Science* **2007**, *315*, 220.
[37] J. Oliver-Meseguer, J. R. Cabrero-Antonino, I. Domínguez, A. Leyva-Pérez, A. Corma, *Science* **2012**, *338*, 1452.
[38] J. P. Wilcoxon, B. L. Abrams, *Chem. Soc. Rev.* **2006**, *35*, 1162.
[39] L. Shang, S. Dong, G. U. Nienhaus, *Nano Today* **2011**, *6*, 401.
[40] H. Haekkinen, *Chem. Soc. Rev.* **2008**, *37*, 1847.
[41] H. Qian, M. Zhu, Z. Wu, R. Jin, *Acc. Chem. Res.* **2012**, *45*, 1470.
[42] J. Zheng, P. R. Nicovich, R. M. Dickson, *Annu. Rev. Phys. Chem.* **2007**, *58*, 409.
[43] J. Zheng, C. Zhou, M. Yu, J. Liu, *Nanoscale* **2012**, *4*, 4073.
[44] Y. Zhu, H. Qian, R. Jin, *J. Mater. Chem.* **2011**, *21*, 6793.
[45] S. Yamazoe, K. Koyasu, T. Tsukuda, *Acc. Chem. Res.* **2014**, *47*, 816.
[46] I. Diez, R. H. A. Ras, *Springer Ser. Fluoresc.* **2010**, *9*, 307.
[47] P. Lourdu Xavier, K. Chaudhari, A. Baksi, T. Pradeep, *Nano Rev.* **2012**, *3*, 14767.
[48] Y.-C. Shiang, C.-C. Huang, W.-Y. Chen, P.-C. Chen, H.-T. Chang, *J. Mater. Chem.* **2012**, *22*, 12972.
[49] X. Yuan, Z. Luo, Y. Yu, Q. Yao, J. Xie, *Chem. Asian J.* **2013**, *8*, 858.
[50] J. W. Hamilton, R. C. Kaltreider, O. V. Bajenova, M. A. Ihnat, J. McCaffrey, B. W. Turpie, E. E. Rowell, J. Oh, M. J. Nemeth, C. A. Pesce, J. P. Lariviere, *Environ. Health Perspect.* **1998**, *106*, 1005.
[51] R. C. Price, R. L. Whetten, *J. Am. Chem. Soc.* **2005**, *127*, 13750.
[52] Z. Wu, E. Lanni, W. Chen, M. E. Bier, D. Ly, R. Jin, *J. Am. Chem. Soc.* **2009**, *131*, 16672.
[53] T. P. Ang, T. S. A. Wee, W. S. Chin, *J. Phys. Chem. B* **2004**, *108*, 11001.
[54] S. Y. Kang, K. Kim, *Langmuir* **1998**, *14*, 226.
[55] T. U. B. Rao, B. Nataraju, T. Pradeep, *J. Am. Chem. Soc.* **2010**, *132*, 16304.
[56] T. Udayabhaskararao, M. S. Bootharaju, T. Pradeep, *Nanoscale* **2013**, *5*, 9404.
[57] I. Chakraborty, W. Kurashige, K. Kanehira, L. Gell, H. Häkkinen, Y. Negishi, T. Pradeep, *J. Phys. Chem. Lett.* **2013**, *4*, 3351.
[58] I. Chakraborty, A. Govindarajan, J. Erusappan, A. Ghosh, T. Pradeep, B. Yoon, R. L. Whetten, U. Landman, *Nano Lett.* **2012**, *12*, 5861.
[59] Z. Shen, H. Duan, H. Frey, *Adv. Mater.* **2007**, *19*, 349.
[60] L. Li, Z. Li, H. Zhang, S. Zhang, I. Majeed, B. Tan, *Nanoscale* **2013**, *5*, 1986.
[61] M. A. Habeeb Muhammed, P. K. Verma, S. K. Pal, A. Retnakumari, M. Koyakutty, S. Nair, T. Pradeep, *Chem. Eur. J.* **2010**, *16*, 10103.
[62] A. Mathew, P. R. Sajanlal, T. Pradeep, *J. Mater. Chem.* **2011**, *21*, 11205.
[63] P. L. Xavier, K. Chaudhari, P. K. Verma, S. K. Pal, T. Pradeep, *Nanoscale* **2010**, *2*, 2769.
[64] J. Zheng, J. T. Petty, R. M. Dickson, *J. Am. Chem. Soc.* **2003**, *125*, 7780.

[65] J. Zheng, R. M. Dickson, *J. Am. Chem. Soc.* **2002**, *124*, 13982.
[66] I. Chakraborty, T. Udayabhaskararao, T. Pradeep, *J. Hazard. Mater.* **2012**, *211–212*, 396.
[67] J. Zhang, S. Xu, E. Kumacheva, *Adv. Mater.* **2005**, *17*, 2336.
[68] J. T. Petty, J. Zheng, N. V. Hud, R. M. Dickson, *J. Am. Chem. Soc.* **2004**, *126*, 5207.
[69] H.-C. Yeh, J. Sharma, J. J. Han, J. S. Martinez, J. H. Werner, *Nano Lett.* **2010**, *10*, 3106.
[70] J. Xie, Y. Zheng, J. Y. Ying, *J. Am. Chem. Soc.* **2009**, *131*, 888.
[71] D. M. Chevrier, A. Chatt, P. Zhang, *J. Nanophotonics* **2012**, *6*, 064504.
[72] H. Xu, K. S. Suslick, *ACS Nano* **2010**, *4*, 3209.
[73] A. Ledo-Suárez, J. Rivas, C. F. Rodríguez-Abreu, M. J. Rodríguez, E. Pastor, A. Hernández-Creus, S. B. Oseroff, M. A. López-Quintela, *Angew. Chem. Int. Ed.* **2007**, *46*, 8823.
[74] B. G. Ershov, A. Henglein, *J. Phys. Chem. B* **1998**, *102*, 10667.
[75] T. Linnert, P. Mulvaney, A. Henglein, H. Weller, *J. Am. Chem. Soc.* **1990**, *112*, 4657.
[76] N. Vilar-Vidal, M. C. Blanco, M. A. López-Quintela, J. Rivas, C. Serra, *J. Phys. Chem. C* **2010**, *114*, 15924.
[77] T. Liu, Y. Su, H. Song, Y. Lv, *Analyst* **2013**, *138*, 6558.
[78] L. Dhanalakshmi, T. Udayabhaskararao, T. Pradeep, *Chem. Commun.* **2011**, *48*, 859.
[79] Y. Shichibu, Y. Negishi, H. Tsunoyama, M. Kanehara, T. Teranishi, T. Tsukuda, *Small* **2007**, *3*, 835.
[80] E. S. Shibu, M. A. H. Muhammed, T. Tsukuda, T. Pradeep, *J. Phys. Chem.C* **2008**, *112*, 12168.
[81] Y. Niihori, M. Matsuzaki, T. Pradeep, Y. Negishi, *J. Am. Chem. Soc.* **2013**, *135*, 4946.
[82] M. J. Hostetler, A. C. Templeton, R. W. Murray, *Langmuir* **1999**, *15*, 3782.
[83] Y. Negishi, K. Nobusada, T. Tsukuda, *J. Am. Chem. Soc.* **2005**, *127*, 5261.
[84] Y. Negishi, Y. Takasugi, S. Sato, H. Yao, K. Kimura, T. Tsukuda, *J. Am. Chem. Soc.* **2004**, *126*, 6518.
[85] C. Kumara, A. Dass, *Nanoscale* **2012**, *4*, 4084.
[86] R. L. Donkers, D. Lee, R. W. Murray, *Langmuir* **2004**, *20*, 1945.
[87] S. Knoppe, J. Boudon, I. Dolamic, A. Dass, T. Burgi, *Anal. Chem.* **2011**, *83*, 5056.
[88] L. Beqa, D. Deschamps, S. P. Perrio, A.-C. Gaumont, S. Knoppe, T. Bürgi, *J. Phys. Chem. C* **2013**, *117*, 21619.
[89] I. Dolamic, S. Knoppe, A. Dass, T. Bürgi, *Nat. Commun.* **2012**, *3*, 798.
[90] W. Wurth, M. Martins, D. P. Woodruff, in *The Chemical Physics of Solid Surfaces*, Vol. *12*, Elsevier, Amsterdam, **2007**, pp. 471.
[91] A. Baksi, T. Pradeep, B. Yoon, C. Yannouleas, U. Landman, *Chem. Phys. Chem.* **2013**, *14*, 1272.
[92] A. Baksi, T. Pradeep, *Nanoscale* **2013**, *5*, 12245.
[93] P. D. Jadzinsky, G. Calero, C. J. Ackerson, D. A. Bushnell, R. D. Kornberg, *Science* **2007**, *318*, 430.
[94] M. W. Heaven, A. Dass, P. S. White, K. M. Holt, R. W. Murray, *J. Am. Chem. Soc.* **2008**, *130*, 3754.
[95] M. Zhu, C. M. Aikens, F. J. Hollander, G. C. Schatz, R. Jin, *J. Am. Chem. Soc.* **2008**, *130*, 5883.
[96] H. Qian, W. T. Eckenhoff, Y. Zhu, T. Pintauer, R. Jin, *J. Am. Chem. Soc.* **2010**, *132*, 8280.
[97] C. Zeng, H. Qian, T. Li, G. Li, N. L. Rosi, B. Yoon, R. N. Barnett, R. L. Whetten, U. Landman, R. Jin, *Angew. Chem. Int. Ed.* **2012**, *51*, 13114.
[98] A. Das, T. Li, K. Nobusada, Q. Zeng, N. L. Rosi, R. Jin, *J. Am. Chem. Soc.* **2012**, *134*, 20286.
[99] C. Zeng, T. Li, A. Das, N. L. Rosi, R. Jin, *J. Am. Chem. Soc.* **2013**, *135*, 10011.
[100] A. Das, T. Li, K. Nobusada, C. Zeng, N. L. Rosi, R. Jin, *J. Am. Chem. Soc.* **2013**, *135*, 18267.
[101] H. Yang, J. Lei, B. Wu, Y. Wang, M. Zhou, A. Xia, L. Zheng, N. Zheng, *Chem. Commun.* **2012**, *49*, 300.
[102] H. Yang, Y. Wang, N. Zheng, *Nanoscale* **2013**, *5*, 2674.
[103] H. Yang, Y. Wang, H. Huang, L. Gell, L. Lehtovaara, S. Malola, H. Häkkinen, N. Zheng, *Nat. Commun.* **2013**, *4*, 2422.
[104] A. Desireddy, B. E. Conn, J. Guo, B. Yoon, R. N. Barnett, B. M. Monahan, K. Kirschbaum, W. P. Griffith, R. L. Whetten, U. Landman, T. P. Bigioni, *Nature* **2013**, *501*, 399.
[105] H. Yang, Y. Wang, J. Lei, L. Shi, X. Wu, V. Mäkinen, S. Lin, Z. Tang, J. He, H. Häkkinen, L. Zheng, N. Zheng, *J. Am. Chem. Soc.* **2013**, *135*, 9568.
[106] R. L. Whetten, J. T. Khoury, M. M. Alvarez, S. Murthy, I. Vezmar, Z. L. Wang, P. W. Stephens, C. L. Cleveland, W. D. Luedtke, U. Landman, *Adv. Mater.* **1996**, *8*, 428.
[107] T. G. Schaaff, M. N. Shafigullin, J. T. Khoury, I. Vezmar, R. L. Whetten, W. G. Cullen, P. N. First, C. Gutiérrez-Wing, J. Ascensio, M. J. Jose-Yacamán, *J. Phys. Chem. B* **1997**, *101*, 7885.
[108] M. M. Alvarez, J. T. Khoury, T. G. Schaaff, M. Shafigullin, I. Vezmar, R. L. Whetten, *Chem. Phys. Lett.* **1997**, *266*, 91.
[109] M. M. Alvarez, J. T. Khoury, T. G. Schaaff, M. N. Shafigullin, I. Vezmar, R. L. Whetten, *J. Phys. Chem. B* **1997**, *101*, 3706.
[110] S. L. Logunov, T. S. Ahmadi, M. A. El-Sayed, J. T. Khoury, R. L. Whetten, *J. Phys. Chem. B* **1997**, *101*, 3713.
[111] M. J. Hostetler, J. E. Wingate, C.-J. Zhong, J. E. Harris, R. W. Vachet, M. R. Clark, J. D. Londono, S. J. Green, J. J. Stokes, G. D. Wignall, G. L. Glish, M. D. Porter, N. D. Evans, R. W. Murray, *Langmuir* **1998**, *14*, 17.
[112] C. M. Aikens, *J. Phys. Chem. Lett.* **2010**, *2*, 99.
[113] E. Hulkko, O. Lopez-Acevedo, J. Koivisto, Y. Levi-Kalisman, R. D. Kornberg, M. Pettersson, H. Häkkinen, *J. Am. Chem. Soc.* **2011**, *133*, 3752.
[114] O. Lopez-Acevedo, J. Akola, R. L. Whetten, H. Grönbeck, H. Häkkinen, *J. Phys. Chem. C* **2009**, *113*, 5035.
[115] J. Akola, M. Walter, R. L. Whetten, H. Häkkinen, H. Grönbeck, *J. Am. Chem. Soc.* **2008**, *130*, 3756.
[116] D. Lee, R. L. Donkers, G. Wang, A. S. Harper, R. W. Murray, *J. Am. Chem. Soc.* **2004**, *126*, 6193.
[117] K. M. Harkness, Y. Tang, A. Dass, J. Pan, N. Kothalawala, V. J. Reddy, D. E. Cliffel, B. Demeler, F. Stellacci, O. M. Bakr, J. A. McLean, *Nanoscale* **2012**, *4*, 4269.
[118] O. M. Bakr, V. Amendola, C. M. Aikens, W. Wenseleers, R. Li, L. Dal Negro, G. C. Schatz, F. Stellacci, *Angew. Chem. Int. Ed.* **2009**, *48*, 5921.
[119] S. Malola, L. Lehtovaara, J. Enkovaara, H. Häkkinen, *ACS Nano* **2013**, *7*, 10263.
[120] A. Dass, *J. Am. Chem. Soc.* **2011**, *133*, 19259.
[121] Z. Wu, R. Jin, *Nano Lett.* **2010**, *10*, 2568.
[122] I. Díez, M. Pusa, S. Kulmala, H. Jiang, A. Walther, A. S. Goldmann, A. H. E. Müller, O. Ikkala, R. H. A. Ras, *Angew. Chem. Int. Ed.* **2009**, *48*, 2122.
[123] A. Mooradian, *Phys. Rev. Lett.* **1969**, *22*, 185.
[124] G. T. Boyd, Z. H. Yu, Y. R. Shen, *Phys. Rev. B* **1986**, *33*, 7923.
[125] T. P. Bigioni, R. L. Whetten, Ã. Dag, *J. Phys. Chem. B* **2000**, *104*, 6983.
[126] S. Link, A. Beeby, S. FitzGerald, M. A. El-Sayed, T. G. Schaaff, R. L. Whetten, *J. Phys. Chem. B* **2002**, *106*, 3410.
[127] G. Wang, T. Huang, R. W. Murray, L. Menard, R. G. Nuzzo, *J. Am. Chem. Soc.* **2004**, *127*, 812.
[128] M. S. Devadas, J. Kim, E. Sinn, D. Lee, T. Goodson, G. Ramakrishna, *J. Phys. Chem. B* **2010**, *114*, 22417.
[129] S. A. Miller, J. M. Womick, J. F. Parker, R. W. Murray, A. M. Moran, *J. Phys. Chem. B* **2009**, *113*, 9440.
[130] J. Zheng, C. Zhang, R. M. Dickson, *Phys. Rev. Lett.* **2004**, *93*, 077402.
[131] X. Wen, P. Yu, Y.-R. Toh, J. Tang, *J. Phys. Chem.C* **2012**, *116*, 11830.

[132] X. Wen, P. Yu, Y.-R. Toh, A.-C. Hsu, Y.-C. Lee, J. Tang, *J. Phys. Chem. C* **2012**, *116*, 19032.
[133] I. Diez, M. I. Kanyuk, A. P. Demchenko, A. Walther, H. Jiang, O. Ikkala, R. H. A. Ras, *Nanoscale* **2012**, *4*, 4434.
[134] F. Qu, L. L. Dou, N. B. Li, H. Q. Luo, *J. Mater. Chem. C* **2013**, *1*, 4008.
[135] A. Mathew, P. R. Sajanlal, T. Pradeep, *Angew. Chem. Int. Ed.* **2012**, *51*, 9596.
[136] T. G. Schaaff, G. Knight, M. N. Shafigullin, R. F. Borkman, R. L. Whetten, *J. Phys. Chem. B* **1998**, *102*, 10643.
[137] O. Lopez-Acevedo, H. Tsunoyama, T. Tsukuda, H. Häkkinen, C. M. Aikens, *J. Am. Chem. Soc.* **2010**, *132*, 8210.
[138] T. G. Schaaff, R. L. Whetten, *J. Phys. Chem. B* **2000**, *104*, 2630.
[139] Z. Wu, C. Gayathri, R. R. Gil, R. Jin, *J. Am. Chem. Soc.* **2009**, *131*, 6535.
[140] M. Zhu, H. Qian, X. Meng, S. Jin, Z. Wu, R. Jin, *Nano Lett.* **2011**, *11*, 3963.
[141] G. Ramakrishna, O. Varnavski, J. Kim, D. Lee, T. Goodson, *J. Am. Chem. Soc.* **2008**, *130*, 5032.
[142] S. A. Patel, C. I. Richards, J.-C. Hsiang, R. M. Dickson, *J. Am. Chem. Soc.* **2008**, *130*, 11602.
[143] S. H. Yau, N. Abeyasinghe, M. Orr, L. Upton, O. Varnavski, J. H. Werner, H.-C. Yeh, J. Sharma, A. P. Shreve, J. S. Martinez, T. Goodson, *Nanoscale* **2012**, *4*, 4247.
[144] P. Crespo, R. Litrán, T. C. Rojas, M. Multigner, J. M. de la Fuente, J. C. Sánchez-López, M. A. García, A. Hernando, S. Penadés, A. Fernández, *Phys. Rev. Lett.* **2004**, *93*, 087204.
[145] Y. Yamamoto, T. Miura, M. Suzuki, N. Kawamura, H. Miyagawa, T. Nakamura, K. Kobayashi, T. Teranishi, H. Hori, *Phys. Rev. Lett.* **2004**, *93*, 116801.
[146] H. Hori, Y. Yamamoto, T. Iwamoto, T. Miura, T. Teranishi, M. Miyake, *Phys. Rev. B* **2004**, *69*, 174411.
[147] Y. Negishi, H. Tsunoyama, M. Suzuki, N. Kawamura, M. M. Matsushita, K. Maruyama, T. Sugawara, T. Yokoyama, T. Tsukuda, *J. Am. Chem. Soc.* **2006**, *128*, 12034.
[148] M. Zhu, C. M. Aikens, M. P. Hendrich, R. Gupta, H. Qian, G. C. Schatz, R. Jin, *J. Am. Chem. Soc.* **2009**, *131*, 2490.
[149] R. S. McCoy, S. Choi, G. Collins, B. J. Ackerson, C. J. Ackerson, *ACS Nano* **2013**, *7*, 2610.
[150] M. Walter, J. Akola, O. Lopez-Acevedo, P. D. Jadzinsky, G. Calero, C. J. Ackerson, R. L. Whetten, H. Gronbeck, H. Häkkinen, *Proc. Natl. Acad. Sci.* **2008**, *105*, 9157.
[151] B. M. Quinn, P. Liljeroth, V. Ruiz, T. Laaksonen, K. S. Kontturi, *J. Am. Chem. Soc.* **2003**, *125*, 6644.
[152] J. B. Tracy, G. Kalyuzhny, M. C. Crowe, R. Balasubramanian, J.-P. Choi, R. W. Murray, *J. Am. Chem. Soc.* **2007**, *129*, 6706.
[153] A. Tlahuice-Flores, R. L. Whetten, M. Jose-Yacaman, *J. Phys. Chem. C* **2013**, *117*, 20867.
[154] Y. Negishi, N. K. Chaki, Y. Shichibu, R. L. Whetten, T. Tsukuda, *J. Am. Chem. Soc.* **2007**, *129*, 11322.
[155] M. A. Tofanelli, C. J. Ackerson, *J. Am. Chem. Soc.* **2012**, *134*, 16937.
[156] J. Jung, S. Kang, Y.-K. Han, *Nanoscale* **2012**, *4*, 4206.
[157] A. Mathew, G. Natarajan, L. Lehtovaara, H. Häkkinen, R. M. Kumar, V. Subramanian, A. Jaleel, T. Pradeep, *ACS Nano* **2014**, *8*, 139.
[158] J. C. Azcárate, G. N. Corthey, E. Pensa, C. Vericat, M. H. Fonticelli, R. C. Salvarezza, P. Carro, *J. Phys. Chem. Lett.* **2014**, *4*, 3127.
[159] Y. Gao, *J. Phys. Chem. C* **2013**, *117*, 8983.
[160] S. Kumar, R. Jin, *Nanoscale* **2012**, *4*, 4222.
[161] W. Kurashige, M. Yamaguchi, K. Nobusada, Y. Negishi, *J. Phys. Chem. Lett.* **2012**, *3*, 2649.
[162] K. P. Remya, T. Udayabhaskararao, T. Pradeep, *J. Phys. Chem. C* **2012**, *116*, 26019.
[163] Y. Negishi, K. Munakata, W. Ohgake, K. Nobusada, *J. Phys. Chem. Lett.* **2012**, *3*, 2209.
[164] Y. Negishi, W. Kurashige, Y. Niihori, T. Iwasa, K. Nobusada, *Phys. Chem. Chem. Phys.* **2010**, *12*, 6219.
[165] A. George, E. S. Shibu, S. M. Maliyekkal, M. S. Bootharaju, T. Pradeep, *ACS Appl. Mater. Interfaces* **2012**, *4*, 639.
[166] A. Samanta, B. B. Dhar, R. N. Devi, *J. Phys. Chem. C* **2011**, *116*, 1748.
[167] M. A. Habeeb Muhammed, T. Pradeep, *Small* **2011**, *7*, 204.
[168] T. Chen, Y. Hu, Y. Cen, X. Chu, Y. Lu, *J. Am. Chem. Soc.* **2013**, *135*, 11595.
[169] T. Udaya Bhaskara Rao, T. Pradeep, *Angew. Chem. Int. Ed.* **2010**, *49*, 3925.
[170] E. S. Shibu, T. Pradeep, *Chem. Mater.* **2011**, *23*, 989.
[171] C. Wang, J. Li, C. Amatore, Y. Chen, H. Jiang, X.-M. Wang, *Angew. Chem. Int. Ed.* **2011**, *50*, 11644.
[172] A. Chandrasekar, T. Pradeep, *J. Phys. Chem. C* **2012**, *116*, 14057.
[173] C.-L. Liu, H.-T. Wu, Y.-H. Hsiao, C.-W. Lai, C.-W. Shih, Y.-K. Peng, K.-C. Tang, H.-W. Chang, Y.-C. Chien, J.-K. Hsiao, J.-T. Cheng, P.-T. Chou, *Angew. Chem. Int. Ed.* **2011**, *50*, 7056.
[174] G.-H. Yang, J.-J. Shi, S. Wang, W.-W. Xiong, L.-P. Jiang, C. Burda, J.-J. Zhu, *Chem. Commun.* **2013**, *49*, 10757.
[175] I.-S. Hwang, J.-K. Choi, H.-S. Woo, S.-J. Kim, S.-Y. Jung, T.-Y. Seong, I.-D. Kim, J.-H. Lee, *ACS Appl. Mater. Interfaces* **2011**, *3*, 3140.
[176] G. Aragay, J. Pons, A. Merkoçi, *Chem. Rev.* **2011**, *111*, 3433.
[177] J. H. Duffus, *Pure Appl. Chem.* **2003**, *75*, 1357.
[178] B. L. Vallee, D. D. Ulmer, *Annu. Rev. Biochem.* **1972**, *41*, 91.
[179] T. Partanen, P. Heikkila, S. Hernberg, T. Kauppinen, G. Moneta, A. Ojajarvi, *Scand. J. Work Environ. Health* **1991**, *17*, 231.
[180] E. V. Ohanian, *Clin. Chem.* **1991**, *37*, 1104.
[181] N. H. Bings, A. Bogaerts, J. A. C. Broekaert, *Anal. Chem.* **2006**, *78*, 3917.
[182] K. E. Lorber, *Waste Manag. Res.* **1986**, *4*, 3.
[183] R. Kunkel, S. E. Manahan, *Anal. Chem.* **1973**, *45*, 1465.
[184] M. López-Artíguez, A. Cameán, M. Repetto, *J. Anal. Toxicol.* **1993**, *17*, 18.
[185] K. W. Jackson, T. M. Mahmood, *Anal. Chem.* **1994**, *66*, 252R.
[186] C. Guo, J. Irudayaraj, *Anal. Chem.* **2011**, *83*, 2883.
[187] M. S. Bootharaju, T. Pradeep, *Langmuir* **2011**, *27*, 8134.
[188] J. Xie, Y. Zheng, J. Y. Ying, *Chem. Commun.* **2010**, *46*, 961.
[189] C.-C. Huang, Z. Yang, K.-H. Lee, H.-T. Chang, *Angew. Chem. Int. Ed.* **2007**, *46*, 6824.
[190] J. H. Park, S. Hwang, J. Kwak, *ACS Nano* **2010**, *4*, 3949.
[191] Y.-H. Lin, W.-L. Tseng, *Anal. Chem.* **2010**, *82*, 9194.
[192] W. Guo, J. Yuan, E. Wang, *Chem. Commun.* **2009**, 3395.
[193] B. Adhikari, A. Banerjee, *Chem. Mater.* **2010**, *22*, 4364.
[194] X. Le Guével, B. Hötzer, G. Jung, K. Hollemeyer, V. Trouillet, M. Schneider, *J. Phys. Chem. C* **2011**, *115*, 10955.
[195] C.-C. Huang, Z. Yang, K.-H. Lee, H.-T. Chang, *Angew. Chem. Int. Ed.* **2007**, *119*, 6948.
[196] G.-Y. Lan, C.-C. Huang, H.-T. Chang, *Chem. Commun.* **2010**, *46*, 1257.
[197] Y. Li, X. Wang, G. Chen, S. Xu, W. Xu, *Anal. Methods* **2013**, *5*, 3853.
[198] Y.-T. Su, G.-Y. Lan, W.-Y. Chen, H.-T. Chang, *Anal. Chem.* **2010**, *82*, 8566.
[199] S. Yunfeng, L. Sujuan, Z. Yahui, Z. Qingpan, H. Mengyue, C. Fensha, D. Jimin, L. Jiamiao, Z. Xinyuan, *Nanotechnology* **2012**, *23*, 485603.
[200] S. Liu, F. Lu, J.-J. Zhu, *Chem. Commun.* **2011**, *47*, 2661.
[201] J.-A. Annie Ho, H.-C. Chang, W.-T. Su, *Anal. Chem.* **2012**, *84*, 3246.
[202] Z. Yuan, M. Peng, Y. He, E. S. Yeung, *Chem. Commun.* **2011**, *47*, 11981.
[203] W. Chen, X. Tu, X. Guo, *Chem. Commun.* **2009**, 1736.
[204] C. V. Durgadas, C. P. Sharma, K. Sreenivasan, *Analyst* **2011**, *136*, 933.
[205] A. Henglein, *Chem. Mater.* **1998**, *10*, 444.

Part. Part. Syst. Charact. **2014**,
DOI: 10.1002/ppsc.201400033

[206] Y. Liu, K. Ai, X. Cheng, L. Huo, L. Lu, *Adv. Funct. Mater.* **2010**, *20*, 951.
[207] F. Qu, N. B. Li, H. Q. Luo, *Anal. Chem.* **2012**, *84*, 10373.
[208] W.-Y. Chen, G.-Y. Lan, H.-T. Chang, *Anal. Chem.* **2011**, *83*, 9450.
[209] J. Zhang, C. Chen, X. Xu, X. Wang, X. Yang, *Chem. Commun.* **2013**, *49*, 2691.
[210] M. S. Bootharaju, G. K. Deepesh, T. Udayabhaskararao, T. Pradeep, *J. Mater. Chem. A* **2013**, *1*, 611.
[211] M. Haruta, T. Kobayashi, H. Sano, N. Yamada, *Chem. Lett.* **1987**, *16*, 405.
[212] G. C. Bond, D. T. Thompson, *Catal. Rev.* **1999**, *41*, 319.
[213] M. Haruta, *Nature* **2005**, *437*, 1098.
[214] M. D. Hughes, Y. J. Xu, P. Jenkins, P. McMorn, P. Landon, D. I. Enache, A. F. Carley, G. A. Attard, G. J. Hutchings, F. King, E. H. Stitt, P. Johnston, K. Griffin, C. J. Kiely, *Nature* **2005**, *437*, 1132.
[215] M. Chen, Y. Cai, Z. Yan, D. W. Goodman, *J. Am. Chem. Soc.* **2006**, *128*, 6341.
[216] M. Stratakis, H. Garcia, *Chem. Rev.* **2012**, *112*, 4469.
[217] M. Chen, D. W. Goodman, *Chem. Soc. Rev.* **2008**, *37*, 1860.
[218] J. Gong, *Chem. Rev.* **2011**, *112*, 2987.
[219] A. S. K. Hashmi, G. J. Hutchings, *Angew. Chem. Int. Ed.* **2006**, *45*, 7896.
[220] Y. Zhu, H. Qian, M. Zhu, R. Jin, *Adv. Mater.* **2010**, *22*, 1915.
[221] Y. Liu, H. Tsunoyama, T. Akita, T. Tsukuda, *Chem. Commun.* **2010**, *46*, 550.
[222] M. Turner, V. B. Golovko, O. P. H. Vaughan, P. Abdulkin, A. Berenguer-Murcia, M. S. Tikhov, B. F. G. Johnson, R. M. Lambert, *Nature* **2008**, *454*, 981.
[223] X. Nie, H. Qian, Q. Ge, H. Xu, R. Jin, *ACS Nano* **2012**, *6*, 6014.
[224] X. Nie, C. Zeng, X. Ma, H. Qian, Q. Ge, H. Xu, R. Jin, *Nanoscale* **2013**, *5*, 5912.
[225] G. Ma, A. Binder, M. Chi, C. Liu, R. Jin, D.-E. Jiang, J. Fan, S. Dai, *Chem. Commun.* **2012**, *48*, 11413.
[226] O. Lopez-Acevedo, K. A. Kacprzak, J. Akola, H. Häkkinen, *Nat. Chem.* **2010**, *2*, 329.
[227] H. Tsunoyama, N. Ichikuni, T. Tsukuda, *Langmuir* **2008**, *24*, 11327.
[228] H. Tsunoyama, H. Sakurai, Y. Negishi, T. Tsukuda, *J. Am. Chem. Soc.* **2005**, *127*, 9374.
[229] S. Xie, H. Tsunoyama, W. Kurashige, Y. Negishi, T. Tsukuda, *ACS Catal.* **2012**, *2*, 1519.
[230] Y. Liu, H. Tsunoyama, T. Akita, S. Xie, T. Tsukuda, *ACS Catal.* **2010**, *1*, 2.
[231] Y. Zhu, Z. Wu, C. Gayathri, H. Qian, R. R. Gil, R. Jin, *J. Catal.* **2010**, *271*, 155.
[232] H. Yamamoto, H. Yano, H. Kouchi, Y. Obora, R. Arakawa, H. Kawasaki, *Nanoscale* **2012**, *4*, 4148.
[233] W. Chen, S. Chen, *Angew. Chem. Int. Ed.* **2009**, *48*, 4386.
[234] W. Wei, W. Chen, *Int. J. Smart Nano Mater.* **2012**, *4*, 62.
[235] C. Jeyabharathi, S. Senthil Kumar, G. V. M. Kiruthika, K. L. N. Phani, *Angew. Chem. Int. Ed.* **2010**, *49*, 2925.
[236] Y. Lu, W. Chen, *J. Power Sources* **2012**, *197*, 107.
[237] Y. Liu, H. Tsunoyama, T. Akita, T. Tsukuda, *J. Phys. Chem. C* **2009**, *113*, 13457.
[238] D. P. Anderson, J. F. Alvino, A. Gentleman, H. A. Qahtani, L. Thomsen, M. I. J. Polson, G. F. Metha, V. B. Golovko, G. G. Andersson, *Phys. Chem. Chem. Phys.* **2013**, *15*, 3917.
[239] Z. Jiang, W. Zhang, L. Jin, X. Yang, F. Xu, J. Zhu, W. Huang, *J. Phys. Chem. C* **2007**, *111*, 12434.
[240] C. Wen, Y. Zhu, Y. Ye, S. Zhang, F. Cheng, Y. Liu, P. Wang, F. Tao, *ACS Nano* **2012**, *6*, 9305.
[241] B. Yoon, H. Häkkinen, U. Landman, A. S. Wörz, J.-M. Antonietti, S. Abbet, K. Judai, U. Heiz, *Science* **2005**, *307*, 403.
[242] N. Yi, R. Si, H. Saltsburg, M. Flytzani-Stephanopoulos, *Appl. Catal. B: Environ.* **2010**, *95*, 87.
[243] N. Yi, R. Si, H. Saltsburg, M. Flytzani-Stephanopoulos, *Energy Environ. Sci.* **2010**, *3*, 831.
[244] C. J. Harding, S. Kunz, V. Habibpour, U. Heiz, *Phys. Chem. Chem. Phys.* **2008**, *10*, 5875.
[245] Y. Fukamori, M. König, B. Yoon, B. Wang, F. Esch, U. Heiz, U. Landman, *Chem. Cat. Chem.* **2013**, *5*, 3330.
[246] C. Zhang, B. Yoon, U. Landman, *J. Am. Chem. Soc.* **2007**, *129*, 2228.
[247] C. Harding, V. Habibpour, S. Kunz, A. N.-S. Farnbacher, U. Heiz, B. Yoon, U. Landman, *J. Am. Chem. Soc.* **2008**, *131*, 538.
[248] Y. Gao, N. Shao, Y. Pei, Z. Chen, X. C. Zeng, *ACS Nano* **2011**, *5*, 7818.
[249] W. Huang, H.-J. Zhai, L.-S. Wang, *J. Am. Chem. Soc.* **2010**, *132*, 4344.
[250] D. R. Kauffman, D. Alfonso, C. Matranga, H. Qian, R. Jin, *J. Am. Chem. Soc.* **2012**, *134*, 10237.
[251] M. Arenz, U. Landman, U. Heiz, *Chem. Phys. Chem.* **2006**, *7*, 1871.
[252] S. R. Panikkanvalappil, M. A. Mahmoud, M. A. Mackey, M. A. El-Sayed, *ACS Nano* **2013**, *7*, 7524.
[253] P. R. Sajanlal, T. Pradeep, *Nanoscale* **2012**, *4*, 3427.
[254] K. Kneipp, H. Kneipp, I. Itzkan, R. R. Dasari, M. S. Feld, *Chem. Rev.* **1999**, *99*, 2957.
[255] S. R. Panikkanvalappil, M. A. Mackey, M. A. El-Sayed, *J. Am. Chem. Soc.* **2013**, *135*, 4815.
[256] M. R. K. Ali, P. R. Sajanlal, M. A. El-Sayed, *J. Am. Chem. Soc.* **2014**,*136*, 4464.
[257] I. Chakraborty, S. Bag, U. Landman, T. Pradeep, *J. Phys. Chem. Lett.* **2013**, *4*, 2769.
[258] W. Zhang, M. Saliba, S. D. Stranks, Y. Sun, X. Shi, U. Wiesner, H. J. Snaith, *Nano Lett.* **2013**, *13*, 4505.
[259] G. Chen, J. Seo, C. Yang, P. N. Prasad, *Chem. Soc. Rev.* **2013**, *42*, 8304.
[260] C. C. D. Wang, W. C. H. Choy, C. Duan, D. D. S. Fung, W. E. I. Sha, F.-X. Xie, F. Huang, Y. Cao, *J. Mater. Chem.* **2012**, *22*, 1206.
[261] H. Choi, J.-P. Lee, S.-J. Ko, J.-W. Jung, H. Park, S. Yoo, O. Park, J.-R. Jeong, S. Park, J. Y. Kim, *Nano Lett.* **2013**, *13*, 2204.
[262] D. Zhang, W. C. H. Choy, C. C. D. Wang, X. Li, L. Fan, K. Wang, H. Zhu, *Appl. Phys. Lett.* **2011**, *99*, 223302.
[263] Y.-S. Chen, H. Choi, P. V. Kamat, *J. Am. Chem. Soc.* **2013**, *135*, 8822.
[264] R. S. Khnayzer, L. B. Thompson, M. Zamkov, S. Ardo, G. J. Meyer, C. J. Murphy, F. N. Castellano, *J. Phys. Chem. C* **2011**, *116*, 1429.
[265] Solutions for medical problems have been a major concern throughout all civilizations. References to the use of noble metals in medicinal preparations exist in numerous ancient cultures for the treatment of a variety of conditions such as smallpox, skin ulcers, measles, etc. The *Ayurvedic* system of medicine (whose celebrated text, *Sushruta Samhita* dates back to 6th century BC), mentions the use of metallic preparations in healthcare. Use of *Swarna bhasma* (meaning "gold ash"), a form of gold, for medicinal purposes started during the *Vedic* period in ancient India [C. L. Brown, G. Bushell, M. W. Whitehouse, D. S. Agrawal, S. G. Tupe, K. M. Paknikar, E. R. T. Tiekink, *Gold Bull.* 2007, *40*, 245].
[266] Many of these noble metal preparations have withstood the test of time and are still prevelant and practised by many. References on the use of gold for medicinal purposes also exist in the Chinese literature, and it was thought to act as the elixir of life [References exist in a book titled *Handbook of Prescription of Emergencies* authored by Ko Hung (Tsin dynasty, 265–419 AD)]. However, many of such treatments are not considered reliable or safe by modern medical practitioners as they contain substantial quantities of heavy metals and involve strict dietary regulations to be followed by the patient. Also, success of the treatment is mostly based on individual preference and their testimonies. Often, such

testimonies may not be verifiable accurately by the principles of modern medicine. The unique properties offered by noble metal QCs are currently being studied and exploited in a range of potential applications in biology.

[267] R. Archana, S. Sonali, M. Deepthy, R. Prasanth, M. Habeeb, P. Thalappil, N. Shantikumar, K. Manzoor, *Nanotechnology* **2010**, *21*, 055103.
[268] H. Wei, Z. Wang, L. Yang, S. Tian, C. Hou, Y. Lu, *Analyst* **2010**, *135*, 1406.
[269] F. Wen, Y. Dong, L. Feng, S. Wang, S. Zhang, X. Zhang, *Anal. Chem.* **2011**, *83*, 1193.
[270] X. Wang, P. Wu, Y. Lv, X. Hou, *Microchemical J.* **2011**, *99*, 327.
[271] Z. Chen, S. Qian, X. Chen, W. Gao, Y. Lin, *Analyst* **2012**, *137*, 4356.
[272] X. Chen, Y. Zhou, X. Peng, J. Yoon, *Chem. Soc. Rev.* **2010**, *39*, 2120.
[273] X. Yuan, Y. Tay, X. Dou, Z. Luo, D. T. Leong, J. Xie, *Anal. Chem.* **2012**, *85*, 1913.
[274] B. Han, E. Wang, *Biosens. Bioelectron.* **2011**, *26*, 2585.
[275] L. Shang, S. Dong, *Biosens. Bioelectron.* **2009**, *24*, 1569.
[276] Z. Huang, F. Pu, Y. Lin, J. Ren, X. Qu, *Chem. Commun.* **2011**, *47*, 3487.
[277] R. C. Triulzi, M. Micic, S. Giordani, M. Serry, W.-A. Chiou, R. M. Leblanc, *Chem. Commun.* **2006**, 5068.
[278] C.-C. Huang, C.-K. Chiang, Z.-H. Lin, K.-H. Lee, H.-T. Chang, *Anal. Chem.* **2008**, *80*, 1497.
[279] C.-C. Huang, C.-T. Chen, Y.-C. Shiang, Z.-H. Lin, H.-T. Chang, *Anal. Chem.* **2009**, *81*, 875.
[280] Y.-C. Shiang, C.-A. Lin, C.-C. Huang, H.-T. Chang, *Analyst* **2011**, *136*, 1177.
[281] C.-T. Chen, W.-J. Chen, C.-Z. Liu, L.-Y. Chang, Y.-C. Chen, *Chem. Commun.* **2009**, 7515.
[282] C.-C. Huang, Y.-L. Hung, Y.-C. Shiang, T.-Y. Lin, Y.-S. Lin, C.-T. Chen, H.-T. Chang, *Chem. Asian J.* **2010**, *5*, 334.
[283] C.-C. Huang, T.-Y. Lin, W.-S. Yu, C.-T. Chen, H.-T. Chang, *J. Biomed. Nanotechnol.* **2009**, *5*, 579.
[284] G.-Y. Lan, W.-Y. Chen, H.-T. Chang, *Analyst* **2011**, *136*, 3623.
[285] J. Sharma, H.-C. Yeh, H. Yoo, J. H. Werner, J. S. Martinez, *Chem. Commun.* **2011**, *47*, 2294.
[286] H. Liu, X. Wu, X. Zhang, C. Burda, J.-J. Zhu, *J. Phys. Chem. C* **2011**, *116*, 2548.
[287] M. Zhang, S.-M. Guo, Y.-R. Li, P. Zuo, B.-C. Ye, *Chem. Commun.* **2012**, *48*, 5488.
[288] H. Dong, S. Jin, H. Ju, K. Hao, L.-P. Xu, H. Lu, X. Zhang, *Anal. Chem.* **2012**, *84*, 8670.
[289] X. Liu, F. Wang, A. Niazov-Elkan, W. Guo, I. Willner, *Nano Lett.* **2012**, *13*, 309.
[290] H.-C. Yeh, J. Sharma, J. J. Han, J. S. Martinez, J. H. Werner, *Nano Lett.* **2010**, *10*, 3106.
[291] A. P. Demchenko, M. A. H. Muhammed, T. Pradeep, in *Advanced Fluorescence Reporters in Chemistry and Biology II*, Vol. *9*, Springer, Berlin, Heidelberg **2010**, pp. 333.
[292] N. Makarava, A. Parfenov, I. V. Baskakov, *Biophys. J.* **2005**, *89*, 572.
[293] J. Yu, S. A. Patel, R. M. Dickson, *Angew. Chem. Int. Ed.* **2007**, *46*, 2028.
[294] J. Yu, S. Choi, C. I. Richards, Y. Antoku, R. M. Dickson, *Photochem. Photobiol.* **2008**, *84*, 1435.
[295] C.-A. J. Lin, T.-Y. Yang, C.-H. Lee, S. H. Huang, R. A. Sperling, M. Zanella, J. K. Li, J.-L. Shen, H.-H. Wang, H.-I. Yeh, W. J. Parak, W. H. Chang, *ACS Nano* **2009**, *3*, 395.
[296] M. A. H. Muhammed, P. K. Verma, S. K. Pal, R. C. A. Kumar, S. Paul, R. V. Omkumar, T. Pradeep, *Chem. Eur. J.* **2009**, *15*, 10110.
[297] Y. Tao, Y. Lin, Z. Huang, J. Ren, X. Qu, *Adv. Mater.* **2013**, *25*, 2594.
[298] J. Wang, G. Zhang, Q. Li, H. Jiang, C. Liu, C. Amatore, X. Wang, *Sci. Rep.* **2013**, *3*, 1157.
[299] Y. Wang, J. Chen, J. Irudayaraj, *ACS Nano* **2011**, *5*, 9718.
[300] G. Sun, L. Zhou, Y. Liu, Z. Zhao, *New J. Chem.* **2013**, *37*, 1028.
[301] G. Liang, D. Ye, X. Zhang, F. Dong, H. Chen, S. Zhang, J. Li, X. Shen, J. Kong, *J. Mater. Chem. B* **2013**, *1*, 3545.
[302] C. Zhou, M. Long, Y. Qin, X. Sun, J. Zheng, *Angew. Chem. Int. Ed.* **2011**, *50*, 3168.
[303] C. A. Simpson, B. J. Huffman, A. E. Gerdon, D. E. Cliffel, *Chem. Res.Toxicol.* **2010**, *23*, 1608.
[304] C. A. Simpson, A. C. Agrawal, A. Balinski, K. M. Harkness, D. E. Cliffel, *ACS Nano* **2011**, *5*, 3577.
[305] Y. Pan, S. Neuss, A. Leifert, M. Fischler, F. Wen, U. Simon, G. Schmid, W. Brandau, W. Jahnen-Dechent, *Small* **2007**, *3*, 1941.
[306] M. Tsoli, H. Kuhn, W. Brandau, H. Esche, G. Schmid, *Small* **2005**, *1*, 841.
[307] M. Zhu, E. Lanni, N. Garg, M. E. Bier, R. Jin, *J. Am. Chem. Soc.* **2008**, *130*, 1138.
[308] E. G. Castro, R. V. Salvatierra, W. H. Schreiner, M. M. Oliveira, A. J. G. Zarbin, *Chem. Mater.* **2010**, *22*, 360.
[309] X. Yuan, Z. Luo, Q. Zhang, X. Zhang, Y. Zheng, J. Y. Lee, J. Xie, *ACS Nano* **2011**, *5*, 8800.
[310] M. A. H. Muhammed, F. Aldeek, G. Palui, L. Trapiella-Alfonso, H. Mattoussi, *ACS Nano* **2012**, *6*, 8950.
[311] L. Shang, S. Dong, *Chem. Commun.* **2008**, 1088.
[312] C. I. Richards, S. Choi, J.-C. Hsiang, Y. Antoku, T. Vosch, A. Bongiorno, Y.-L. Tzeng, R. M. Dickson, *J. Am. Chem. Soc.* **2008**, *130*, 5038.
[313] T. Vosch, Y. Antoku, J.-C. Hsiang, C. I. Richards, J. I. Gonzalez, R. M. Dickson, *Proc. Natl. Acad. Sci.* **2007**, *104*, 12616.
[314] W. Guo, J. Yuan, Q. Dong, E. Wang, *J. Am. Chem. Soc.* **2009**, *132*, 932.
[315] J. Yu, S. Choi, R. M. Dickson, *Angew. Chem. Int. Ed.* **2009**, *48*, 318.
[316] T. Shimizu, T. Teranishi, S. Hasegawa, M. Miyake, *J. Phys. Chem. B* **2003**, *107*, 2719.
[317] I. Chakraborty, T. Udayabhaskararao, T. Pradeep, *Chem. Commun.* **2012**, *48*, 6788.
[318] H. Qian, Y. Zhu, R. Jin, *ACS Nano* **2009**, *3*, 3795.
[319] T. G. Schaaff, R. L. Whetten, *J. Phys. Chem. B* **1999**, *103*, 9394.
[320] T. Udayabhaskararao, Y. Sun, N. Goswami, S. K. Pal, K. Balasubramanian, T. Pradeep, *Angew. Chem. Int. Ed.* **2012**, *51*, 2155.
[321] W. Kurashige, K. Munakata, K. Nobusada, Y. Negishi, *Chem. Commun.* **2013**, *49*, 5447.
[322] S. L. Christensen, M. A. MacDonald, A. Chatt, P. Zhang, H. Qian, R. Jin, *J. Phys. Chem. C* **2012**, *116*, 26932.
[323] H. Qian, W. T. Eckenhoff, M. E. Bier, T. Pintauer, R. Jin, *Inorg. Chem.* **2011**, *50*, 10735.
[324] C. Kumara, C. M. Aikens, A. Dass, *J. Phys. Chem. Lett.* **2014**, *5*, 461.
[325] D. Crasto, S. Malola, G. Brosofsky, A. Dass, H. Häkkinen, *J. Am. Chem. Soc.* **2014**.
[326] H. Yang, Y. Wang, J. Lei, L. Shi, X. Wu, V. Mäkinen, S. Lin, Z. Tang, J. He, H. Häkkinen, L. Zheng, N. Zheng, *J. Am. Chem. Soc.* **2013**, *135*, 9568.
[327] D. Hu, Z. Sheng, P. Gong, P. Zhang, L. Cai, *Analyst* **2010**, *135*, 1411.
[328] S. Roy, G. Palui, A. Banerjee, *Nanoscale* **2012**, *4*, 2734.
[329] L. Shang, S. Dong, *J. Mater. Chem.* **2008**, *18*, 4636.
[330] T.-Y. Zhou, L.-P. Lin, M.-C. Rong, Y.-Q. Jiang, X. Chen, *Anal. Chem.* **2013**.
[331] H. Qian, D.-e. Jiang, G. Li, C. Gayathri, A. Das, R. R. Gil, R. Jin, *J. Am. Chem. Soc.* **2012**, *134*, 16159.
[332] S. Kanaoka, N. Yagi, Y. Fukuyama, S. Aoshima, H. Tsunoyama, T. Tsukuda, H. Sakurai, *J. Am. Chem. Soc.* **2007**, *129*, 12060.

Part. Part. Syst. Charact. **2014**,
DOI: 10.1002/ppsc.201400033

[333] N. K. Chaki, H. Tsunoyama, Y. Negishi, H. Sakurai, T. Tsukuda, *J. Phys. Chem. C* **2007**, *111*, 4885.
[334] G. Li, C. Liu, Y. Lei, R. Jin, *Chem. Commun.* **2012**, *48*, 12005.
[335] C. Yu, G. Li, S. Kumar, H. Kawasaki, R. Jin, *J. Phys. Chem. Lett.* **2013**, *4*, 2847.
[336] P. Maity, S. Yamazoe, T. Tsukuda, *ACS Catal.* **2013**, *3*, 182.
[337] G. Li, H. Qian, R. Jin, *Nanoscale* **2012**, *4*, 6714.
[338] A. Leelavathi, T. Bhaskara Rao, T. Pradeep, *Nanoscale Res. Lett.* **2011**, *6*, 123.
[339] S. W. Yang, T. Vosch, *Anal. Chem.* **2011**, *83*, 6935.
[340] H.-C. Yeh, J. Sharma, J. J. Han, J. S. Martinez, J. H. Werner, *Nano Lett.* **2010**, *10*, 3106.
[341] J. T. Petty, B. Sengupta, S. P. Story, N. N. Degtyareva, *Anal. Chem.* **2011**, *83*, 5957.